

LUND'S UNIVERSITETS ÅRSSKRIFT N. F. Avd. 2. Bd 54. Nr 1.

KUNGL. FYSIOGRAFISKA SÄLLSKAPETS HANDLINGAR. N. F. Bd 69. Nr 1.

MEDDELANDE FRÅN LUND'S ASTRONOMISKA OBSERVATORIUM

Ser. II. Nr. 136.

# A PHOTOGRAPHIC PHOTOMETRY OF EXTRAGALACTIC NEBULAE

BY

ERIK HOLMBERG

I. A STUDY OF INTEGRATED MAGNITUDES  
AND COLORS OF 300 GALAXIES

LUND  
C. W. K. GLEERUP

(

(

-(

F1

Read before the Royal Physiographic Society, Nov. 13, 1957.

- [1] .
- [2] :
- [3] (
- [4] )
- [5] :
- [6] :
- [7] (
- [8] .
- [9] )
- [10] (
- [11] :
- [12] '
- [13] :
- [14]
- [15] :
- [16] )
- [17] '
- [18] )

LUND

HÅKAN OHLSSONS BOKTRYCKERI

1 9 5 8

## Summary

The present paper gives the results of a photographic photometry of 300 extra-galactic nebulae. The photometric work is based on observations with the 60-inch and 100-inch telescopes at Mt. Wilson, made by the writer during three different periods as guest investigator at the Mount Wilson and Palomar Observatories. The program, which covers the entire northern sky, mainly includes nebulae brighter than the 12th magnitude.

*Chapter I* gives an account of the photometric procedure. The integrated photogr. and photovis. magnitudes (int. scale), which are referred to a homogeneous system, have been derived by integrations based on photometer tracings, the plates being calibrated by means of extrafocal exposures of stars of NPS, or SA 57. As a rule, 2 photogr. and 2 photovis. plates have been available for each object, the total number of individual magnitude measures amounting to 1205. The final mean errors appear to be small (Table 2). A detailed comparison with the photoelectric measures by Stebbins-Whitford does not reveal any systematic differences.

*Chapter II* gives the results of an investigation of the integrated colors of the nebulae. The color index of a spiral system depends on the inclination (Fig. 2). The observed color includes a color excess that is a linear function of the cosecant of gal. lat. (Fig. 3), the selective absorption at lat.  $90^\circ$  being  $0^m062$ ; a slight difference between northern and southern hemispheres is indicated. The redshift effect in color index, as derived for spiral nebulae, amounts to  $+0^m018$  per  $10^3$  km/sec. The mean colors of nebulae of different types, as listed in Table 7, range from  $+0^m28$  (type *Ir I*) to  $+0^m85$  (type *E*).

*Chapter III* deals with the internal absorption in spiral nebulae. The inclination effect in selective absorption is derived from the observed colors. The corresponding effect in photographic absorption, as derived from the variation in surface magnitude, appears to be proportional to the cosecant of the incl. of the object to the line of sight (Fig. 4). For incl.  $90^\circ$ , the total photogr. absorption is, on an average, equal to  $0^m28$  (type *Sc*), and  $0^m43$  (type *Sb, Sa*); for incl.  $0^\circ$ , the corresponding results are  $1^m3$  and  $1^m8$ , resp. The ratio of photogr. to selective absorption is rather high for incl.  $0^\circ$ , but approaches 4 as the incl. increases (Fig. 5); the ratios agree with those derived for a theoretical system. A special investigation based on the *main bodies* of the spiral nebulae gives similar results. The internal absorption known, the intrinsic colors of the stellar contents of nebulae of different types may be determined (Table 13); the colors range from  $+0^m12$  (type *Ir I*) to  $+0^m77$ .

(type *E*). Finally, a study of the surface magnitudes leads to a total galactic absorption of the same size as that found by Hubble from nebular counts.

*Chapter IV* presents the results of an investigation of the Virgo cluster. A study of the colors derived by the writer for 53 cluster members indicates that about 50 % of the nebulae suffer from a color excess of approximately  $+0^m16$ . The color excess is accompanied by a decrease in photogr. surface magnitude, the ratio of the two effects possibly being 1:4 (Fig. 10). An examination of the "normal" cluster members indicates a rather pronounced correlation between absolute magnitude and surface magnitude (Fig. 11). If the latter quantity is used as distance indicator, we find for nebulae outside the cluster mean absolute luminosities of the same order of size as those derived from redshifts (Table 17); with an app. modulus of the Virgo cluster of 30.2, as obtained from the photometric material, we arrive at a Hubble parameter  $H$  of 134 km/sec per  $10^6$  ps. A study of the magnitude distribution (corr. for background) of the cluster nebulae leads to the absolute luminosity curve reproduced in Fig. 13; the highest abs. magn.,  $-20.9$ , is found for the elliptical nebula NGC 4472.

[1] *Chapter V* gives the details of an investigation of double nebulae included in the writer's program. From the material assembled in Table 19 a pronounced correlation is found between the components of close pairs as regards integrated color index (Fig. 14), and as regards surface magnitude (Fig. 15). The agreements indicate that physically related nebulae have similar stellar contents, and similar luminosity densities (mass densities). The results strongly suggest that double systems have been formed by disintegrations of single nebulae. Individually, the members of double systems seem to be comparable to a random selection of extragalactic objects.

[2] The *Catalogue* gives galactic coordinates, types, apparent diameters, integrated magnitudes, and integrated color indices for the 300 nebulae included in the photometric program.

[3] The writer wishes to acknowledge his sincere gratitude to Dr. I. S. Bowen, Director of the Mount Wilson and Palomar Observatories, who has rendered this investigation possible by making the telescopes and other facilities at Mount Wilson available for the photometric work. The writer's thanks are also extended to the night assistants, in particular Mr. E. Hancock and Mr. A. H. Olmstead, who have always done all in their power to help carry through the usually rather crowded nightly programs. For the measuring and reduction work at the Lund Observatory, the writer has been fortunate in being able to secure the help of a number of reliable assistants and computers, among them Mr. G. Lyngå, Mrs. Inga Appeltoft, Miss Irene Lundqvist, and Miss Anna Johnsson. Finally, the writer is indebted to the Swedish Natural Science Research Council, and to the Royal Physiographic Society in Lund, which have provided the financial support necessary to carry through the investigation.

## CHAPTER I

### Observational Method and Photometric Results

#### 1. Scope of photometric program.

The present photometric work is an extension of the photographic photometry of extragalactic nebulae begun by the writer at Mount Wilson in 1947–48. The earlier investigation (Holmberg 1950a) included nearby nebulae for which distance moduli could be derived with some degree of accuracy (local group; groups around NGC 3031 and NGC 5457), and the results were used for a study of, among other things, absolute luminosities and dimensions of extragalactic objects. The extended program, which is based on observations with the 60-inch and 100-inch telescopes at Mount Wilson, includes altogether 300 external nebulae, for which integrated magnitudes, color indices, and apparent dimensions have been measured. The objects are distributed over the entire northern sky, the observations (in 1951 and 1954–55) covering all hours of right ascension.

The nebulae included in the photometric program have been selected by means of the plate collection of the Mount Wilson and Palomar Observatories, and by means of the redshift catalogue by Humason, Mayall, and Sandage (1956). By using the degree of resolution, the apparent magnitudes and dimensions, and the redshifts as distance indicators, the writer has tried to assemble a material referring to the nearer extragalactic space; the great majority of the selected objects presumably have distance moduli below 30.0. The material includes (a) nebulae showing a pronounced resolution on the 60-inch or 100-inch plates (individual stars, emission knots), (b) nebulae with app. magnitudes and diameters brighter than 12<sup>m</sup>0 and above 5'0, respectively, and (c) nebulae with moderately large redshifts (below 1200 km/sec). Owing to the practical observing conditions it has, of course, not always been possible to adhere strictly to these rules. The material includes the majority of the objects which in the Shapley-Ames (1932) survey catalogue are listed as brighter than the 12th magnitude (above decl. –10°). It should be noted that in the Virgo cluster area (comp. sect. 25) the program has been extended to nebulae that are fainter than the magnitude mentioned.

The program includes a number of interesting nebulae which have been discovered in the recent years on survey plates from the Palomar Schmidt telescopes. The *Leo B* system and the *Regulus* system (Harrington and Wilson 1950), the latter having a position close to  $\alpha$  Leonis, are both remarkable elliptical nebulae of the “Sculptor type”, well resolved into stars and of very low surface luminosity. The

*Pegasus* and *Sextans B* systems are somewhat smaller irregular nebulae, the latter showing a good resolution. The objects denoted *Leo A* and *Sextans A*, discovered by Zwicky (1942), are also well resolved nebulae of the irregular type. The coordinates of all objects not listed in NGC or IC are given in the notes at the end of the catalogue.

Among the other anonymous objects we may mention the eight nebulae denoted *Ho I* to *Ho VIII*. Some of these have been discovered earlier by the writer on survey plates covering the regions around NGC 3031 and NGC 5457, while others have been found on the 60-inch or 100-inch plates as companions to brighter nebulae already included in the photometric program. The most remarkable of these objects are *Ho I* and *Ho II*, well resolved systems of the irregular type.

Unfortunately, it has not been possible to include the four most important discoveries, the *Fornax* and *Sculptor* systems (Shapley 1938), and the *Draco* and *Ursa Minor* systems (Wilson 1955). The first two nebulae have rather low declinations ( $-35^\circ$  and  $-34^\circ$ , resp.); the latter two (decl.  $+58^\circ$  and  $+67^\circ$ , resp.) are too well resolved for the 60-inch telescope, and their surface magnitudes are, furthermore, below the practical measuring limit at Mount Wilson.

All nebulae included in the photometric program are listed in the catalogue at the end of the paper. Except for magnitudes, colors, and diameters, the catalogue also gives the type of each object, as determined by the writer from the 60-inch or 100-inch plates; the classification system, which is based on the traditional system by Hubble, is described in sect. 12.

## 2. Photometric method.

The observations have aimed at a determination, on the international scale, of the integrated photographic and photovisual magnitudes of the selected nebulae. As measured by the writer, each magnitude represents the light contained within a certain isophote, corresponding to a surface luminosity that is more or less the same for the entire material. All magnitudes are thus comparable measures, and form a homogeneous system. As is found below in sect. 4, the limiting surface luminosities (corresp. to the standard exp. times) amount to about  $26^m5$  and  $26^m0$  per square second in the photographic and photovisual regions, respectively. According to the writer's experience from the analyses of the photometer registrations, a nebular magnitude thus defined must in most cases be very close to the total (or asymptotic) magnitude that includes *all* the light of the nebula. For all practical purposes, the magnitude measures listed in the catalogue may be assumed to represent the total magnitudes of the nebulae; in the following sections the measures will frequently be referred to by this term. For the difference between photographic and photovisual magnitudes, the term integrated color index will be used.

As a by-product of the photometric measures, the major and minor apparent diameters of the nebulae are obtained in a similar, homogeneous system.

The photometric method may be described as a comparison, by means of a micro-photometer, between two exposures of the same duration, each made on one half of

a plate. The exposures refer to the nebula (focal image), and to the stars of a comparison field (extrafocal images). The photometer recordings of the stars give the relation between plate density and surface luminosity, needed for the evaluation of the tracings of the nebula. The results are thus independent of any artificial calibrations of the plate, by sensitometer or other means.

As a comparison field either the north polar region (60-inch tel.), or the selected area 57 (100-inch tel.) has been used. The polar exposures have been centered on the NPS star 18, and the calibration has been based on stars 16, 17, 18, 20, 21, 22, 7r, 8r, and 12r; besides, the stars  $89^{\circ}, 33$  and  $89^{\circ}, 36$  of the Mount Wilson polar catalogue (Seares, Ross, and Joyner 1941) have been used. As regards photographic magnitudes and color indices, the results listed in the Rome Report (Seares 1922) have been accepted, the revisions by Seares-Joyner (1945) and the adjustments indicated by modern photoelectric observations (Stebbins, Whitford, and Johnson 1950) being taken into account. The exposures of SA 57 have been centered on star 29, the calibrations being based on stars 7, 8, 11, 16, 25, 29, 40, 52, 54, and 58 (numbers ref. to the Mount Wilson Cat. of Sel. Areas, 1930); for these stars, the magnitudes and colors derived photoelectrically by Stebbins-Whitford-Johnson in the above-mentioned paper have been adopted. For an accurate determination of the mean densities of the calibration stars, it is important that the extrafocal images are as smooth and homogeneous as possible. Since the mirrors of the two main telescopes used are optically perfect, this condition is fulfilled in the present case.

The nebulae have in most cases been measured in directions parallel to their minor axes, the number of photometer tracings depending on the size of the object. The measuring procedure will be further described below (sect. 4). By means of the calibration curve, each registration is transformed into a curve giving the distribution of surface brightness. The total luminosity of the nebula, as represented by the amount of light within the isophote corresponding to the limiting surface magnitude of the plate, is then derived by integrations along the minor and major axes.

It may be noted that, since we are dealing with surface objects, the final results are practically independent of possible changes in atmospheric seeing conditions from nebular exposure to calibration exposure and, likewise, of possible changes as regards focussing and guiding of the telescope. As is well known, these three effects may give rise to appreciable systematic errors in the traditional stellar photometry based on focal images.

The photometric procedure is laborious, but leads to results of considerable accuracy and high homogeneity. Besides, the procedure yields not only integrated magnitudes and color indices, but also internal distributions of surface luminosity and color. The results referring to the internal distributions are not discussed in this paper; a detailed report will be given in a subsequent publication.

The photometric program includes a number of nebulae of rather low surface brightness. These objects do not usually present any serious difficulties in the measuring work, the photometer tracings indicating a clear separation between nebula and background. There are, however, some exceptional nebulae of exceedingly

low surface luminosity which demand special attention. The most interesting of these objects is the local group member *Leo B* (comp. sect. 1), for which the mean photographic surface magnitude, as derived by the writer, amounts to only 26<sup>m</sup>.6 per square second; the surface magnitude is thus lower than the limiting magnitude mentioned above. For a few nebulae of this abnormal type, it has been necessary to increase the exposure times of the plates, the standard exposure not being sufficient to bring out a measurable contrast between nebula and background.

In two following sections, comparisons will be made between the writer's measures and results derived by photoelectric observations. As to the advantages and disadvantages of the two photometric methods, it is quite clear that the photoelectric procedure, as based on a fixed diaphragm, gives the best results for concentrated nebulae of high (or medium) surface luminosity; on account of the small size and the steep density gradients, nebulae of this type are less suitable (although not really difficult) objects for the photographic method. In the case of nebulae of low surface luminosity, it seems possible to get reliable results only by the photographic method; owing to the disturbance caused by the superposed star field, it would be very difficult (if at all possible) to measure objects of this kind by the usual photoelectric technique.

Attempts have been made (van Houten, Oort, and Hiltner 1954) to overcome the difficulty of superposed stars in the photoelectric work by tracing the nebula at the telescope, a method principally the same as that used by the writer (but without the photogr. plate as intermediary step); the laboratory measuring work is thus shifted to the telescope. Very likely, the procedure could never be used for any larger number of nebulae on account of the enormous observing times involved. Furthermore, the tracings may, especially in the case of objects of low surface luminosity, be noticeably disturbed by the small, accidental variations in sky brightness. The photographic measures are naturally not influenced by this effect, nebula and background being observed simultaneously.

### **3. Instruments and plate material.**

The photometric data listed in the final catalogue are based on a total of 1205 individual magnitude measures. Of these, 886 have been derived from plates taken with the 60-inch, and 256 from plates taken with the 100-inch telescope. At the request of Dr. R. Minkowski, the southern nebula NGC 5128 has been included in the photometric list; 4 plates from the Palomar 48-inch Schmidt telescope have been available for this object. The remaining plates refer to observations with the 10-inch refractor at Mount Wilson, and with the 60-cm and 100-cm reflectors of the Hamburg Observatory; details about the latter observations have been given in the earlier publication (Holmberg 1950 a).

A summary of the observational work at Mount Wilson is found in Table 1. The material has been collected during three observation periods in the years 1947 to 1955. The results of the first period have been discussed in the paper mentioned above. The great majority of the plates have been secured during the second and

Table 1. *Observational material from the Mount Wilson Observatory used in the present investigation.*

Observation period	Number of exp. of nebulae	Instrument
Aug. 1947—Febr. 1948	105	60-inch
	31	10-inch
July 1951—Dec. 1951	320	60-inch
Dec. 1954—May 1955	256	100-inch
	461	60-inch

1173

third periods, which together cover all hours of right ascension. Especially in 1955, the writer has been able to get a considerable number of exposures, the telescopes being available for the photometric work on practically all moon-free nights each month. It may be mentioned that most of the 100-inch plates refer to nebulae in the Virgo cluster area; a larger scale has been desirable for these objects, their average dimensions being comparatively small.

Both at the 60-inch and the 100-inch telescope the observations have been made at Newton focus; all plates have been taken by the writer. Since guiding has not been necessary for the extrafocal exposures of the NPS stars, the polar region can be reached by the 60-inch instrument even with the cage mounted in the southern position. Practically all observations have been made in negative hour angles. Since the majority of the nebulae have positive declinations, the observations have thus been restricted to the northeastern quadrant of the sky; between this region and the polar area there is usually no noticeable difference in sky brightness at Mount Wilson. With the exception of those nights when the valley has been covered by clouds, observations in south and west have been avoided.

The photographic magnitudes have been derived from Eastman 103a-O plates, and the photovisual magnitudes from 103a-D (in 1947-48, 103a-C) plates exposed behind a 2 mm Schott GG 11 filter. Since no blue stars are used for calibration, it has not been deemed necessary to combine the 103a-O plates with a filter cutting out ultraviolet light. As will be shown below (sect. 5), the magnitudes based on the above plate material are rather closely related to the int. system.

In order to obtain a photometric material that is homogeneous, standard exposures of 10 min. (103a-O) and 15 min. (103a-D) have been used in practically all cases. With these comparatively short exposure times the sky fog is reduced to a minimum; the exposures are, on the other hand, sufficient to bring out the faint outer parts of the objects. For nebulae having exceptionally high surface luminosities in the central regions, it has been necessary to supplement the standard exposures with exposures of shorter duration.

It has been the aim of the writer to secure for each nebula two pairs of plates, a pair comprising one photographic and one photovisual exposure. The two exposures have as a rule been made in immediate succession; the two pairs are, however, taken

on different nights. The observational conditions have in a few cases permitted only 1+1 plates, in other cases it has been possible to increase the number to 3+3. For nine nebulae observed in 1947–48 only one photographic plate is available.

As has already been mentioned, the nebular exposures have been made in focus. Only in the case of a few very nearby systems, the plates have been taken slightly out of focus in order to smear out an incipient resolution into individual stars. The NPS stars (60-inch tel.) have been exposed at extrafocal distances of 12–20 mm, the displacement depending on the desired range in plate density. As regards SA 57 (100-inch tel.), the stars included in the comparatively small field do not have a sufficient range in magnitude; the calibration has in each case been based on two exposures, with extrafocal displacements of about 12 mm and 35 mm.

At the beginning of the observational work each plate was calibrated individually, the exposure of the nebula on one half of the plate being followed by the polar exposure on the other half. In order to save observing time, a slightly modified procedure has been adopted later on; the two plates facing each other within a sub-package of the box have been treated as one photometric unit. In this way three nebular exposures (100-inch, 2 exp.) have been referred to the same calibration. The modified procedure has not led to any noticeable increase in accidental errors.

#### 4. Measuring procedure.

The measuring of the plates, and the subsequent reductions, which represent the most laborious part of the program, have been done at the Lund Observatory. In order to speed up the work, the writer has secured the help of a number of assistants; all calibration plates and about one third of the nebular exposures have, however, been measured and reduced by the writer alone. By the end of 1956 practically all measuring and reduction work had been completed.

The plates have been measured in a thermoelectric, selfrecording microphotometer, the linear enlargement from plate to registration paper usually being about 7 times, and the total galvanometer deflection (zero point to clear plate) about 100 mm. The size of the slit, as projected on the plate, has been varied according to the type of the nebula and the steepness of the density gradients. In the case of extended nebulae with smooth distributions of surface luminosity, the use of even a rather large slit will not give rise to any appreciable systematic errors. The maximum size of the slit used in the present case has been  $1.0 \times 0.1$  mm<sup>2</sup>.

The nebulae have been measured in directions perpendicular, or almost perpendicular, to their major axes. The measured cross-sections have been distributed in the most suitable way over the nebular image, their number depending on the size of the object and on the density gradients; in the case of elliptical and spiral nebulae one cross-section always passes through the central region. The number of photometer registrations of each plate ranges from 10 to over 20, the mean being about 15. In addition, a few tracings have been made along the major axis of each nebula in order to determine the maximum extension of the object. The total number of nebular tracings analysed amounts to about 20000.

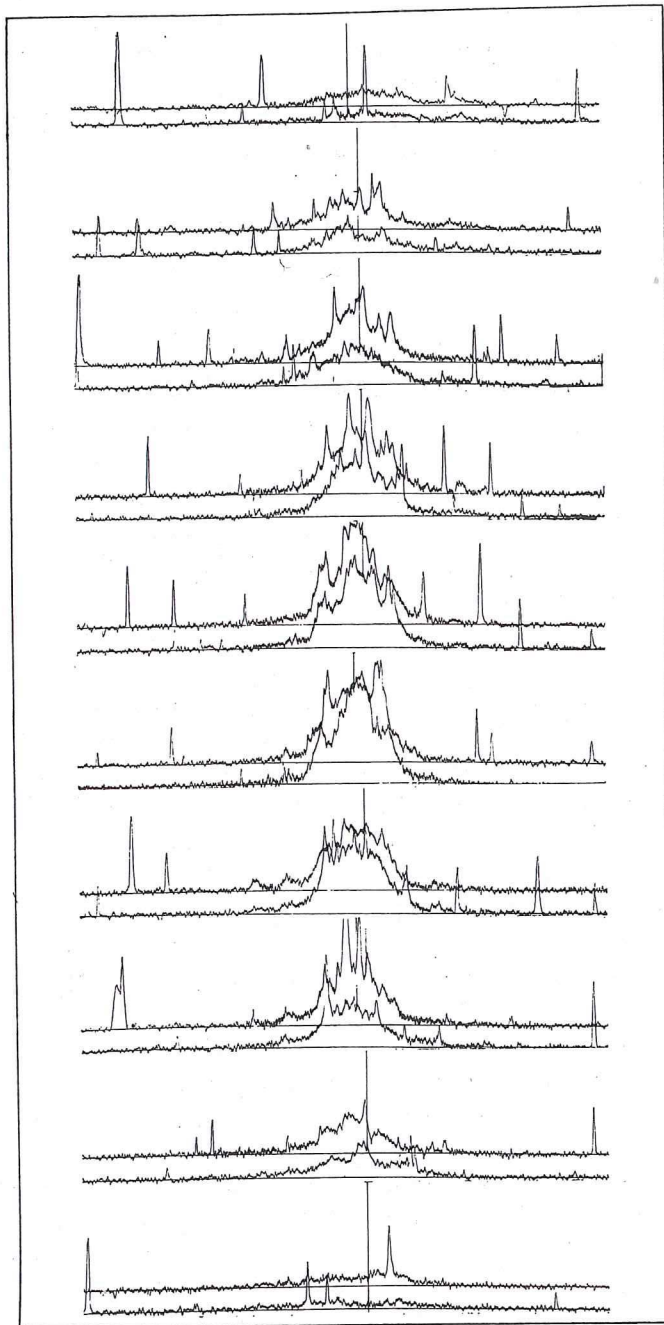


Fig. 1. Reproduction of 20 microphotometer tracings of the spiral nebula NGC 2403 (*103a-0* plate, 60-inch tel.). Each tracing (length = 400 mm) represents the distribution of surface luminosity in a cross-section parallel to the minor axis of the object; the galvanometer zero point marks are not shown.

It may be noted that only in exceptional cases can the background (sky fog) of the plate be represented by a perfectly straight line. For an accurate definition of the background it is thus very important that the photometer registrations include, on both sides of the measured nebula, sufficiently large areas of the plate. In the present case, each tracing has usually been extended over a distance on the plate at least three times the minor diameter of the object.

The extrafocal calibration stars have been measured in the photometer in exactly the same way as the nebulae. Each star image has been traced through the center, and in a direction where the least disturbance is caused by neighboring stars. When the extrafocal displacement is moderately large, a slight coma effect may be noticed in stars located at the edge of the calibration field; these stars have been measured in two directions perpendicular to each other. From the tracings we get the relation between relative plate density (defl. clear plate minus star, divided by total defl.) and surface luminosity, as corresponding to the adopted stellar magnitudes and the diameter of the extrafocal images (derived from tracings). In the reduction work it has appeared most convenient to use a calibration curve based on the surface brightness, as defined by the amount of light per square mm of the plate. This curve starts from a point very close to the zero points of the two scales, and is, for relative plate densities smaller than about 15 %, practically a straight line; with a suitable choice of light unit, the surface brightness will in the latter interval be equal to the relative plate density.

The extrafocal exposures usually yield calibration curves that are very well defined; the dispersion of the individual stars around the curve may be as small as 0<sup>m</sup>02. As regards plates of standard exposures, a relative plate density of 0.5 % corresponds, on an average, to surface magnitudes of 26<sup>m</sup>5 (photogr. reg.), and 26<sup>m</sup>0 (photov. reg.), per square second. Since a density of 0.5 % is close to the practical measuring limit, the two magnitudes mentioned represent the *limiting surface magnitudes* of the plates.

By means of the calibration curve the density distributions obtained for the different cross-sections of a nebula are transformed into distributions of surface brightness. The superposed stars are naturally not included; in doubtful cases, a comparison between photographic and photovisual plates immediately reveals the foreground stars. A numerical integration yields the integrated amount of light,  $\Sigma i$ , corresponding to each cross-section. A second integration (along the major axis), based on the curve defined by the different  $\Sigma i$ -values, then gives the luminosity of the entire system. The result is expressed in the units of light adopted for the calibration stars, and is easily transformed into magnitudes. It may be remarked that the total extension of the  $\Sigma i$ -curve, which cannot be accurately derived from the cross-section measures, has been determined from the tracings along the major axis of the nebula.

##### 5. Color equation and extinction.

The integrated magnitudes have been reduced to the international system by means of the color equations derived from the calibration stars. If the corrections

to be applied to the photographic and photovisual magnitudes are represented by the linear expressions  $p(C-0^m 60)$  and  $v(C-0^m 60)$ , respectively, the following results are obtained for the 60-inch plates:

$$\begin{array}{lll} p = -0.11 \text{ (1947-48)}, & p = -0.08 \text{ (1951)}, & p = -0.15 \text{ (1954-55)}. \\ v = 0.00 & v = -0.03 & v = 0.00 \end{array}$$

The coefficients  $p$  and  $v$  are thus approximately the same for the three observation periods; the maximum correction to the photographic magnitudes amounts to  $0^m 04$ — $0^m 05$ . For the 100-inch plates the corrections are the same as those derived for the 60-inch plates of the same period.

In a following section the magnitudes and color indices derived by the writer are compared with the photoelectric results (int. syst.) by Stebbins-Whitford. It is very gratifying to note that the comparison does not reveal any differential color equation, either in the magnitudes or the colors. Since the writer has not been able to investigate a possible variation in color equation with magnitude, it should be pointed out that no such effect is indicated.

Only those nights have been used for observations when the atmospheric conditions seemed to be favorable for photometric work. No special arrangements have been made to determine the extinction each night. Indirectly, it is however possible to check the extinction constants by a comparison between the magnitudes derived for nebulae observed on different nights, and by a comparison between the calibration curves derived from the polar stars. Most of the nebulae have been observed on two nights, and frequently at different zenith distances. Since the exposure times are the same, and a standard procedure has been used in developing the plates, the polar exposures are comparable; the difference found between the surface magnitudes corresponding to a given plate density is for the most part caused by a difference in extinction.

For the 1947—48 and 1951 observation periods the standard extinction constants,  $0^m 295$  (photogr. reg.) and  $0^m 128$  (photov. reg.) at zenith, have been adopted. Comparisons between nebular magnitudes, and between calibration curves, have not revealed any noticeable deviations from these values.

For the 1954—55 period a general increase by 25 % has been found in the photographic extinction, whereas the photovisual extinction appeared to be unchanged; on a few nights both extinction constants deviated by the same amounts from these "normal" values. The change in extinction is undoubtedly due to the slight deterioration in the observing conditions at Mount Wilson caused by the gradual increase in the altitude of the smog level. For the 1954—55 observations the writer has adopted the extinction constants as derived from the photometric material.

#### 6. Discussion of possible systematic errors.

Among the sources of error that could possibly influence the photometric results systematically, the following ones may be mentioned: (a) a difference in sky fog

between nebular region and calibration field, (b) a change in sensitivity of the photographic emulsion from first to second exposure, (c) the smoothing effect caused by the use of a too large slit for the photometer registrations, and (d) an incorrect extrapolation over the nebular region of the background curves representing the sky fog. The four effects, which refer to the observations (*a*, *b*), to the measuring work (*c*), and to the reductions (*d*), will be briefly discussed below.

Although the nebulae have, as a rule, been observed in the northeastern quadrant of the sky, a comparison between nebular exposure and corresponding polar exposure (60-inch tel.) in some cases reveals a slight difference in sky fog (darkest sky usually at the pole). The resulting effect in the integrated magnitude derived for the nebula depends on the shape of the calibration curve. Since all the curves obtained from the writer's polar plates have such a shape that the surface brightness (amount of light per unit area) is more or less proportional to  $-\log(1-d)$ , where  $d$  represents the relative plate density, the effect should in the present case be very small, or negligible (comp. Holmberg 1950 a).

An examination of the final magnitudes confirms the assumption that no appreciable errors are caused by a sky fog difference. The majority of the nebulae have been observed on two different nights, and in some cases a difference in sky fog between nebula and pole may be found on one of the nights, but not on the other. A comparison between the corresponding nebular magnitudes does not, within the limits of the accidental errors, reveal any systematic difference.

At the 100-inch telescope, the exposures of nebulae and SA 57 have always been made in roughly the same azimuth and altitude, and the plates do not show any noticeable differences in sky fog. It may in this connection be noted that 11 nebulae have been observed both at the 60-inch and the 100-inch telescope. A comparison between the resulting magnitudes gives a mean difference, 60-inch minus 100-inch, of  $-0^m01$  in both the photographic and photovisual regions.

Usually, one exposure (nebula or calibration stars) has been made on each half of a plate. Since no filter has been used in the photographic region, the emulsion of the second half of the plate (covered by slide) may be influenced by the humidity of the air during the first exposure, and a systematic effect of type (b) could possibly be expected. This source of error is easily investigated by a comparison between "first exposure magnitudes" and "second exposure magnitudes" derived for the same nebulae. No effect of this kind seems to be present in the material.

For the measuring of the plates, the most suitable size of photometer slit to be used in each case has to some degree been decided by compromise. A large slit will result in very smooth and well-defined background tracings. If the slit is made too large, however, the distributions of surface luminosity in the different cross-sections of the nebula, as derived from the density curves, may be systematically falsified, resulting in an integrated magnitude that is too faint. By comparing tracings obtained with slits of different size, the writer has tried to estimate the systematic smoothing effects and to determine, for nebulae of different types and of different size, the maximum slit permissible; the aim has been to keep the "smoothing error"

in the final magnitude below  $0^m02$ . As projected on the plate, the slits used in the present case range from  $0.2 \times 0.1 \text{ mm}^2$  to  $1.0 \times 0.1 \text{ mm}^2$ .

It has been mentioned previously that the background tracings representing the sky fog of the plate are in most cases not straight lines. Owing to secondary reflections inside the telescope tube, the density of the sky fog is a function of the distance from the center of the plate, the maximum fog usually being found at the center. The effect is naturally very small, but is easily noticeable as a slight curvature in the background tracings. If this curvature is not taken into account, we may get appreciable systematic errors in the final magnitudes, especially in the case of nebulae of faint surface brightness. In order to make possible a correct extrapolation of the background over the area covered by the nebula, it is necessary that each registration includes sufficiently long sections of the plate outside the nebula. The extrapolation is facilitated by the fact that the curvature of the tracings obtained for the different cross-sections is practically the same. For the drawing of the background curves the writer has used a set of slightly curved, transparent rulers, which have proved very practical. It is difficult to make a correct estimate of the errors that may possibly remain in the final magnitudes due to inaccuracies in the adopted backgrounds. Since the extrapolations of the background curves have been done with the greatest care, the errors, if any, are supposedly small.

In a subsequent comparison (sect. 8) of the writer's magnitudes with those measured photoelectrically by Stebbins-Whitford a very satisfactory agreement is found, both as regards zero point and scale. Indirectly, the agreement may be interpreted as a proof that the writer's results do not contain any serious systematic errors due to the effects discussed above.

#### 7. The final magnitudes and their mean errors.

In column 6 of the catalogue we find the integrated photographic and photovisual magnitudes (int. syst.), as derived by the procedure described above for the 300 nebulae included in the photometric program. The catalogue magnitudes are usually means of two independent measures; the number of measures, or plates, in each case is denoted by the figure in parentheses. As has been mentioned above, the total number of individual measures amounts to 1205. The photographic magnitudes range from  $4^m33$  to  $14^m59$ , and the color indices (column 7) from  $+0^m18$  to  $+1^m03$ . It may be added, that the apparent major and minor diameters, as derived from photometer tracings of  $103a-O$  plates (photogr. reg.), are listed in column 5 of the catalogue. Since the limiting magnitude of the plates is more or less constant, the diameters and the integrated magnitudes form a homogeneous material.

The mean errors of the catalogue magnitudes can be derived from the dispersion of the individual values. For each object with at least two independent measures (photogr. or photov.), a mean error,  $\varepsilon$ , may be computed in the usual way from the relation  $(n-1) \cdot \varepsilon^2 = \sum (m - \bar{m})^2$ , where  $n$  is the number of measures (plates). By taking the mean of all the quantities  $\varepsilon^2$ , we arrive at the following final mean error of one plate:

Table 2. Mean errors of integrated magnitudes and color indices.

Number of plates	$\varepsilon(m_{pg}), \varepsilon(m_{pv})$	Number of plates	$\varepsilon(C)$
1	0 <sup>m</sup> 060	1+1	0 <sup>m</sup> 074
2	0. 042	1+2	0. 066
3	0. 035	2+2	0. 052
4	0. 030	2+3	0. 049
5	0. 027	3+3	0. 043

$$\varepsilon(m) = 0^m 056 \text{ (1947-48)}, \varepsilon(m) = 0^m 055 \text{ (1951)}, \varepsilon(m) = 0^m 062 \text{ (1954-55)}.$$

The photographic and photovisual magnitude series give results that are practically identical. The mean error obtained for the third observation period is slightly larger than the errors of the two first periods.

Although the accuracy of a magnitude measure to some extent depends on the instrument used, and on the magnitude and size of the nebula, we will for the entire material accept the weighted mean of the above mean errors. For one plate, photographic or photovisual, the (internal) mean error may thus be assumed to be 0<sup>m</sup>060.

The mean errors of the color indices may be computed in a similar way. In this case we can include only those objects for which there are at least 2+2 plates, or two photographic and two photovisual measures. For the combination 1+1 plates we get a mean result that is more or less the same for the three observation periods,

$$\varepsilon(C) = 0^m 074.$$

We might have expected that the mean error of the color index would be equal to  $\sqrt{2} \cdot \varepsilon(m)$ , or 0<sup>m</sup>085. However, the photographic and photovisual exposures of a nebula have as a rule been made on the same night, and in immediate succession, and the resulting correlation between accidental and systematic errors due to similar observing conditions is demonstrated by a certain decrease in the mean error of the color index.

Table 2 gives the resulting mean errors of integrated magnitudes and color indices, corresponding to different numbers of plates. Since most of the nebulae have been measured on 2+2 plates, the standard mean errors of the catalogue data are 0<sup>m</sup>042 and 0<sup>m</sup>052, respectively.

The above mean errors may possibly represent minimum values, since they have been derived from internal agreement. A comparison with the results by Stebbins-Whitford (sect. 8), or an examination of the color dispersions within different type classes of nebulae (sect. 16), indicates however that the mean error derived for the color indices apparently is of the right order of size. As regards the integrated magnitudes, it seems likely that the real (external) mean error is somewhat larger than the error listed in Table 2.

**8. Comparison with Stebbins-Whitford.**

In their photoelectric photometry of extragalactic nebulae, Stebbins and Whitford (1952) have derived integrated photographic magnitudes, and in more than half the cases also color indices, for 176 external systems. The observations have been made with the same telescopes as those used in the present case; the diameters of the focal diaphragms range from 0'3 to 8'6 at the 60-inch, and from 0'2 to 5'1 at the 100-inch telescope. Since the diaphragm in most cases is large enough to include the main bulk of the nebula, the photoelectric magnitudes and colors furnish a suitable material for a comparison with the writer's results.

It may be noted that the earlier photometric list by Stebbins-Whitford (1937) will not be included. On account of the small diaphragms, and the use of an unsatisfactory zero point, the results of this list are not directly comparable with the writer's data.

In the comparison with the SW 1952 list five nebulae have been omitted — NGC 147, 185, 3726, 4244, and 5005. On account of the low surface brightness of the very extended outer regions, and the dense star field, the two first objects are rather difficult objects from a photometric point of view. The major diameters, as derived from the tracings, are 18' and 14', respectively. As regards integrated colors, the agreement between SW and the writer is reasonably good. If the photoelectric magnitudes, 11<sup>m</sup>2 (diaphr. 8'6) and 11<sup>m</sup>4 (diaphr. 4'1), respectively, are corrected for diaphragm effect in the manner described below, they will however still be about 0<sup>m</sup>3 fainter than the writer's measures (see notes at end of cat.). The photometric difficulties are illustrated by the fact that a decrease in diaphragm from 4'1 to 2'4 for NGC 185 gives a change in photoelectric magnitude by only 0<sup>m</sup>2, from 11<sup>m</sup>4 to 11<sup>m</sup>6. If we, for instance, apply the diaphragm correction to the latter magnitude, we obtain a result in close agreement with the total magnitude measured by the writer. As regards NGC 3726, the SW observations apparently do not refer to the same nebula as that measured by the writer; the object listed in the present catalogue has the position given in the NGC for 3726, and the descriptions by Reinmuth (1926) of nebula and surrounding star field do not seem to leave any doubt about a correct identification. The photoelectric magnitude given for NGC 4244 is based on a rectangular diaphragm; the object has no pronounced nuclear region, and it is not quite clear what part of the nebula has been measured. Finally, the quality of the sky has been denoted as doubtful in the SW list as regards NGC 5005.

If we also omit NGC 205, 224, 4501, and 4565, for which only the nuclear (central) regions have been measured by SW, there are 51 nebulae left for a comparison of magnitudes. The objects are listed in Table 3, where the second and third columns give the total photographic magnitudes according to the writer and SW, respectively. The fourth column gives the correction to be applied to the photoelectric measure on account of the omission of the outmost parts of the nebula, the diaphragm in practically all cases not being quite large enough. This quantity has been derived from the writer's photometer tracings, on the assumption that the diaphragm

Table 3. Comparison between Holmberg and Stebbins-Whitford.

NGC	Total magnitudes				Color indices				
	Ho	SW	corr.	Ho-SW <sub>c</sub>	Ho	SW	corr.	Ho-SW <sub>c</sub>	
221	9 <sup>m</sup> 06	9 <sup>m</sup> 4	-0 <sup>m</sup> 25	-0 <sup>m</sup> 09	+0 <sup>m</sup> 90	+0 <sup>m</sup> 90	0 <sup>m</sup> 00	0 <sup>m</sup> 00	
2146	11. 26	11. 6	-0. 11	-0. 23	0. 58	-	-	-	
2300	12. 25	12. 5	-0. 11	-0. 14	1. 03	0. 97	0. 00	+0. 06	
2655	10. 92	11. 1	-0. 13	-0. 05	0. 76	0. 79	-0. 02	-0. 01	
2681	11. 33	11. 4	-0. 23	+0. 16	0. 68	0. 66	-0. 01	+0. 03	
2685	12. 04	12. 1	-0. 09	+0. 03	0. 66	-	-	-	
2976	10. 73	10. 9	-0. 09	-0. 08	0. 64	0. 51	+0. 11	+0. 02	
3034	9. 20	9. 4	-0. 03	-0. 17	0. 81	0. 72	0. 00	+0. 09	
3166	11. 49	11. 6	-0. 08	-0. 03	0. 79	(0. 85)	-	-	
3184	10. 28	10. 4	-0. 03	-0. 09	0. 44	-	-	-	
	3556	10. 57	10. 7	-0. 08	-0. 05	0. 45	0. 50	0. 00	-0. 05
	3623	10. 18	10. 4	-0. 07	-0. 15	0. 81	(0. 98)	-	-
	3627	9. 65	9. 7	-0. 09	+0. 04	0. 63	(0. 87)	-	-
[1]	3642	11. 52	11. 8	-0. 18	-0. 10	0. 35	-	-	-
[2]	3953	10. 71	11. 1	-0. 16	-0. 23	0. 57	-	-	-
[3]	3992	10. 62	10. 6	-0. 05	+0. 07	0. 70	-	-	-
[4]	4036	11. 48	11. 7	-0. 01	-0. 21	0. 78	0. 82	-0. 01	-0. 03
[5]	4051	10. 81	11. 2	-0. 22	-0. 17	0. 61	-	-	-
[6]	4111	11. 63	11. 6	-0. 04	+0. 07	0. 72	-	-	-
[7]	4168	12. 32	12. 4	-0. 14	+0. 06	0. 93	0. 79	0. 00	+0. 14
[8]	4214	10. 12	10. 2	-0. 05	-0. 03	0. 27	0. 32	-0. 02	-0. 03
[9]	4216	10. 88	11. 2	-0. 03	-0. 29	0. 94	(1. 01)	-	-
[10]	4254	10. 37	10. 4	-0. 01	-0. 02	0. 47	0. 44	0. 00	+0. 03
[11]	4258	8. 90	9. 4	-0. 40	-0. 10	0. 52	-	-	-
[12]	4270	13. 13	13. 1	0. 00	+0. 03	0. 89	-	-	-
[13]	4278	11. 20	11. 4	-0. 32	+0. 12	0. 77	0. 87	0. 00	-0. 10
[14]	4283	13. 27	13. 2	-0. 10	+0. 17	0. 81	0. 82	0. 00	-0. 01
[15]	4321	10. 07	9. 9	0. 00	+0. 17	0. 62	0. 57	0. 00	+0. 05
[16]	4374	10. 21	10. 5	-0. 15	-0. 14	0. 85	0. 92	0. 00	-0. 07
[17]	4382	10. 05	10. 2	-0. 16	+0. 01	0. 78	0. 81	-0. 04	+0. 01
[18]	4406	10. 10	10. 5	-0. 21	-0. 19	0. 85	0. 93	0. 00	-0. 08
	4449	9. 90	9. 8	0. 00	+0. 10	0. 22	0. 23	0. 00	-0. 01
	4450	10. 81	11. 2	-0. 33	-0. 06	0. 70	0. 77	-0. 08	+0. 01
	4472	9. 33	9. 5	-0. 08	-0. 09	0. 84	0. 89	0. 00	-0. 05
	4485	12. 24	12. 4	-0. 15	-0. 01	0. 22	-	-	-
	4486	9. 56	9. 9	-0. 28	-0. 06	0. 82	0. 89	0. 00	-0. 07
	4490	10. 09	10. 1	-0. 01	0. 00	0. 28	0. 27	0. 00	+0. 01
	4579	10. 32	10. 6	-0. 10	-0. 18	0. 71	0. 79	-0. 03	-0. 05
	4594	9. 18	9. 2	-0. 07	+0. 05	0. 89	0. 92	-0. 07	+0. 04
	4649	9. 88	10. 2	-0. 42	+0. 10	0. 91	0. 91	0. 00	0. 00

Table 3 (cont.)

NGC	Total magnitudes				Color indices			
	Ho	SW	corr.	Ho-SW <sub>c</sub>	Ho	SW	corr.	Ho-SW <sub>c</sub>
4725	10 <sup>m</sup> 07	10 <sup>m</sup> 1	-0 <sup>m</sup> 15	+0 <sup>m</sup> 12	0 <sup>m</sup> 61	(0 <sup>m</sup> 93)	-	-
4736	8. 91	9. 0	-0. 20	+0. 11	0. 63	0. 66	-0. 01	-0. 02
4826	9. 27	9. 4	-0. 05	-0. 08	0. 76	0. 77	-0. 05	+0. 04
5055	9. 26	9. 3	-0. 08	+0. 04	0. 61	(0. 56)	-	-
5194	8. 88	9. 0	-0. 01	-0. 11	0. 53	0. 47	-0. 02	+0. 08
5195	10. 47	10. 6	-0. 13	0. 00	0. 98	(0. 77)	-	-
5363	11. 13	11. 4	-0. 35	+0. 08	0. 86	0. 95	-0. 06	-0. 03
5846	11. 16	11. 3	-0. 07	-0. 07	0. 86	-	-	-
6015	11. 69	11. 7	-0. 03	+0. 02	0. 45	0. 45	-0. 03	+0. 03
6503	10. 77	11. 0	-0. 20	-0. 03	0. 53	0. 57	-0. 04	0. 00
7217	11. 00	11. 0	-0. 15	+0. 15	0. 80	0. 86	-0. 01	-0. 05

has always been centered on the nucleus of the object. It may be noted that the correction sometimes includes a small color effect, also derived from the tracings; in reducing the observed magnitudes to the int. syst. (corr. = +0.29 C), SW have not always been able to ascertain the correct color corresponding to the part of the nebula covered by the diaphragm. The corrections range from 0<sup>m</sup>00 to -0<sup>m</sup>42, the mean being -0<sup>m</sup>13. For 43 of the nebulae SW have assumed that the diaphragm includes the entire object (*Pg*, not in parentheses); for this part of the material the mean correction amounts to -0<sup>m</sup>12.

In the fifth column of the table we find the differences between the Ho magnitudes and the corrected SW measures. The deviations range from -0<sup>m</sup>29 to +0<sup>m</sup>17; for the mean and the dispersion, we get the following results:

$$\overline{Ho-SW_c} = -0^m03 \pm 0^m016 \text{ (m.e.)}, \sigma(Ho-SW_c) = 0^m11.$$

We may conclude that the zero points of the two photometric systems are practically the same. Considering the possibility that in some cases the diaphragm has not been centered exactly in the way assumed above, we have in fact to expect a small, negative mean deviation.

Since a plot of the differences Ho-SW<sub>c</sub> against magnitude (Ho or SW<sub>c</sub>) does not indicate any systematic dependence, we may assume that the magnitude scales of the two systems are also in agreement; if the material is divided in two halves according to the Ho magnitudes (Ho < 10<sup>m</sup>50, Ho > 10<sup>m</sup>50), we get for both groups a mean deviation of -0<sup>m</sup>03. A similar result is obtained as regards differential color equation; an examination of the relation between magnitude difference and color index (Ho) does not reveal any systematic run.

The dispersion found in the magnitude differences represents the combined effect

of (a) accidental errors in the Ho magnitudes, (b) accidental errors in the photoelectric magnitudes (meas. errors and var. in star field), and (c) errors in the adopted diaphragm corrections. Of these effects, the photoelectric measuring errors can be neglected, whereas the errors due to fluctuations in the stellar foreground (from nebula to comp. field) are comparatively large. An examination of the accidental variations in the star numbers (in area of same size as aver. diaphr.) indicates, that even in high galactic latitudes these variations may give rise to a mean error larger than  $0^m05$ . Errors of type (c) are due to the uncertainty as regards the exact position of the diaphragm with respect to the center of the nebula, especially in the case of objects not having a pronounced central condensation; the size of these errors is not known. Although it is not possible to make a correct estimate of the mean error of the Ho magnitudes from the comparison material discussed here, it seems likely that the mean error is somewhat larger than that derived in the preceding section from internal agreement.

In the right half of Table 3 a comparison has been made between the color measures; columns 6 and 7 give the integrated color indices according to Ho and SW, respectively. We find that photoelectric measures are not available for all objects. Some of the color indices are in parentheses, the photoelectric measures referring only to the nuclear regions. In this group we have also included NGC 5195, for which the diaphragm used is large enough; however, the superposed, blue spiral arm extending from NGC 5194 makes the color measure very dependent on the position of the diaphragm. The comparison will be based on the remaining 32 nebulae. The diaphragm corrections, as derived from the photometer tracings, are listed in column 8. The corrections are zero for elliptical nebulae, and usually negative for spiral systems. The last column gives the difference between Ho and corrected SW.

For the mean and the dispersion of the color differences, we get the following results:

$$\overline{Ho-SW_c} = -0^m001 \pm 0^m009 \text{ (m.e.)}, \sigma(Ho-SW_c) = 0^m053.$$

The zero points of the two color systems are thus in good agreement. A plot of the individual differences against the Ho color does not reveal any systematic scale deviations; if the material is divided in four equally large groups according to Ho color, we get the following mean differences:  $+0^m007$  ( $\overline{Ho}=0^m40$ ),  $+0^m009$  ( $0^m69$ ),  $-0^m026$  ( $0^m80$ ), and  $+0^m007$  ( $0^m90$ ). A negative result is also obtained in an examination of the relation between color difference and photographic magnitude; if the material is divided in four groups according to Ho magnitude, we find mean differences of  $+0^m014$  ( $\overline{Ho}=9^m17$ ),  $-0^m015$  ( $10^m05$ ),  $-0^m012$  ( $10^m69$ ), and  $+0^m011$  ( $11^m83$ ).

As regards color, the photoelectric measures are certainly very accurate, the results being only to a very small degree dependent on the projected star field; the diaphragm corrections are also rather small. The dispersion found in the differences  $Ho-SW_c$  is practically the same as the mean error (2+2 pl.) in the Ho colors, as

derived in the preceding section from internal agreement. Accordingly, we may accept this mean error as a correct measure of the accuracy of the writer's color determinations.

The measures by Stebbins-Whitford are undoubtedly the most homogeneous and reliable results available so far in the field of photoelectric nebular photometry. The good agreement obtained in the above, rather detailed comparisons, both as regards magnitudes and colors, seems to confirm the accuracy of the writer's photometric system.

#### 9. Comparison with Pettit.

In the extensive list by Pettit (1954), photoelectric measures of magnitudes and colors are given for nebulae included in the redshift programs of the Mount Wilson-Palomar and Lick Observatories. The listed data are supposed to be on the int. scale. All the observations have been made at Mount Wilson, the focal diaphragms used ranging from 0'3 to 8'6 at the 60-inch, and from 0'2 to 5'1 at the 100-inch telescope.

Since the accidental errors of the Pettit magnitude measures are unexpectedly large, a fact that appears already in a comparison between the magnitudes of NPS stars as derived by Pettit and by other photoelectric observers, the writer has in this case refrained from the rather laborious determination of diaphragm corrections from the photometer tracings. Corrections of a similar kind have however been derived by Sandage (Humason-Mayall-Sandage 1956) in his very detailed discussion of the magnitudes of nebulae with known redshifts. The corrections have been determined by means of the Palomar 48-inch survey plates, the Pettit magnitude being reduced to a standard isophote corresponding to 2.5 times the maximum radius of the object found by visual inspection of the plates. The reduction depends on the distribution of surface luminosity in the outer parts of the nebula; since the distribution curve is not known in each individual case, the curve has for all types of nebulae been assumed to be similar to that derived for the elliptical object NGC 3379. Although the procedure is based on an assumption that is only approximately true, it will undoubtedly lead to final magnitudes that are more homogeneous than the original data, and which probably rather closely approach the total luminosities of the nebulae.

In a comparison between the corrected Pettit magnitudes and the Stebbins-Whitford magnitudes, corrected in a similar way, Sandage got the following results from 79 nebulae in common to both lists:

$$\overline{SW_c - P_c} = +0^m 026 \pm 0^m 021 \text{ (m.e.)}, \sigma(SW_c - P_c) = 0^m 191.$$

The mean deviation is thus close to zero; the dispersion in the individual differences is comparatively large.

In order to check the diaphragm corrections, as derived by Sandage, it would be of great interest to compare the  $P_c$  magnitudes with the writer's magnitude measures. A preliminary comparison has already been made by Sandage by means of the  $H_o$  magnitudes that were available in 1955; a mean difference  $H_o - P_c$  of  $-0^m 04 \pm 0^m 025$

was then found for 56 nebulae. Of the objects listed in the writer's final catalogue, 132 are also included in Sandage's list of  $P_c$  magnitudes. If four nebulae with exceptional differences ( $Ho - P_c < -0^m 6$ ) are omitted, a comparison leads to the following results:

$$\overline{Ho - P_c} = -0^m 011 \pm 0^m 017 \text{ (m.e.)}, \sigma(Ho - P_c) = 0^m 188.$$

The zero points of the two systems are thus in very good agreement. The dispersion is about the same as that found for  $\overline{SW_c - P_c}$ . It may be noted that if the above results as regards  $\overline{SW_c - P_c}$  and  $\overline{Ho - P_c}$  are combined, we get a mean difference between  $Ho$  and  $SW_c$  of the same size, and the same sign, as that derived in the preceding section.

A plot of  $Ho - P_c$  against  $Ho$  does not reveal any systematic deviations in the magnitude scales. We may conclude that the procedure used by Sandage leads to diaphragm corrections that are substantially correct, and that the *standard isophote adopted is close to that corresponding to the writer's magnitudes*.

An examination of the colors derived by Pettit for the NPS stars indicates the presence of a rather large color equation; besides, the examination reveals large accidental errors (or possibly systematic errors due to unfavorable observing conditions on certain nights). A study of the colors measured for different types of nebulae, for instance type *E* or type *Ir I*, leads to similar results.

#### 10. Comparison with Shapley-Ames.

Since it comprises the entire sky, the Shapley-Ames (1932) catalogue of nebulae supposedly brighter than the 13th magnitude still is of importance in many respects as a survey catalogue. For this reason, we shall briefly examine the estimated total magnitudes as regards accidental and systematic errors.

In the following analysis the estimated magnitude of a nebula will be denoted by  $ShA$ , and the apparent diameters (in min., as listed in the survey cat.) by  $a$  and  $b$ . It has been found previously by the writer that the systematic error in a  $ShA$  magnitude is mainly a function of surface magnitude. The dependence of the error on the latter quantity will be determined by means of the writer's magnitudes ( $Ho$ ) and the Stebbins-Whitford magnitudes ( $SW - 0^m 1$ ), the photoelectric measures being corrected for mean diaphragm effect as derived in sect. 8. Two least squares solutions, based on 194 and 106 nebulae, respectively, yield the preliminary relations,

$$\begin{aligned} Ho - ShA &= -0.23x - 0.28y - 0.29, \\ (SW - 0.1) - ShA &= -0.22x - 0.22y - 0.37, \end{aligned} \quad (1a)$$

where  $x$  stands for  $(ShA - 12.0)$ , and  $y$  for  $(2.5 \log ab - 1.0)$ . The two solutions give very similar results, the four coefficients of  $x$  and  $y$  being of the same order of size.

In the final solution we shall derive the systematic error as a function of only one variable — the quantity  $(x+y)$ . The solution will however include two constant terms

corresponding to galactic latitudes above and below  $50^\circ$ . On account of the heavy galactic "absorption" (about  $0^m 4$  in dir. of gal. pole, van de Kamp 1932) resulting from an analysis of the distribution of the Shapley-Ames objects over different latitude intervals, it has been known that the estimated magnitudes must contain a systematic error dependent on latitude. The solution, based on the entire material, gives as final result,

$$\frac{Ho}{(SW - 0.1)} - ShA = -0.25(x+y) - \begin{cases} 0.3 & (|B| > 50^\circ) \\ 0.5 & (|B| < 50^\circ) \end{cases} \quad (1b)$$

This relation leads to corrections to the estimated magnitudes that, with a few exceptions, range from  $+0^m 5$  to  $-1^m 5$ .

An examination of the residuals between photometric magnitudes and estimated magnitudes, corrected by the above formula, shows that the dispersion amounts to  $0^m 32$ . The mean error of a corrected ShA magnitude is thus comparatively large, about  $0^m 31$ .

If the statistical distribution of the corrected ShA magnitudes is examined (sect. 29), we find that the distribution curve has such a shape as may be expected on the assumption of a constant space density of nebulae; we also find that the survey catalogue seems to be complete down to, and including, a corrected magnitude of 11.9.

#### 11. Comparison with other magnitude lists.

Although it is not the intention of the writer to examine all results that have been derived previously in the field of nebular photometry, it may be of interest to extend the comparison to a few other magnitude lists.

In the pioneer work by Redman (1936), and by Redman-Shirley (1938), integrated photographic magnitudes were derived for 15 elliptical nebulae. The results were obtained by integrations based on the surface luminosity distributions along the major and minor axes of the objects, as measured on photographic plates. For the 4 nebulae also included in the writer's catalogue (NGC 205, 221, 4111, 4649) a comparison reveals a noticeable systematic magnitude difference. Since the magnitudes listed by the writer for these nebulae agree very well with the photoelectric measures by Stebbins-Whitford, the deviation apparently represents a zero point error in the Redman-Shirley magnitude scale.

By a special photographic procedure, the "Fabry method", Bigay (1951) has derived integrated photographic magnitudes (int. syst.) for a rather large number (175) of extragalactic nebulae. The method is based on surface photometry of the photographic image of the objective, illuminated by the nebula, and is thus not free from the disturbing effects of the projected star field. The present catalogue includes 98 of the objects measured by Bigay. If three objects with exceptional magnitude deviations are omitted, we find a mean difference,  $Ho$  minus Bigay, of  $+0^m 03 \pm 0^m 04$  (m.e.); the zero points of the two systems are thus in good agreement.

A more detailed comparison indicates that the agreement also extends to the scales. The dispersion in the individual magnitude differences,  $0^m36$ , is however rather large. It may be noted that a dispersion of the same order of size is obtained if the Bigay measures are compared with the results by Stebbins-Whitford.

In two subsequent lists, based on photoelectric observations, Bigay and collaborators (Bigay, Dumont, Lenouvel, and Lunel 1953; Bigay and Dumont 1954) have given photographic magnitudes and color indices (int. syst.) for 66 nebulae. From 24 objects in common with the writer's list we find a mean difference in photographic magnitude,  $H_o$  minus Bigay, of  $-0^m12$ , the dispersion in the individual differences being reasonably small. The deviation presumably represents the average diaphragm effect. In the color indices a corresponding mean difference of  $+0^m01$  is obtained.

Fi

- [1]
- [2]
- [3]
- [4]
- [5]
- [6]
- [7]
- [8]
- [9]
- [10]
- [11]
- [12]
- [13]
- [14]
- [15]
- [16]
- [17]
- [18]

## CHAPTER II

### Integrated Colors of Extragalactic Nebulae

#### 12. Classification system.

The integrated color indices, or the differences between integrated photographic and photovisual magnitudes (int. syst.), are listed in the catalogue for 289 nebulae. The mean errors of the colors have been examined in sect. 7 (comp. Table 2); in most cases ( $2+2$  plates) the mean error amounts to  $0^m05$ . In this chapter a detailed analysis will be made of the colors of nebulae of different types, especially with regard to the systematic effects produced by internal nebular absorption, by galactic absorption, and by redshift.

On account of the large variations in the intrinsic colors of extragalactic nebulae it is as a first step necessary to divide the material in a number of suitable type classes. As may be expected, a division according to type will lead to a considerable reduction in the color dispersion. The systematic color deviations to be investigated are of a limited size, and can be determined with any degree of accuracy only if the intrinsic dispersion, as well as the observational mean error, is sufficiently small. The classification system used in the present case is based on the traditional Mount Wilson system; with the addition of three more classes the latter system has proved very practical. Attention may here be called to the classification proposed by Morgan and Mayall (1957) based on nebular spectra, which eventually may prove helpful as a complementary system.

As appears from the catalogue, the following nine type classes have been used: *E*, *Ir II*, *SO*, *Sa*, *Sb-*, *Sb+*, *Sc-*, *Sc+*, and *Ir I*. All elliptical nebulae are, as usual, referred to class *E*. Since the apparent diameters of each object are listed in the catalogue, the writer has refrained from a subdivision based on elongation; it may be noted that the color of an elliptical nebula is apparently independent of the diameter ratio. The irregular nebulae have been divided into two separate groups according to their stellar content: *Ir I* (type I population) and *Ir II* (presumably type II population). The need of this distinction has been pointed out previously by the writer (1950a), and is confirmed by a study of the present material. On the 60-inch or 100-inch plates there is usually no difficulty in separating the two types, the *Ir I* systems being characterized by a pronounced resolution (supergiant stars, emission objects).

As regards the spiral nebulae, it has seemed desirable (and feasible) to make a further division of types *Sb* and *Sc* into "early" and "late" subtypes, denoted by

— and +, respectively. The following short description gives the general characteristics of each subtype, together with some typical specimens.

Type *Sb*—. Extended nuclear region, representing a considerable fraction of the total luminosity; mean surface brightness comparatively high; symmetrical and rather closed system of spiral arms (many revolutions) with no pronounced contrast between arms and main body; in most cases no appreciable resolution. NGC 224, 3031.

Type *Sb*+. Comparatively small nuclear region; mean surface brightness lower than in previous case; symmetrical and more open system of arms with good contrast against main body; noticeable resolution in structural details. NGC 3953, 3992.

Type *Sc*—. Small, sometimes semistellar nucleus; mean surface brightness about the same as for *Sb*+; more or less symmetrical, open, and rather pronounced spiral arms; resolution well advanced. NGC 5194, 5457.

Type *Sc*+. No prominent nuclear region; mean surface brightness lower than for *Sc*—; confused, and loosely defined spiral arm system (short arms); high resolution, comparable to that of *Ir I* nebulae. NGC 598, 2403.

In most cases, the practical application of the classification scheme does not present any difficulties, at least as regards nebulae having moderately large distance moduli. Some experience may be needed in the case of spirals with an edgewise orientation; for these objects the degree of resolution, as observed on the 60-inch or 100-inch plates, is an important classification parameter. Naturally there are some nebulae which do not fit into any of the above subgroups; they may represent transitions between two types, or they may be abnormal objects. In the catalogue a number of spirals (usually faint nebulae) have been classified simply as *S*, or *Sp*.

It may be noted that the main types, as estimated by the writer, in most cases are in agreement with the types listed in the recent redshift catalogue by Humason, Mayall, and Sandage (1956).

The classification system does not include any special type classes referring to *barred* spirals. A detailed study of the writer's plate material reveals that the majority of spiral nebulae exhibit a more or less pronounced bar; the bar may not always be recognizable on the blue plate, but is usually visible on the photovisual exposure. It seems quite possible that a bar is a structural detail common to all, or most, spiral nebulae, and that the observed differences are of a quantitative rather than a qualitative nature. In the subsequent analysis a further subdivision of the spiral systems with respect to the conspicuousness of the bar has not been deemed necessary.

### 13. Inclination effect in color index.

The observed color index of an extragalactic nebula includes two absorption effects, one produced by galactic obscuration, and the other by absorbing material in the nebula. In addition, a color excess effect is caused by the redshift. As will be

shown below, it is possible to determine all three effects by an analysis of the present material.

In this section we shall examine the variation in color index with apparent diameter ratio,  $b/a$ ; the latter quantity may, at least in the case of spiral nebulae, be assumed to be a rather good measure of the inclination of the object to the line of sight (comp. sect. 18). The results will give us some information about the *differential* selective absorption in the external systems and enable us to reduce the observed colors to an inclination of  $90^\circ$  ( $b/a=1$ ). A more complete investigation of the total and selective absorption produced by obscuring matter in spiral nebulae will be made in Chap. III.

The diameter ratio effect in the observed color will be examined separately for each of the six types of spiral nebulae in the writer's classification scheme. For comparison, irregular nebulae of type *Ir I* will also be included (but not *E* nebulae, which are apparently free from int. abs.). The investigation will, with some exceptions, be based on all the nebulae of the types mentioned that are listed in the catalogue. The exceptions are NGC 157 (*Sc-*, abnormally high color index), NGC 4236, 4395 (abnormal *Sc+* nebulae of exceedingly low surface brightness), NGC 4594 (*Sa*, diameter ratio not representative of inclination due to enormous central bulge), and NGC 7640 (*Sc+*, abnormally low color index). Furthermore, members of the Virgo cluster (comp. Table 15) are omitted as regards types *Ir I*, *Sc+*, *Sc-*, and *Sb+*; according to the results obtained in sect. 26 a considerable number of the cluster objects have abnormal colors. In order to get a sufficiently large material, cluster members have not been omitted as regards types *Sb-* and *Sa*; the 12 cluster nebulae included in these groups seem to have more or less normal colors. As regards type *SO*, all but 5 of the nebulae in the writer's material are Virgo cluster members; owing to the limited number of objects, the results to be derived for this group are in any case uncertain. As appears from the second column of Table 4, the final number of nebulae in each type group ranges from 18 to 55.

The color indices of the selected nebulae have been reduced to gal. lat.  $90^\circ$  by the provisional correction  $-0^m063$  ( $\text{cosec } B - 1$ ), as derived by the writer in a previous investigation (unpublished) based on a smaller material. The absorption parameter happens to be practically the same as the definitive parameter derived in the next section from the colors (freed from incl. effects) of the present material. It may be noted that for about 75 % of the nebulae the correction is numerically smaller than  $0^m05$ , and that a minor change in the adopted absorption parameter would have no noticeable effect on the results to be derived below. As regards the redshift effect, the color indices of the Virgo cluster members included have been given a differential correction of  $-0^m01$ , the redshift of the cluster objects being on an average somewhat larger than that of the "field" nebulae (comp. sect. 15).

In Fig. 2, the corrected color indices have, for each type class, been plotted against the apparent diameter ratio  $b/a$ . Types *Sb-* and *Sa*, for which the inclination effect seems to be about the same, have been taken together in one group in order to

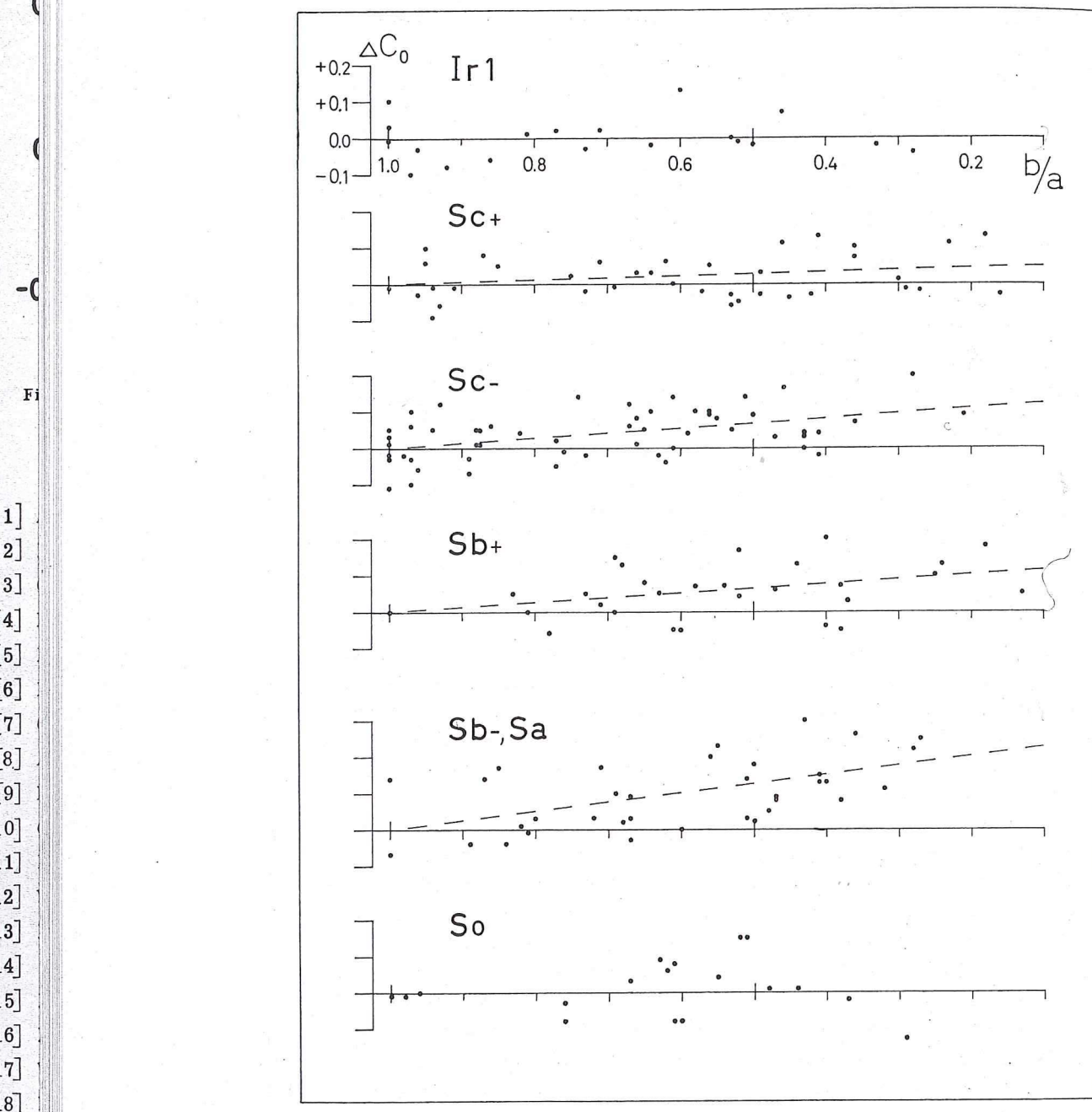


Fig. 2. Inclination effects in the integrated color index, as derived for nebulae of types *Ir I* to *SO*. Relation between color index residual (obs. color minus mean color, both red. to gal. lat.  $90^\circ$ ) and apparent diameter ratio ( $b/a$ ); mean relation indicated by broken line.

Table 4. Color excess parameter  $\beta$  as derived for nebulae of different types.

Type	N	$\beta$
Ir I	19	—
Sc+	37	+0 <sup>m</sup> 049
Sc-	55	+0.136
Sb+	28	+0.123
Sb-	16	+0.251
Sa	19	
SO	18	(+0.015)

secure a more reliable result. For each group a least squares solution has been made, based on the linear relation,

$$C_0 - \bar{C}'_0 = \Delta C_0 = \beta(1 - b/a), \quad (2)$$

where  $C_0$  denotes the observed color index reduced to  $B=90^\circ$ , and  $\bar{C}'_0$  is the color index reduced to  $B=90^\circ$  and  $b/a=1.0$ . For the moment we are interested only in the coefficient  $\beta$ , representing the inclination effect in the color. According to the results listed in the last column of Table 4, the coefficient is always positive, and reaches a maximum of about 0<sup>m</sup>25 ( $Sb-$ ,  $Sa$ ).

A study of the figure shows that for nebulae of type *Ir I* the inclination effect is probably small; owing to the limited number of objects, no numerical solution has been made in this case. It seems possible that some of the irregular objects do not possess the same rotational symmetry as is found in spiral nebulae, and that, accordingly, the observed diameter ratio is not a measure of the inclination. For the  $Sc+$  spirals an inclination effect, although small, is clearly indicated. The increase in the coefficient  $\beta$ , as we proceed from type  $Sc+$  to types  $Sb-$ ,  $Sa$ , presumably reflects a corresponding increase in internal absorption. For type *SO* the inclination effect, although uncertain, seems to be small; there are other indications that *SO* nebulae contain a very limited amount of obscuring matter (comp. Baade 1951).

#### 14. Selective galactic absorption.

For an investigation of the color excess produced by galactic obscuration the same material will be used as in the preceding section, with the exception of type *SO*; it has been noted above that the latter group mainly comprises Virgo cluster members. The number of nebulae thus amounts to 174.

The analysis is based on the quantity  $C'$ , or the observed color index corrected for inclination effect (no corr. for type *Ir I*); the correction is  $-\beta(1 - b/a)$ . As a first approximation, the selective absorption (supposedly the same for both gal. hemispheres) may be assumed to be a linear function of  $\text{cosec } B$ ,

$$C' = \bar{C}'_0 + E(\text{cosec } B - 1), \quad (3)$$

where  $E$  denotes the color excess in the directions of the galactic poles. The quantity  $E$ , as well as the mean colors  $\bar{C}'_0$  of the six groups of nebulae, have been determined by a least squares solution. As regards the absorption parameter, the solution yields

$$E = 0^m 062 \pm 0^m 007 \text{ (m.e.)}.$$

The resulting mean colors will be discussed below (sect. 16).

The relation between color residual and cosec  $B$  is shown by the plot reproduced in Fig. 3. As far as can be judged from the present material, the assumption of a linear relation seems to be justified. As appears from the figure, the great majority of the nebulae are located in high galactic latitudes. The lowest latitudes are found for NGC 6946 ( $Sc-$ ,  $11^{\circ}3$ ), NGC 2525 ( $Sc-$ ,  $12^{\circ}0$ ), and NGC 1569 ( $Ir\ I$ ,  $12^{\circ}1$ ); in spite of their positions close to the milky way region, these objects are still outside Hubble's zone of avoidance.

The selective absorption constant derived above amounts to 25 % of the total photographic absorption,  $0^m 25$ , as found by Hubble (1934) from his nebular counts. On account of the importance of the absorption ratio, it may be noted that the two absorption constants are comparable quantities. They are both *mean* results, derived indirectly by the cosecant relation from a study of nebulae with a wide range in galactic latitude; besides, the distribution of the objects in galactic longitude, and over the two hemispheres, is more or less the same. For a comparison, we refer to sect. 20, where the absorption ratios derived for external nebulae are discussed.

It would from several points of view be of interest to examine the deviations of the colors of individual nebulae, or groups of nebulae, from the mean relation of Fig. 3. Since  $C'_0$  represents the observed color index corrected for inclination effect and differential galactic absorption, the residual ( $= C'_0 - \bar{C}'_0$ ) may be denoted by  $\Delta C'_0$ .

Of the 174 nebulae investigated above, 132 are located in northern galactic latitudes and 42 in southern latitudes. In the third and fourth columns of Table 5 we find the corresponding means of cosec  $B$ , and of  $\Delta C'_0$ . A systematic difference is indicated, the colors of southern nebulae being on an average  $0^m 02$  redder than the colors of northern objects. It should be noted that the color difference does not include any differential redshift effect (comp. next sect.), the mean redshifts of the two groups being of the same order of size. If the means of  $\Delta C'_0$  are divided by the respective means of cosec  $B$  — that is, reduced to the galactic poles — the difference will amount to  $0^m 012$ . It may be assumed that the sun's position north of the galactic plane is the principal cause of this effect. If the asymmetric location is responsible for the entire amount, the color difference would represent the selective absorption corresponding to twice the distance of the sun from the galactic plane. If the absorption ratio is assumed to be equal to 4, and if the sun's distance from the plane is 20 ps (10 ps), the photographic absorption in our immediate neighborhood would amount to  $0^m 001$  per ps ( $0^m 002$  per ps). On account of the comparatively large mean error, the latter result should, of course, be accepted with some caution. In

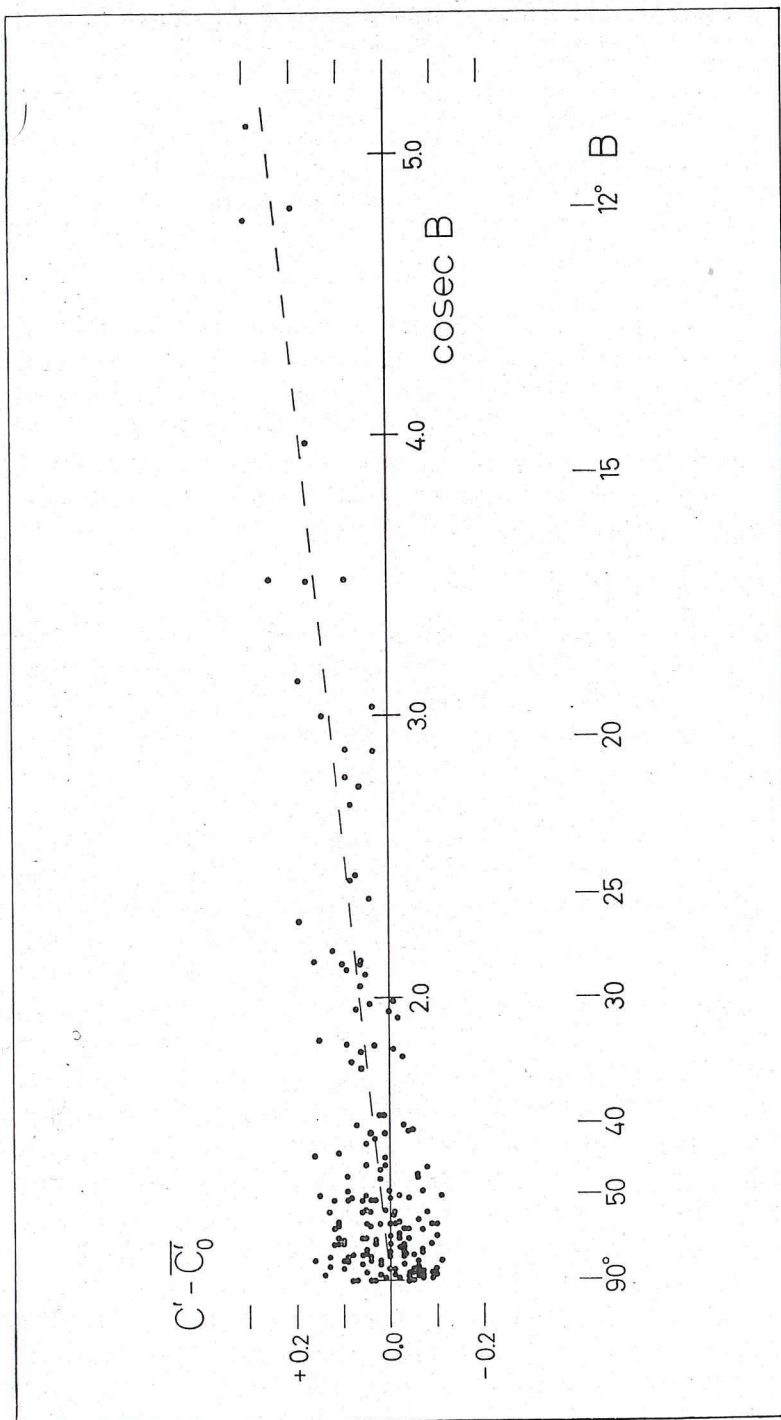


Fig. 3. Selective galactic absorption, as derived from nebulae of types  $Ir\ I$  to  $Sa$ . Relation between color index residual, obs. color (red. to incl.  $90^\circ$ ) *minus* mean color (red. to incl.  $90^\circ$  and to lat.  $90^\circ$ ), and cosecant of galactic latitude; the mean relation corresponds to a selective absorption at the gal. pole of  $0^{\circ}062$ .

Table 5. Mean color residuals, with mean errors, as found for the northern and southern galactic hemispheres.

B	N	cosec B	$\Delta C'_0$	$\Delta C'_0 / \text{cosec } B$
$0^\circ - +90^\circ$	132	1.41	$-0^m 005 \pm 0^m 006$	$-0^m 004 \pm 0^m 004$
$0^\circ - -90^\circ$	42	1.80	$+0.015 \pm 0.009$	$+0.008 \pm 0.005$
diff.: $0^m 012 \pm 0^m 006$				

order not to introduce any unnecessary complications, the slight difference in selective absorption between northern and southern hemispheres will not be taken into account in the color investigations of the following chapters.

A plot of the color residuals against galactic longitude shows that the writer's material has an unfavorable distribution for an examination of longitude variations in galactic absorption. In the most important area, the low-latitude region, the number of objects is also too small.

### [1] 15. Redshift effect in color index.

The systematic changes in the photographic and photovisual magnitudes of an external nebula that are caused by a displacement of the energy distribution due to redshift, will give rise to a systematic effect also in the observed color. The size of the color deviation is not the same for nebulae of different types, the shape of the energy curve presumably varying from one type to another. The only results available so far are those derived by Stebbins-Whitford (1948; comp. also Whitford 1954) in their well-known photoelectric photometry of elliptical nebulae, indicating a color excess that amounts to  $0^m 0133$  per  $10^3$  km/sec. With the exception of a few observations by Whitford (1953), we have in the case of spiral nebulae as yet had no observational data of sufficient accuracy suitable for a study of the redshift effect in color.

Since the redshift effect to be expected is comparatively small, and may easily be obscured by slight color variations due to other causes, it is important that the analysis be based on a material as homogeneous as possible. In order to reduce the selection effects, the following objects will be omitted from the material discussed in sect. 14: (a) nebulae of type *Ir I*, (b) members of the Virgo cluster (only *Sa* and *Sb*— previously incl.), (c) nebulae with apparent major diameters smaller than  $5'0$ , and (d) nebulae with galactic latitudes below  $15^\circ$ . The material ( $N=113$ ) will thus comprise only spiral systems of types *Sa* to *Sc+*. With the exception of NGC 4490 (*Sc+*,  $C'_0=0^m 26$ ) and NGC 5194 (*Sc-*,  $C'_0=0^m 49$ ), the selected objects are found in Tables 14a and 14b; these tables also list the color indices  $C'_0$ , corrected for inclination effect and differential galactic absorption.

Redshifts, as observed at Mount Wilson-Palomar and at Lick, are listed for 97 of the above spiral nebulae in the catalogue by Humason, Mayall, and Sandage (1956); if two independent measures are available, the arithmetical mean has been

Table 6. Mean color deviations derived for different intervals of redshift.

V (km/sec)	N	$\overline{\Delta C'_0}$
0—500	19	-0 <sup>m</sup> 002
500—1000	34	+0.015
1000—1500	25	+0.028
1500—2000	11	+0.026
2000—2500	6	+0.036
All ( $\bar{V} = 977$ )	95	+0.018

accepted. With the exclusion of two objects (NGC 1961, 3646), which would carry unduly large weights on account of exceptionally high redshifts, we find that the redshifts range from about zero to about +2500 km/sec.

The analysis is thus based on a final material of 95 spiral nebulae. On account of the limited range in redshift a linear relation has been assumed. Thus

$$C'_0 = p + q V, \quad (4)$$

where the parameter  $q$  represents the sought color excess effect. Two separate least squares solutions have been made, one for the group  $Sc-$ ,  $Sc+$  and one for  $Sa$ ,  $Sb-$ ,  $Sb+$ . The results, with mean errors, are as follows:

$$Sc-, Sc+ : q = +0^m016 \text{ per } 10^3 \text{ km/sec } (N=55) \\ \pm .015$$

$$Sa, Sb-, Sb+ : q = +0^m021 \text{ per } 10^3 \text{ km/sec } (N=40). \\ \pm .017$$

The solutions also yield five values of the parameter  $p$ , one for each type.

The results of the two independent solutions are more or less the same. If the results are combined, we find that the integrated color indices of spiral nebulae, as measured by the writer, include a *color excess proportional to redshift of*  $+0^m018 \pm 0^m011$  per  $10^3$  km/sec.

In the third column of Table 6 we have, taking the two groups together, computed the means of the color residuals  $\Delta C'_0 = C'_0 - p$ , as corresponding to different intervals of the redshift. A more or less linear increase of color index with redshift seems to be indicated. For the entire material, the mean color excess amounts to  $+0^m018$ . It may be noted that the material includes 25 nebulae of the southern galactic hemisphere, and that these objects are rather evenly distributed over the different redshift classes.

An investigation of the relation between color and redshift may easily be influenced by systematic effects of various kinds. Attention will be called to two possible sources of error, which may give rise to color deviations that are, indirectly, a function of the distance (or the redshift).

In the first place, the colors would be systematically affected in the way mentioned

if the photographic and (or) photovisual magnitudes contained a residual color equation depending on the apparent magnitude. However, there does not seem to be any reason to assume, in the present case, that a color equation of this kind is hidden in the photometric data. It may be recollect that a comparison (sect. 8) of the writer's color indices with the photoelectric colors by Stebbins-Whitford, corrected for diaphragm effect, does not indicate any systematic differences. Since the color of a spiral nebula changes from nuclear region to outer parts, it will be emphasized that the color index, as measured by the writer, refers to the light contained within a certain isophote (comp. sect. 2); the definition is thus independent of the apparent magnitude, or the apparent size, of the object.

The second effect to be considered is the observational selection, which may lead to a correlation between absolute magnitude and distance. In the next section, where the mean colors of nebulae of different types are derived, we shall find that the color index increases by  $0^m 41$  along the type sequence from *Sc+* to *Sa*. Along the same sequence there is also an increase in the mean absolute luminosity of the nebulae (comp. Table 17). A similar relation between color and absolute magnitude, although on a much smaller scale, may possibly exist within each type class. If the observational selection favors high-luminosity objects as the distance grows larger, we may, accordingly, get a false positive correlation between color and redshift. It is naturally rather difficult to estimate the size of this effect. The situation is complicated by the possible presence of another selection effect that works in the opposite direction. It has been mentioned previously that the photometric program to a large extent has been based on the plate collection of the Mount Wilson and Palomar Observatories. Since these plates refer to the photographic region, it seems possible that the selection may have favored exceptionally blue nebulae as the apparent magnitude decreases.

According to the previous determination by Stebbins-Whitford of the energy distribution in elliptical nebulae, the observed redshift effect in color is more than twice as large as the effect computed from the distribution curve. It is interesting to note that the redshift effect found above for spiral nebulae is also about two times the "theoretical" effect, as derived by Merle Walker (comp. Humason, Mayall, and Sandage 1956, p. 159) for *Sb* and *Sc* nebulae. According to Walker, the color deviation to be expected would amount to  $0^m 010$  (type *Sb*), and  $0^m 008$  (type *Sc*), per  $10^3$  km/sec.

From certain investigations in progress (comp. report by Whitford 1956), both Whitford and Arthur Code have succeeded in proving that there really are no differences between observed and "theoretical" redshift effects in color as regards elliptical nebulae. The previous discrepancies may be traced to two causes: (a) systematic deviations in Pettit's solar energy curve, which was used to transform the relative six-color measures to absolute values, and (b) the fact that the six-color curve, as derived by Stebbins-Whitford for the comparison nebula NGC 221 (M 32), is not detailed enough for a determination of the true energy distribution. If the observed redshift effect is satisfactorily explained for elliptical nebulae, it

seems quite likely that a renewed analysis of the energy distribution in spiral nebulae, based on revised data, will lead to a color deviation of the same order as that derived from the present material.

#### 16. Mean colors of different types of nebulae.

According to the results obtained in the preceding sections, the observed color index of a nebula is reduced to gal. lat.  $90^\circ$  by the correction  $-0^m062$  ( $\text{cosec } B - 1$ ), and to incl.  $90^\circ$  to line of sight (only spirals) by the correction  $-\beta (1 - b/a)$ ; the latitude,  $B$ , and the apparent diameters,  $a$  and  $b$ , are listed in the catalogue. The color index thus corrected has been denoted by  $C'_0$ .

The observed color index is given in the catalogue for each object. The individual values of  $C'_0$  have not been listed, except for the objects contained in Tables 14a and 14b; the latter tables, which include the nebulae selected for the absorption investigation of Chap. III, give the indices  $C'_0$  for the majority of the spiral systems.

In the second column of Table 7 we find, for each of the nine type classes, the number of nebulae as listed in the catalogue; members of the Virgo cluster have however not been included as regards types *Ir I* to *Sb+* (5 other objects also omitted; comp. sect. 13). The third column gives the mean color,  $\bar{C}'_0$ , with mean error. The means for the first six groups, *Ir I* to *Sa*, are the results of the least squares solution of sect. 14, whereas the remaining means have been computed directly from the observed colors. The color dispersion within each group is found in the fourth column of the table.

The mean colors  $\bar{C}'_0$  include the selective absorption in the direction of the galactic pole. They also include a color deviation due to redshift. It may be assumed that the redshift effect for type *Ir I* is comparable to that found for the spiral nebulae, and that the effect for types *SO*, *E*, and *Ir II* is equal to that derived by Stebbins-Whitford; since the average redshift does not vary too much from one group to another, the mean deviation in color will be about the same for all the types. *If the listed mean colors are corrected by  $-0^m08$ , they are reduced to outside the Galaxy and to zero redshift.*

In order to get the intrinsic color of the stellar content of a nebula, the color index has to be corrected for the effect of internal nebular absorption (comp. Table 13). The internal absorption in spiral nebulae will be investigated in Chap. III.

According to Table 7, the mean color index ranges from  $0^m28$  for *Ir I* nebulae to  $0^m85$  for elliptical objects. The color found for *Sc+* spirals is very nearly the same as that for *Ir I*, indicating a similarity between the two types as regards stellar content. A similar color agreement exists between types *SO*, *E*, and *Ir II*. The large difference in color between *Ir I* and *Ir II* confirms the need of a separation of irregular nebulae into two groups.

In their photoelectric work Stebbins and Whitford (1948) have derived a mean color (int. syst.; zero redshift) for elliptical nebulae of  $0^m84$ ; the result does not include any diaphragm effect, the color of an elliptical object apparently being the same in the central and outer parts. The mean color, reduced to zero redshift,

Table 7. Means and dispersions of integrated color indices, as derived for nebulae of different types.  
(red. to gal. lat.  $90^\circ$  and to incl.  $90^\circ$ )

Type	N	$\bar{C}_o'$	Disp.
Ir I	19	$+0^m28 \pm 0^m013$	$0^m057$
Sc+	37	0.31 0.009	0.056
Sc-	55	0.40 0.008	0.059
Sb+	28	0.56 0.013	0.069
Sb-	16	0.67 0.018	0.071
Sa	19	0.72 0.021	0.090
SO	18	0.85 0.018	0.076
E	14	0.85 0.015	0.057
Ir II	6	0.84 —	—

found by the writer for type *E* is also  $0^m84$ . For three nebulae of type *Ir I*, included in the photoelectric program (Stebbins-Whitford 1952), the mean color ( $0^m27$ ) is practically the same as that derived in Table 7. The photoelectric mean colors determined for different types of spiral nebulae are however not comparable to the writer's results, the photoelectric measures including diaphragm effect, inclination effect, and differential galactic absorption.

As appears from the last column of Table 7, there is in most of the type classes a comparatively small color dispersion. As regards types *Ir I*, *Sc+*, *Sc-*, and *E*, the dispersions are only slightly larger than the mean error, about  $0^m05$ , of the color indices. We may conclude that these groups are very homogeneous, and that the mean error, as derived from internal agreement, is of the right order of size. The largest color dispersions are found for nebulae of the earlier spiral types; on account of the heavy internal absorption this result is not unexpected.

## CHAPTER III

## Internal Absorption in Spiral Nebulae

## 17. Previous results.

On account of the comparatively few observational data available, our knowledge of the total amount of internal absorption in extragalactic nebulae is still very incomplete. It is quite clear that the spiral nebulae, like the galactic system, contain appreciable amounts of absorbing matter; photographs of spirals, especially of those seen edgewise, give strong indications of heavy obscuration. A more detailed inspection reveals that the absorption effects apparently are not quite the same for spiral nebulae of different types; the internal absorption seems to increase gradually along the sequence from *Sc+* to *Sb*— and *Sa* spirals. For a numerical determination of the mean absorption parameters referring to different type classes, a comprehensive photometric material is needed. Since the differential absorption effects that are available for observation are usually quite small, the photometric data must fulfill rather high requirements as to accuracy and homogeneity.

In a number of previous investigations the amount of absorption has been determined for certain parts of individual nebulae. By means of plates taken with the Mount Wilson 60-inch telescope the writer (1950b) has studied the absorption produced by obscuring matter in the spiral arm which, extending from NGC 5194, partly covers the irregular nebula NGC 5195; it was found that the photographic absorption and the color excess reach maximum values of about 0.8 and 0.2 magnitudes, resp. By using photoelectric observations with the same telescope, Stebbins (1950) has investigated the asymmetrical distributions of luminosity and color along the minor axis of NGC 224; from a comparison between the two halves of the nebula it was possible to derive the ratio of differential total and selective absorption. A similar investigation of NGC 3031 has been made later on by the writer by means of Mount Wilson plates (unpublished paper). Including the results obtained for the galactic system (comp. sect. 14), the data available for spiral nebulae as regards the ratio of photographic absorption and color excess may be summarized as follows:

$$\begin{aligned}
 A/E &= 4.3 && (\text{NGC } 5194; \text{ spiral arm}) \\
 A/E &= 4.0 && (\text{NGC } 224; \text{ central region}) \\
 A/E &= 3.8 && (\text{NGC } 3031; \text{ central region}) \\
 A/E &= 4.0 && (\text{Gal. system; latitude var.})
 \end{aligned}$$

The mean of the four results, which all refer to the int. syst., is close to 4.0. It may be noted that the absorption ratio agrees with the ratios found for numerous dark clouds in our part of the galactic system from photometric studies of background stars.

Among other papers dealing with the absorption in external nebulae we wish to call attention to a number of investigations by Lindblad and collaborators (1941, 1942, 1949, 1952) concerning the distributions of luminosity and color in some spiral systems; detailed analyses of the observational data led to very interesting conclusions as regards the space distribution of absorbing matter. The obscuration in the Magellanic Clouds has been investigated by Shapley and Virginia Nail (1951, 1952) by means of counts of background nebulae (and studies of cepheid variables); the small cloud is apparently more or less transparent, whereas in the large cloud the absorption at some places may be as high as one magnitude. In a very extensive investigation of three fields in NGC 224 Baade and Henrietta Swope (1955) have derived photometric data for more than 700 variable stars, mainly cepheids. A considerable dispersion, apparently an effect of internal absorption, was found in the magnitudes of the cepheids of a given period; in a field 50' from the nucleus, or half way between the nucleus and the edge of the nebula as corresponding to the diameter measured by the writer, the variation in the median magnitudes indicated a total optical thickness of the absorption layer of about 2 magnitudes (comp. also Baade 1951; Baade and Mayall 1951). A similar result as regards the internal absorption has been found by Arp (1956) from his survey of novae in NGC 224. Finally, we wish to cite an interesting investigation by Aina Elvius (1956) concerning the asymmetrical distributions of luminosity and color in spiral systems having small inclinations to the line of sight; from a theoretical analysis, mainly based on NGC 4216, indications were found that the observed asymmetry is caused not only by real absorption effects but also by a dispersion of light due to diffraction.

### **18. Selective absorption in spiral nebulae.**

The photometric data assembled in the catalogue will now be used for a study of the internal absorption in spiral nebulae. It should be noted that the investigation refers to the extinction effects in the observed *integrated* magnitudes and colors, as caused by dust and gas in the nebular bodies. Evidently, the observed magnitude and color do not provide any information about the internal obscuration in an individual object. However, if all nebulae belonging to the same type class are assumed to form a more or less homogeneous group as regards internal absorption, an analysis referring to the entire group will yield definite results concerning the mean absorption parameters. The analysis may follow two different (and independent) lines. An investigation of the integrated colors, and their dependence on the apparent diameter ratio, reveals the differential selective absorption as a function of inclination. On the other hand, we may determine the inclination effect in total absorption by a similar investigation based on the integrated surface magnitudes.

The investigation will include only spiral nebulae. As a first step, it is necessary

to examine the relation between observed diameter ratio and inclination. If the disc of a spiral system is compared to an oblate spheroid, which represents the simplest model, the inclination,  $i$ , of the principal plane to the line of sight is obtained from the relation (comp. Hubble 1926)

$$\sin^2 i = \frac{(b/a)^2 - p^2}{1 - p^2}, \quad (5)$$

where  $b/a$  is the ratio of apparent minor and major diameters, and  $p$  the ratio of smallest to largest axis of the spheroid. In an investigation of the apparent diameters of spiral nebulae, the writer (1946) has previously shown that the mean of the parameter  $p$ , as corresponding to diameters derived from photometer tracings, is close to 0.20. An examination of the diameters listed in the present catalogue also indicates a mean parameter of this size; of the 119 spiral nebulae to be investigated below only 4 have diameter ratios smaller than 1/5. In the following sections, we shall accept the relation given in eq. (5), with a parameter  $p$  equal to 0.20. It may be noted that, for nebulae with inclinations larger than  $20^\circ$ — $25^\circ$ , the inclination derived from this relation is practically independent of a possible deviation in  $p$  from the mean value adopted.

It has been mentioned above (comp. sect. 2) that the diameters listed in the catalogue refer to an isophote which is more or less the same for the entire material. It may be noted that this isophote has an approximately elliptical shape for all the spiral nebulae, and that the shape is not appreciably disturbed by the central bulge; there are, however, a few exceptions (as NGC 4594, not included below; comp. sect. 13).

According to sect. 13, the integrated colors of spiral nebulae are displaced towards the red as the diameter ratio decreases. In fact, the following linear relation was obtained:

$$C_0 - \bar{C}'_0 = \Delta E = \beta(1 - b/a), \quad (6)$$

the coefficient  $\beta$  ranging from  $+0^m 05$  to  $+0^m 25$  (types  $Sc+$  to  $Sa$ ; comp. Table 4). It may be recollected that  $C_0$  denotes the observed color index reduced to gal. lat.  $90^\circ$ , whereas  $C'_0$  is also reduced to incl.  $90^\circ$  to line of sight ( $b/a=1.0$ ). Apart from observational errors and intrinsic color deviations, the difference  $C_0 - \bar{C}'_0$  apparently is an effect of differential selective absorption, and may be denoted by  $\Delta E$ .

It has, for all the types of spiral nebulae investigated, been assumed that the variation in selective absorption with inclination can be adequately described by  $\beta(1 - b/a)$ . In order to ascertain whether this simple expression is really the most suitable inclination function, we may combine all the types of spiral nebulae and examine, for different intervals of  $b/a$ , the mean color deviations from the adopted regression lines. According to Table 8, the mean deviations are small; they range

Table 8. Mean color deviations from adopted linear regression lines, as found for all spiral nebulae of types Sc+ to Sa.

Diam. ratio b/a	N	Mean deviation
$\leq 0.30$	14	+0 <sup>m</sup> 018
0.31–0.40	12	-0. 011
0.41–0.50	24	-0. 010
0.51–0.60	22	+0. 002
0.61–0.70	26	-0. 001
0.71–0.80	14	-0. 007
0.81–0.90	18	+0. 007
0.91–1.00	25	+0. 002
	155	

155

Fi

from  $-0^m011$  to  $+0^m018$  and are evidently of an accidental nature. Accordingly, the function  $\beta(1-b/a)$  may be accepted as the best possible approximation to the true inclination function that can be derived from the present material.

Whereas no difficulties are met in a determination of the inclination effect in the selective absorption, the available color measures do not yield any information as regards the size of this absorption when the nebulae have an inclination of  $90^\circ$  to the line of sight. However, the problem may be solved, indirectly, by a study of the total photographic absorption (comp. sect. 20).

#### 19. Total absorption in spiral nebulae.

In a way similar to the above, we shall investigate the relation between integrated photographic surface magnitude and diameter ratio, and thus get the inclination effect in total, photographic absorption. It may be noted, however, that in the different type classes of spirals the individual variations in surface magnitude are considerably larger than the variations in color. The color dispersion, as caused by deviations in intrinsic color and by observational errors, ranges from  $0^m06$  to  $0^m09$  (comp. Table 7). In the surface magnitudes, the dispersion amounts to about  $0^m3$ , as will be shown below. It should be emphasized, that an investigation of surface magnitudes, in order to yield reliable results, must be based on diameters that are referred to a homogeneous system, a condition supposedly fulfilled in the present case.

The investigation will be based on the quantity  $S_0 = m_0 + 5 \log a$ , where  $m_0$  is the integrated photographic magnitude reduced to gal. lat.  $90^\circ$  by the correction  $-0^m25$  ( $\text{cosec } B - 1$ ), and  $a$  is the apparent major diameter in minutes of arc. The magnitude  $S_0$  (=obs. surf. magn. for nebulae of incl.  $90^\circ$ ) would apparently be independent of inclination if the objects investigated contained no obscuring matter. If absorption is present, the variation in  $S_0$  with inclination will be a reflection of the corresponding variation in total photographic absorption.

On account of the large dispersion in the surface magnitudes, special care has to be taken to avoid systematic effects due to observational selection. In order to get a material that approaches a random sample as closely as possible, it has seemed advisable to omit the following two groups,

- (a) nebulae with major diameters smaller than 5'0,
- (b) nebulae in low galactic latitudes ( $|B| < 15^\circ$ ).

The excluded objects may be expected to have surface magnitudes systematically brighter than the average. In addition, there are two nebulae, NGC 4490 and NGC 5194, which are members of double systems where gravitational disturbances make an accurate definition of the major diameters difficult. Except for these omissions the material will comprise the same spiral nebulae of types  $Sc+$  to  $Sa$  as those included in the investigation of the inclination effect in color index (comp. sect. 13).

In order to get more accurate mean results, the selected nebulae will be taken together in two groups, one comprising  $Sc+$  and  $Sc-$  spirals, and the other spirals of types  $Sb+$ ,  $Sb-$ , and  $Sa$ . The observational data for the two groups, which number 66 and 53 objects, respectively, are summarized in Tables 14a and 14b at the end of this chapter. The second and third columns give the color indices  $C_0$  (red. to gal. lat.  $90^\circ$ ) and  $C'_0$  (red. to gal. lat.  $90^\circ$  and incl.  $90^\circ$ ), whereas the fourth column contains the surface magnitude  $S_0$ , as defined above; in the fifth column we find a quantity  $S'_0$  ( $= S_0$  red. to incl.  $90^\circ$ ), that is derived by the procedure described below.

In Fig. 4 the magnitude  $S_0$  has, for each of the two groups, been plotted against the apparent diameter ratio,  $b/a$ . It is quite evident that the magnitude  $S_0$  increases numerically as the diameter ratio decreases. In spite of the large dispersion in the individual values, the means of  $S_0$  computed for the successive intervals of  $b/a$  permit us to trace mean curves that are rather accurate. For diameter ratios larger than about 0.35 the ordinates of the curves reproduced in the figure are (apart from a constant) proportional to  $\text{cosec } i$ , or to the cosecant of inclination to line of sight as obtained from eq. (5). The curves have, in fact, been derived by least squares solutions based on the relation

$$S_0 - \bar{S}'_0 = \Delta A = \alpha(\text{cosec } i - 1), \quad (7)$$

where  $\bar{S}'_0$  is the mean of  $S_0$  corresponding to inclination  $90^\circ$ . The equation is analogous to eq. (6); the left member may be assumed to represent the inclination effect in photographic absorption,  $\Delta A$ .

The two least squares solutions, which are based on the individual values of  $S_0$  corresponding to diameter ratios larger than 0.30, lead to the numerical results listed in Table 9. The mean surface magnitude  $\bar{S}'_0$  ranges from  $15^m 56$  to  $14^m 87$ , and, as might be expected in advance, the lowest surface luminosity is obtained for  $Sc+$  spirals. It may be mentioned that if the listed quantities are corrected by  $-0^m 26$ , they will be expressed in magnitudes per square minute. The dispersion in  $S'_0$  amounts to about  $0^m 3$ , and is more or less the same for the different types.

Table 9. Mean photographic surface magnitudes and absorption parameters as derived by least squares solutions for spiral nebulae of different types.

Type	N	Surf. magn. S <sub>0</sub> mean	S <sub>0</sub> disp.	Abs. parameter $\alpha$
Sc+	30	+15 <sup>m</sup> 56	0 <sup>m</sup> 32	
Sc-	36	15. 29	0. 34	+0 <sup>m</sup> 28 ± 0 <sup>m</sup> 07 (m.e.)
Sb+	25	15. 25	0. 35	
Sb-	15	14. 87	0. 29	+0. 43 ± 0. 06
Sa	13	15. 10	0. 26	

The most important figures are found in the last column of the table, which gives the resulting values of the absorption parameter  $\alpha$ . It appears that the inclination effect in the photographic absorption is about 50 % larger in the second group than in the first group.

The mean absorption curves of Fig. 4, corresponding to eq. (7), seem to represent the observational data in a very satisfactory way. However, the cosecant law apparently can be applied only down to a diameter ratio of 0.30 to 0.35, or down to inclinations of 13° to 17°. For smaller values of  $b/a$  the curves approach definite maximum values, amounting to about 1<sup>m</sup>03 (Sc+, Sc-) and 1<sup>m</sup>33 (Sb+, Sb-, Sa).

It may be noted that the cosecant law found for the absorption is not unexpected. In fact, any reasonable assumption concerning the space distribution of dark and luminous matter in spiral nebulae seems to lead to this law, at least as a first approximation, as long as the internal absorption is not too pronounced (comp. sect. 22). It is quite evident that the acceptance of the cosecant relation makes possible the determination of one very important quantity, the *total* absorption affecting nebulae of incl. 90° to line of sight. The absorption will apparently be equal to the parameter  $\alpha$  derived above. Accordingly, the total photographic absorption will for the two groups of spiral nebulae range from 0<sup>m</sup>28 (incl. 90°) to 1<sup>m</sup>31 (incl. 0°), and from 0<sup>m</sup>43 (incl. 90°) to 1<sup>m</sup>76 (incl. 0°).

Unfortunately, it is only in a few special cases possible to get confirmatory evidence from other sources as to the amount of internal absorption in spiral nebulae. As regards the Galaxy, a number of facts seem to indicate that our system is a spiral of type *Sb* (comp. Baade 1951). On account of the heavy concentration of obscuring matter in the direction of the galactic center, the optical half-thickness of the absorbing layer is, on an average, probably larger than that found in the solar neighborhood, and may not be too different from the total absorption (incl. 90°) derived above for the same kind of system. It ought to be remarked that the half-thickness of the absorption layer should not be identified with the total absorption; however, if the absorption is moderately large, the two quantities will not differ by any large amount (comp. sect. 22). In the case of NGC 5194 the writer has, in one of the spiral arms, found an optical half-thickness of about 0<sup>m</sup>4 (comp. sect. 17); since the absorbing matter in a spiral system has a strong concentration in the arms,

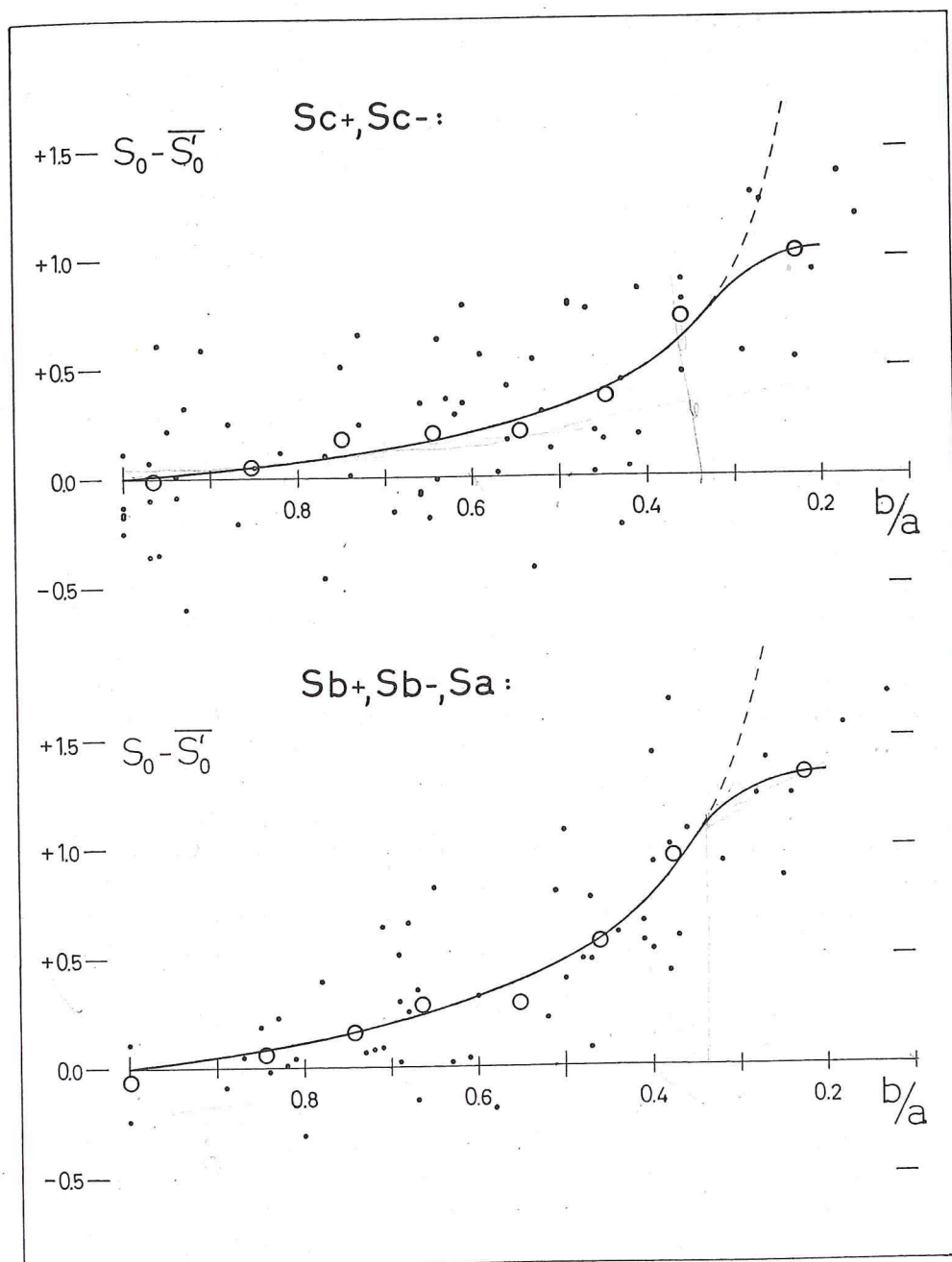


Fig. 4. Variation in total photographic absorption with inclination, as derived for two groups of spiral nebulae. The surface magnitude residuals (obs. magnitude minus mean magnitude, both red. to gal. lat.  $90^\circ$ ) are plotted against the apparent diameter ratios ( $b/a$ ); the open circles represent the mean residuals in different diameter ratio classes.

it seems possible that the absorption referring to the integrated magnitude of the entire nebula is of the same size as that derived for type *Sc* (incl.  $90^\circ$ ). A comparison may also be made with the results obtained by Baade and Swope, and by Arp, in their investigations of cepheids and novae in NGC 224 (comp. sect. 17); from the variation in the observed magnitudes it was found that the optical thickness of the absorption layer at some places probably exceeds 2 magnitudes. If we also in this case assume that the optical thickness is twice the total absorption (as derived above for type *Sb*), which is only approximately correct, we find for NGC 224 an average optical thickness of 2.3 times  $0^m 86$ , or  $2^m 0$ , a result of the same order of size as that derived from the stars investigated; the factor 2.3 (=cosec  $i$ ) represents the increase in total absorption from incl.  $90^\circ$  to incl.  $26^\circ$ , corresponding to the observed diameter ratio of NGC 224.

In conclusion, we shall examine two sources of error that may be of importance in an investigation of integrated surface magnitudes. We have to consider (a) a possible dependence of the observed major diameter on the diameter ratio, and (b) the possibility of residual selection effects in the material. The major diameter, as measured by the writer, refers to an isophote that is approximately the same for all objects. However, the observed surface magnitude of a spiral system depends on the inclination, and there is thus a possibility that the diameter of a nebula having an edgewise orientation is measured too large as compared to the diameter of a nebula oriented in the celestial plane. According to the writer's opinion, the systematic effect is probably small. Firstly, the difference in surface magnitude between nebulae of incl.  $0^\circ$  and  $90^\circ$  is of a moderate size on account of the internal absorption, and, secondly, the surface magnitude gradients are in the outmost parts of spiral nebulae rather steep. One of the most important parameters influencing the observational selection has, of course, been the apparent magnitude. Since spiral nebulae of incl.  $0^\circ$  have, on an average, fainter total magnitudes than nebulae of incl.  $90^\circ$ , it might be suspected that in the former case objects with exceptionally high surface luminosities have been favored. In our analysis of the surface magnitudes, this selection effect (if present in the material) would work in the opposite direction to diameter errors of the kind mentioned. Since objects of small diameters, as well as objects in low latitudes, have not been included in the analysis, it seems likely that the remaining selection effect is small. It may be noted that a comparison (next sect.) between the total and the selective absorption derived for spiral nebulae leads to absorption ratios of a reasonable size — a fact which indicates that the combined effect of the two sources of error discussed here must be inconsiderable. Another fact that permits the same conclusion is the good agreement obtained between Hubble's cosecant law for galactic absorption and the relation derived from the surface magnitudes of the spiral nebulae (sect. 24); down to a latitude of about  $20^\circ$ , corresponding to a differential galactic absorption of  $0^m 5$ , no systematic effect seems to be present in the surface magnitudes.

### 20. Ratio of total to selective absorption.

A comparison between the selective and total absorption derived in the two preceding sections will naturally be of great interest. An examination will first be made of the ratio of differential photographic and differential selective absorption — that is, of the ratio of the two inclination effects found above. The examination will not be based on the mean relations of eq. (6) and eq. (7) but on the individual values of  $\Delta A$  and  $\Delta E$ :

$$\Delta A = S_0 - \bar{S}'_0, \quad \Delta E = C_0 - \bar{C}'_0.$$

The quantities  $\Delta A$  and  $\Delta E$  are easily computed from the data listed in Tables 14a and 14b. As regards the mean colors  $\bar{C}'_0$ , we shall not use the results previously derived in Table 7 but the means computed in Tables 14a and 14b for the different types, the latter means referring to the same material as that used in the investigation of total absorption.

The results of the comparison are listed in Tables 10a and 10b. The means of  $\Delta A$  and  $\Delta E$ , and the corresponding ratios, have been computed for different intervals of the diameter ratio  $b/a$ , the number of objects in each interval being given in column 3. We find that for all of the 66 spirals in Table 10a the absorption ratio is equal to 8.7, whereas the 53 spirals in Table 10b give a ratio of 6.4.

Making allowance for the rather large accidental fluctuations that have to be expected, we find that the absorption ratios derived for the two groups of spirals are comparable; they are of the same order of size, and show a similar variation with  $b/a$ . In order to get more stable mean values it seems permissible to combine the results of the two tables. In Fig. 5 (upper part), the weighted mean ratios (weight prop. to number of obj.) have been plotted against the diameter ratio, and a smoothed relation curve has been drawn. For spirals with an edgewise orientation we now get an absorption ratio of about 11. As  $b/a$  gets larger the ratio becomes smaller, and it is quite evident that, with increasing values of  $b/a$ , the *ratio of the photographic to the selective differential absorption approaches a limiting value close to 4*.

The result obtained for large inclinations agrees nicely with previous determinations of the absorption ratio in spiral nebulae (comp. sect. 17). It should be noted that the earlier determinations refer to dark material supposedly situated in front of the luminous matter investigated. However, it can be shown theoretically (comp. sect. 22) that the ratio of total to selective absorption produced by obscuring material that is mixed in space with the luminous matter is comparable to the "screen ratio", provided that the absorption is of a moderate size; the latter condition is apparently fulfilled in spiral nebulae with large inclinations.

In the analysis of the preceding section we were able to derive the total photographic absorption affecting nebulae of incl.  $90^\circ$ . As regards the selective absorption, only the inclination effect could be determined. If the above absorption ratio is accepted, it is however possible to get the color excess corresponding to incl.  $90^\circ$ ; it will amount to  $0^m 28/4$  ( $Sc+$ ,  $Sc-$ ) and  $0^m 43/4$  ( $Sb+$ ,  $Sb-$ ,  $Sa$ ).

Table 10a. Differential and total values of photographic absorption and color excess as derived for spiral nebulae of types Sc+ and Sc-.

Interval of b/a	$\bar{b}/\bar{a}$	N	Differential absorption			Total absorption		
			$\bar{\Delta}A$	$\bar{\Delta}E$	$\bar{\Delta}A/\bar{\Delta}E$	$\bar{A}$	$\bar{E}$	$\bar{A}/\bar{E}$
$\leq 0.30$	0.23	7	+1 <sup>m</sup> 03	+0 <sup>m</sup> 071	14.5	+1 <sup>m</sup> 31	+0 <sup>m</sup> 141	9.3
0.31–0.40	0.36	3	+0.73	+0.083	8.8	+1.01	+0.153	6.6
0.41–0.50	0.45	11	+0.37	+0.039	9.5	+0.65	+0.109	6.0
0.51–0.60	0.55	8	+0.21	+0.035	6.0	+0.49	+0.105	4.7
0.61–1.00	0.82	37	+0.087	+0.018	4.8	+0.367	+0.088	4.2
All	0.64	66	+0.279	+0.032	8.7	+0.559	+0.102	5.5

Table 10b. Differential and total values of photographic absorption and color excess as derived for spiral nebulae of types Sb+, Sb-, and Sa.

Interval of b/a	$\bar{b}/\bar{a}$	N	Differential absorption			Total absorption		
			$\bar{\Delta}A$	$\bar{\Delta}E$	$\bar{\Delta}A/\bar{\Delta}E$	$\bar{A}$	$\bar{E}$	$\bar{A}/\bar{E}$
[1] $\leq 0.30$	0.22	6	+1 <sup>m</sup> 33	+0 <sup>m</sup> 162	8.2	+1 <sup>m</sup> 76	+0 <sup>m</sup> 269	6.5
[2] 0.31–0.40	0.38	9	+0.96	+0.095	10.1	+1.39	+0.202	6.9
[3] 0.41–0.50	0.46	9	+0.57	+0.108	5.3	+1.00	+0.215	4.7
[4] 0.51–0.60	0.55	4	+0.29	+0.060	4.8	+0.72	+0.167	4.3
[5] 0.61–1.00	0.76	25	+0.162	+0.049	3.3	+0.592	+0.156	3.8
[6] All	0.57	53	+0.509	+0.080	6.4	+0.939	+0.187	5.0

We are now able to determine the ratio of the total photographic absorption,  $A$ , to the total color excess,  $E$ ; the two quantities are evidently obtained from the relations,

$$\begin{aligned} A &= \Delta A + 0^m 28, & E &= \Delta E + 0^m 070 \quad (\text{Sc+}, \text{Sc-}); \\ A &= \Delta A + 0.43, & E &= \Delta E + 0.107 \quad (\text{Sb+}, \text{Sb-}, \text{Sa}). \end{aligned}$$

In the last columns of Tables 10a and 10b we find for the different intervals of  $b/a$  the mean values of  $A$  and  $E$ , and the resulting ratios. As might be expected, the final absorption ratios are usually smaller than those corresponding to the differential absorption. If the results of the two tables are combined, in the same way as above, we obtain the relation between absorption ratio and  $b/a$  that is reproduced in Fig. 5 (lower part). The maximum ratio, corresponding to nebulae of incl.  $0^\circ$ , has now been reduced to 8. As the inclination increases, the absorption ratio gradually approaches the limiting value 4.

## 21. Absorption in the main bodies of spiral nebulae.

The obscuring material in a spiral nebula apparently has a rather heterogeneous distribution. A proportionately large amount of the dark matter seems to be accu-

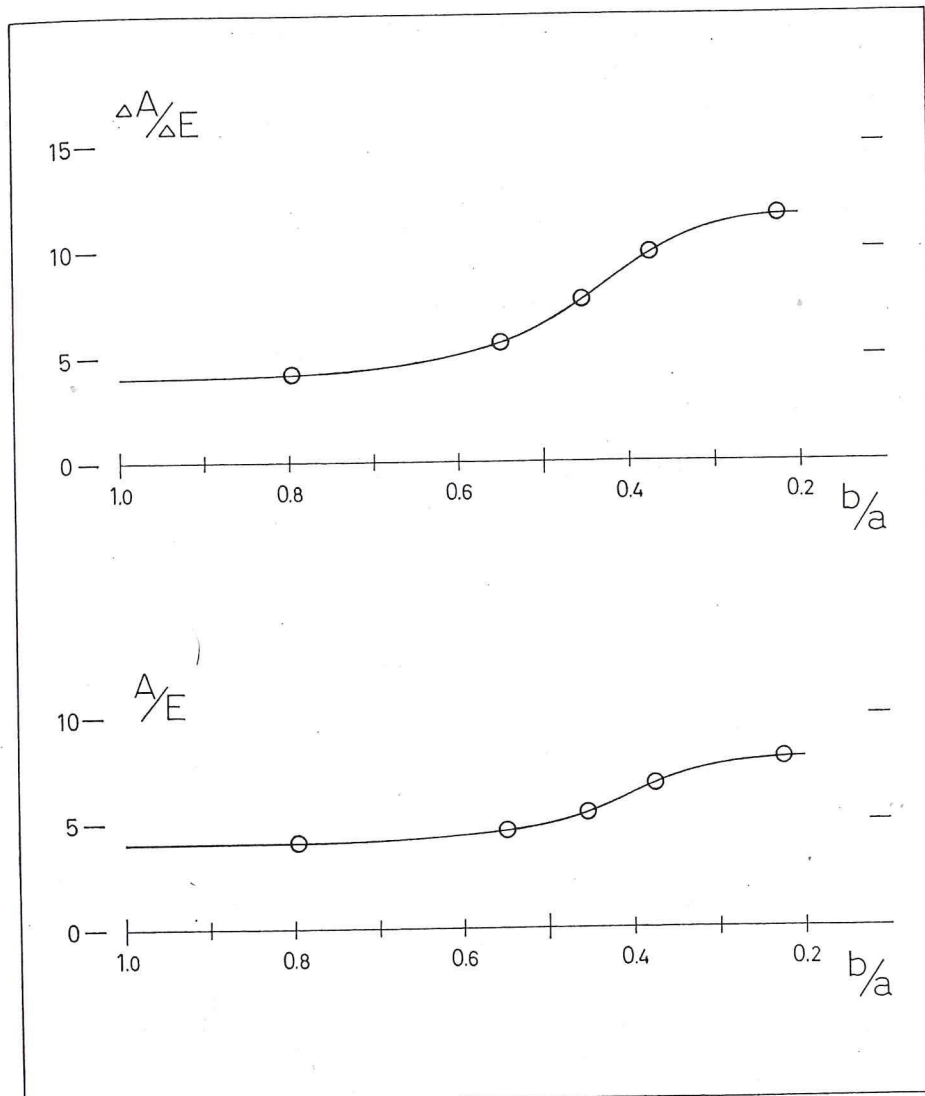


Fig. 5. Ratio of *differential* photographic to selective absorption (inclination effects), and its variation with apparent diameter ratio, as derived for spiral nebulae of types *Sc+* to *Sa* (upper part). Corresponding ratio of *total* photographic to selective absorption, and its variation with diameter ratio (lower part).

mulated in the spiral arms, or in their immediate vicinity; on the other hand, there are indications that the nuclear region is free from obscuration.\* Since the in-

\* An investigation of the internal distribution of luminosity and color in nebulae of different types will be published later by the writer; it will be based on the same observational material as that used in the present paper. Among the preliminary results already available, we may

trinsic color of this region is considerably redder than the mean color of the main body, the observed variation in integrated color with inclination is a rather complex effect. The peculiar distribution of absorbing matter will also influence the inclination variation in total absorption. For all inclinations of the nebula down to a certain minimum value the nucleus remains more or less unobscured — a fact that will tend to reduce the inclination effect in absorption, as derived above. As the inclination approaches  $0^\circ$ , the nuclear region will in many cases be completely hidden by obscuring material, and the result is a sudden increase in total absorption. In order to get a more complete picture of the absorption conditions in the spiral nebulae, it has seemed important to make an additional absorption investigation referring to the main bodies alone.

In order to get rid of the nuclear part we will in each spiral nebula cut off a central area; the region to be rejected is enclosed between two straight lines, parallel to the minor axis of the object, and situated at the same distance from the center of the nucleus. By making the distance between the two lines as large as 20 % of the major diameter, we may be sure that the main part of the nuclear region is cut off. The parts of the nebula that are situated outside the boundary lines will in the following analysis be referred to as the *main body*.

The color index and surface magnitude of the main body are quite easily derived from the photometer registrations of the plates; it has been mentioned previously that the plates have usually been measured in a direction parallel to the minor axis of the object. Both quantities are listed in the right halves of Tables 14a and 14b. As may be expected, the color index  $C_0$  (red. to gal. lat.  $90^\circ$ ) is in practically all cases smaller than the corresponding index referring to the entire nebula. The surface magnitude  $S_0$  is, as before, defined by  $m_0 + 5 \log a$ , where  $m_0$  is the integrated photographic magnitude (red. to gal. lat.  $90^\circ$ ) of the main body, and  $a$  is the major diameter of the nebula in minutes of arc. The magnitudes  $S_0$  are naturally fainter than those referring to the entire nebulae.

The analysis of the inclination effects in  $C_0$  and  $S_0$  will be based on the same relations that have been used previously (comp. eq. 6 and eq. 7). The results of the least squares solutions are listed in Table 11. The mean colors  $\bar{C}'_0$ , corresponding to incl.  $90^\circ$ , are for all the types bluer than the means obtained when nuclear region is included; the deviations amount to  $0^m 04$  ( $Sc+$ ),  $0^m 08$  ( $Sc-$ ),  $0^m 07$  ( $Sb+$ ),  $0^m 10$  ( $Sb-$ ), and  $0^m 06$  ( $Sa$ ). The individual values of  $C'_0$ , as derived from  $C_0$  by applying the correction  $-\beta(1-b/a)$ , are listed in Table 14. The parameter  $\beta$  is the same ( $Sc+$ ), smaller ( $Sc-$ ,  $Sb+$ ), or larger ( $Sb-$ ,  $Sa$ ) than that derived before (comp. Table 4). The mean magnitudes  $\bar{S}'_0$  are considerably fainter than those listed in Table 9, the difference amounting to  $0^m 75$  ( $Sc+$ ),  $0^m 86$  ( $Sc-$ ),  $0^m 94$  ( $Sb+$ ),  $1^m 14$  ( $Sb-$ ), and  $1^m 13$  ( $Sa$ ). The systematic run in these deviations reflects the large

---

mention that the mean color of the nuclear regions of spiral nebulae apparently is independent of inclination (except for incl. close to  $0^\circ$ ) — a fact which indicates that the central regions of the spirals are free from absorbing matter.

Table 11. Mean colors, mean photographic surface magnitudes, and absorption parameters as derived by least squares solutions for the main bodies of spiral nebulae of different types.

Type	N	Color index $C'_0$ mean disp.	Param. $\beta$	Surf. magn. $S'_0$ mean disp.	Param. $\alpha$
Sc+	30	+0 <sup>m</sup> 267 0.316	0 <sup>m</sup> 060 0.086	+16 <sup>m</sup> 31 16.15	0 <sup>m</sup> 31 0.37
Sc-	36	0.484	0.081	+0.062	16.19 0.37
Sb+	25	0.559	0.085	+0.279	16.01 0.26
Sb-	15	0.658	0.089		16.23 0.23
Sa	13				

relative increase in nuclear luminosity along the sequence from  $Sc+$  to  $Sb-$  and  $Sa$ . It may be added that if a correction of  $-0^m58$  is applied to the tabulated values of  $\bar{S}'_0$ , we obtain the surface magnitude of the main body referred to one square minute. The individual values of  $S'_0$ , or  $S'_0 - \alpha$  ( $\text{cosec } i - 1$ ), are listed in Table 14. The results obtained as regards the absorption parameter  $\alpha$  are found in the last column of Table 11.

A plot of the individual values of  $S'_0 - \bar{S}'_0$  against the apparent diameter ratio gives a result similar to that reproduced in Fig. 4. For values of  $b/a$  larger than about 0.35 we find, both for types  $Sc+$ ,  $Sc-$  and for types  $Sb+$ ,  $Sb-$ ,  $Sa$ , that the cosecant curve represents the different class means in a satisfactory way. The maximum absorption, corresponding to inclination  $0^\circ$ , amounts to  $0^m95$  in the group  $Sc+$ ,  $Sc-$  and to  $1^m17$  in the group  $Sb+$ ,  $Sb-$ ,  $Sa$ .

A comparison between the absorption curve derived for the main body and that obtained for the entire nebula shows that for the group  $Sc+$ ,  $Sc-$  the inclination effect is more pronounced when the nuclear region is omitted; the parameter  $\alpha$  has increased from  $0^m28$  to  $0^m32$ . On the other hand, we find that the maximum absorption (incl.  $0^\circ$ ) has been reduced from  $1^m03$  to  $0^m95$ . It has been suggested above that both these changes are a result of the peculiar distribution of absorbing matter in the nebulae. In the group  $Sb+$ ,  $Sb-$ ,  $Sa$  we find a change in the maximum absorption that is twice as large as in the first group; the absorption is reduced from  $1^m33$  to  $1^m17$ . As regards the parameter  $\alpha$ , however, we get an unexpected decrease from  $0^m43$  to  $0^m41$ .

In Tables 12a and 12b the means of the differential absorptions  $\Delta A$  ( $= S'_0 - \bar{S}'_0$ ) and  $\Delta E$  ( $= C'_0 - \bar{C}'_0$ ) have been computed for different intervals of the apparent diameter ratio. The ratios of these means may be compared with the results listed in Tables 10a and 10b (nuclear region included). If Tables 12a and 12b are combined, we arrive at the weighted means and the mean curve of Fig. 6 (upper part). The curve, which gives absorption ratios ranging from about 12 to about 4, is rather similar to the curve derived above (Fig. 5).

In the right halves of Tables 12a and 12b we find the means of the total absorptions  $A$  ( $= \Delta A + \alpha$ ) and  $E$  ( $= \Delta E + \alpha/4$ ), and the corresponding ratios. According

Table 12a. Differential and total values of photographic absorption and color excess as derived for the main bodies of spiral nebulae of types Sc+ and Sc-.

Interval of b/a	$\bar{b}/\bar{a}$	N	Differential absorption			Total absorption		
			$\bar{\Delta}A$	$\bar{\Delta}E$	$\bar{\Delta}A/\bar{\Delta}E$	$\bar{A}$	$\bar{E}$	$\bar{A}/\bar{E}$
$\leq 0.30$	0.23	7	+0 <sup>m</sup> 95	+0 <sup>m</sup> 060	15.8	+1 <sup>m</sup> 27	+0 <sup>m</sup> 140	9.1
0.31–0.40	0.36	3	+0. 98	+0. 080	12.2	+1. 30	+0. 160	8.1
0.41–0.50	0.45	11	+0. 36	+0. 026	13.8	+0. 68	+0. 106	6.4
0.51–0.60	0.55	8	+0. 29	+0. 060	4.8	+0. 61	+0. 140	4.4
0.61–1.00	0.82	37	+0. 104	+0. 013	8.0	+0. 424	+0. 093	4.6
All	0.64	66	+0. 299	+0. 029	10.3	+0. 619	+0. 109	5.7

Table 12b. Differential and total values of photographic absorption and color excess as derived for the main bodies of spiral nebulae of types Sb+, Sb-, and Sa.

Interval of b/a	$\bar{b}/\bar{a}$	N	Differential absorption			Total absorption		
			$\bar{\Delta}A$	$\bar{\Delta}E$	$\bar{\Delta}A/\bar{\Delta}E$	$\bar{A}$	$\bar{E}$	$\bar{A}/\bar{E}$
$\leq 0.30$	0.22	6	+1 <sup>m</sup> 17	+0 <sup>m</sup> 131	8.9	+1 <sup>m</sup> 58	+0 <sup>m</sup> 233	6.8
0.31–0.40	0.38	9	+0. 92	+0. 080	11.5	+1. 33	+0. 182	7.3
0.41–0.50	0.46	9	+0. 50	+0. 115	4.3	+0. 91	+0. 217	4.2
0.51–0.60	0.55	4	+0. 30	+0. 060	5.0	+0. 71	+0. 162	4.4
0.61–1.00	0.76	25	+0. 160	+0. 044	3.6	+0. 570	+0. 146	3.9
All	0.57	53	+0. 472	+0. 073	6.5	+0. 882	+0. 175	5.0

to the resulting mean curve, reproduced in Fig. 6 (lower part), the ratio of total photographic absorption to color excess of the main bodies of spiral nebulae ranges from 8 (incl. 0°) to 4 (incl. 90°). The limiting ratios happen to be the same as those obtained for the nebulae when the nuclear region was included.

## 22. Theoretical analysis of the absorption problem.

According to the observational results available before (comp. sect. 17), the ratio of photographic absorption to color excess produced by obscuring matter in spiral nebulae seems to be very close to 4.0 (int. syst.). A study of the observation procedures shows, that this mean ratio supposedly refers to the ideal case when the obscuring material is located as an absorbing screen entirely in front of the luminous matter. If the absorbing material is mixed in space with the luminous matter, the problem becomes more complicated, the observed absorption representing an integrated effect; the ratio of observed absorption and observed color excess may no longer agree with the normal ratio, or the "screen ratio". In the above investigation of spiral nebulae we have derived absorption ratios ranging from 4 to 8, and it seems important to try to ascertain, by a theoretical analysis of the absorption problem, whether these ratios are of such a size as may be reasonably expected.

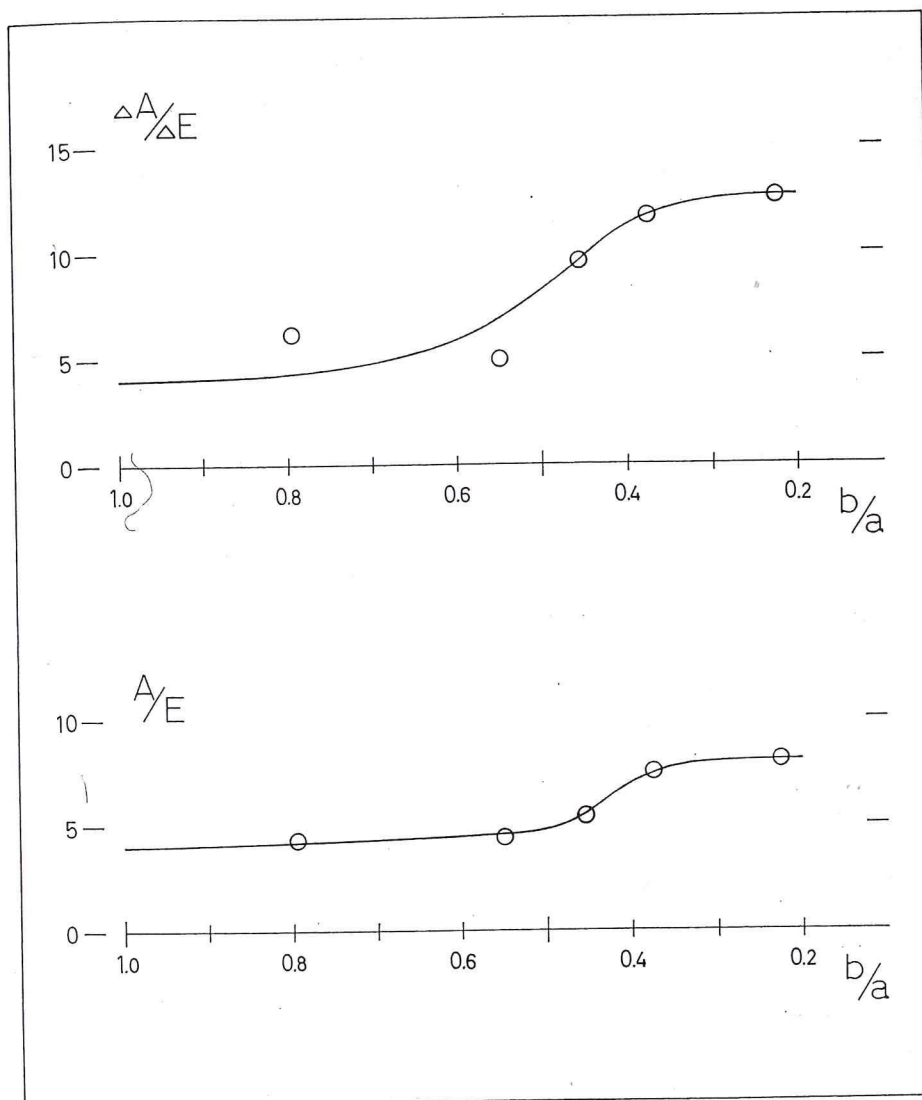


Fig. 6. Ratio of differential photographic to selective absorption, as derived for the main bodies of spiral nebulae of types Sc+ to Sa (upper part). Corresponding ratio of total photographic and selective absorption (lower part).

Since there may be large individual variations among the spiral nebulae as regards the internal distribution of dark and luminous matter, the following analysis will be based on as few assumptions as possible. Let us denote by  $I(x)$  the amount of photographic light in a spiral nebula that, due to internal absorption, suffers an absorption equal to  $x$  magnitudes on its way to the observer. The quantity  $I(x)$  evidently is the sum of a large number of "luminosity elements" emitted by

volume elements distributed over the different parts of the nebula. No assumption is made as regards the space distribution of these volume elements. The total photographic absorption affecting the entire nebula will apparently be equal to

$$A_{pg} = -2.5 \log \left[ \frac{\int_0^a 10^{-0.4x} \cdot I(x) dx}{\int_0^a I(x) dx} \right], \quad (8a)$$

where the integrations are performed over the whole range of the absorption  $x$  from zero to a certain maximum value  $a$ . By expansions in series, the relation may be transformed into the following one:

$$A_{pg} - 0.46 A_{pg}^2 + 0.14 A_{pg}^3 - \dots = \bar{x} - 0.46 \bar{x}^2 + 0.14 \bar{x}^3 - \dots,$$

where the means of  $x^n$  are weighted means, the weights being proportional to  $I(x)$ . If  $A_{pg}$  and  $a$  are moderately large, the two series are rapidly convergent. If terms of the second and higher orders are neglected, we obtain

$$A_{pg} = \frac{\int_0^a x \cdot I(x) dx}{\int_0^a I(x) dx} = \bar{x}. \quad (8b)$$

In the case of a moderately large absorption, we thus find that the total photographic absorption is equal to the weighted mean of the individual absorption quantities  $x$ .

If the second order terms are also included, and if  $A_{pg}^2$  is replaced by  $(\bar{x})^2$ , we obtain the result

$$A_{pg} = \bar{x} - 0.46(\bar{x}^2 - (\bar{x})^2) = \bar{x} - 0.46\sigma^2,$$

where the means of  $x^n$  are the same weighted means as above. The quantity  $\sigma$  represents the dispersion in the individual  $x$ -values. In the previous absorption investigation we have, for spiral nebulae of incl.  $90^\circ$ , found total photographic absorptions of 0.3 to 0.4 magnitudes, which seems to permit the conclusion that the maximum value of  $\sigma$  is about  $0^m 2$ . Accordingly, the last relation gives  $A_{pg} = \bar{x} - c$ , where the correction  $c$  amounts to  $0^m 01$  —  $0^m 02$ . We thus find, that for a total absorption not larger than that derived for incl.  $90^\circ$  relation (8b) represents a very good approximation.

The mean absorption  $\bar{x}$  apparently depends on the inclination of the nebula to the line of sight. With any reasonable assumption regarding the space distribution

of absorbing matter in a spiral nebula, it is quite evident that each individual value of  $x$  is, for inclinations that are not too small, approximately proportional to the cosecant of the inclination angle (comp. the galactic absorption). Accordingly, the total absorption  $A_{pg}$  also obeys a cosecant law.

In the same way as above, we may derive the total photovisual absorption. The function  $I(x)$  is replaced by a function  $p(x) \cdot I(x)$ . If the above result ( $= 4$ ) is accepted as regards the absorption ratio produced by an absorbing screen, a photographic absorption of  $x$  magnitudes apparently corresponds to a photovisual absorption of  $3/4 x$  magnitudes. Consequently,  $p(x) \cdot I(x)$  represents the amount of photovisual light in the object that on its way to the observer suffers an absorption of  $3/4 x$  magnitudes. The function  $p(x)$  depends on the distribution of intrinsic color in the nebula; if there is no variation in color,  $p(x)$  is reduced to a constant. The total photovisual absorption is given by the expression

$$A_{pv} = -2.5 \log \left[ \frac{\int_0^a 10^{-0.3x} p(x) \cdot I(x) dx}{\int_0^a p(x) \cdot I(x) dx} \right], \quad (9a)$$

where the integration limits are the same as before. If  $A_{pv}$  and  $a$  are moderately large, we obtain, as in the previous case, the simple solution

$$A_{pv} = \frac{\frac{3/4}{0} \int_0^a x \cdot p(x) \cdot I(x) dx}{\frac{3/4}{0} \int_0^a p(x) \cdot I(x) dx} \approx \frac{\frac{3/4}{0} \int_0^a x \cdot I(x) dx}{\frac{3/4}{0} \int_0^a I(x) dx} = 3/4 \bar{x}. \quad (9b)$$

The total photovisual absorption is equal to the weighted mean of the individual absorption quantities  $3/4 x$ . The correct weights are given by the function  $p(x) \cdot I(x)$ ; however, if the dispersion in intrinsic color is not too large, these weights may be replaced by weights proportional to  $I(x)$ .

From the total absorption quantities derived in equations (8b) and (9b) we arrive at the following ratio of photographic to selective absorption:

$$\frac{A_{pg}}{E} = \frac{A_{pg}}{A_{pg} - A_{pv}} = 4.$$

On the condition that the total absorption is moderately large, and the variation in intrinsic color not too pronounced, we thus get, for a *mixture* of luminous and absorbing material, an absorption ratio that is comparable to that corresponding to an absorbing screen.

In order to get some information about the order of size of the absorption ratio

corresponding to large values of  $A$  and  $a$ , we are forced to make two assumptions regarding the space distribution of luminous and absorbing material. We shall assume, (1) that the function  $I(x)$  has a constant value in the entire interval from  $x=0$  to  $x=a$ . The assumption implies, as is easily shown, that in each cross-section along the line of sight the space distributions of luminosity and absorption are the same (apart from a constant factor); it may be noted, however, that no assumption is necessary regarding the shape of the space distribution curves. We shall furthermore assume, (2) that the function  $p(x)$  can also be replaced by a constant term — that is, that the intrinsic color is the same for all parts of the nebula; this may be approximately true at least for the main body of a spiral system. Relation (8a) is now transformed into the following one:

$$A_{pg} = -0.089 + 2.5 \log a - 2.5 \log (1 - 10^{-0.4a}). \quad (10)$$

From eq. (9a) we get a similar relation, the only differences being that  $A_{pg}$  is replaced by  $A_{pv}$ , and  $a$  by  $3/4 a$ .

Since the absorbing matter in a spiral nebula apparently has a strong concentration towards the principal plane, it seems probable that, for all inclination angles, certain parts of the object are entirely unobscured. In order to get a better approximation, assumption (1) will be supplemented by the additional assumption that a part (relative size= $q$ ) of the nebular luminosity reaches the observer unabsorbed.

The numerical solutions corresponding to the above assumptions are reproduced in Fig. 7. For  $q=0$  (no part of the nebula unobscured) the absorption ratio increases from the "normal value" 4 to about 6 as the total photographic absorption changes from  $0^m 0$  to  $1^m 7$ . If  $q$  is equal to 0.1 (10 % unobscured), we get in the same absorption interval a change from 4 to about 10. As the parameter  $q$  becomes larger, the absorption ratio attains still higher values. To make possible a comparison, the figure also includes the numerical results obtained in the previous absorption investigations; the open circles represent the results derived in Table 10 (nuclear region included), and the full circles the results of Table 12 (nuclear region omitted). The observed values seem to agree rather well with the curve corresponding to  $q=0.1$ .

The principal aim of this theoretical analysis, which is based on as few and as simple assumptions as possible, has been to demonstrate that the comparatively large absorption ratios obtained in the preceding sections for nebulae with small inclinations to the line of sight need not be in discordance with the assumption that the "screen ratio" is equal to 4.

### 23. Intrinsic colors of stellar contents.

In the second column of Table 13 we have reproduced the mean colors  $\overline{C'_0}$ , as derived for the different types of nebulae in the writer's classification system; the color indices, which are the same as those previously listed in Table 7, are reduced to gal. lat.  $90^\circ$  and to incl.  $90^\circ$  (no incl. corr. for types *Ir I*, *E*, and *Ir II*).

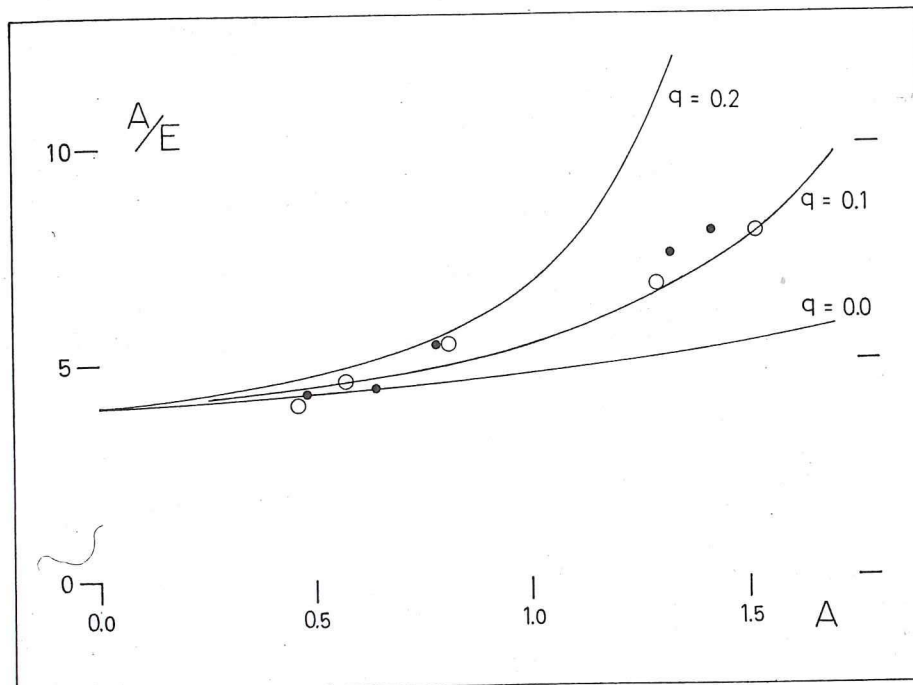


Fig. 7. Ratio of total photographic to selective absorption, and its variation with photographic absorption, as derived for a theoretical system. Observational results obtained for spiral nebulae of types  $Sc+$  to  $Sa$  represented by open circles (nuclear region incl.), and by full circles (nuclear region excl.).

The colors in parentheses refer to the main bodies of spiral nebulae; according to sect. 21, the mean color difference, entire nebula minus main body, amounts to  $+0^m04$  ( $Sc+$ ),  $+0^m08$  ( $Sc-$ ),  $+0^m07$  ( $Sb+$ ),  $+0^m10$  ( $Sb-$ ), and  $+0^m06$  ( $Sa$ ). In the third column of the table the colors have been reduced to outside the Galaxy and to zero redshift by the correction  $-0^m08$  (comp. sect. 16).

In order to get the intrinsic colors of the stellar contents of the nebulae there only remains to correct for the color excess caused by internal absorption. As regards the spiral nebulae, we shall use the results obtained in the previous absorption investigation. It was found in sect. 19 that the total photographic absorption (incl.  $90^\circ$ ) amounts to  $0^m28$  ( $Sc+$ ,  $Sc-$ ) and  $0^m43$  ( $Sb+$ ,  $Sb-$ ,  $Sa$ ); according to sect. 21, the corresponding results referring to the main bodies are  $0^m32$  and  $0^m41$ , respectively. If the ratio of total to selective absorption equals 4, the color excess would amount to 25 % of these values. A study of the inclination effect in color indicates, however, that the internal absorption increases more or less gradually along the type sequence from  $Sc+$  to  $Sa$ . For the entire nebular bodies we shall, accordingly, adopt the following slightly adjusted color excesses:  $0^m06$  ( $Sc+$ ),  $0^m08$  ( $Sc-$ ),  $0^m10$  ( $Sb+$ ), and  $0^m11$  ( $Sb-$ ,  $Sa$ ). As regards the main bodies, the

Table 13. *Intrinsic colors of the stellar contents of nebulae of different types (colors of main bodies in parentheses).*

Type	Mean color index		
	red. to gal. pole and to incl. 90° (C <sub>0</sub> ')	corr. for gal. abs. and for redshift	corr. for internal absorption
Ir I	+0 <sup>m</sup> .28	+0 <sup>m</sup> .20	+0 <sup>m</sup> .12
Sc+	0.31(0.27)	0.23(0.19)	0.17(0.12)
Sc-	0.40(0.32)	0.32(0.24)	0.24(0.15)
Sb+	0.56(0.49)	0.48(0.41)	0.38(0.31)
Sb-	0.67(0.57)	0.59(0.49)	0.48(0.39)
Sa	0.72(0.66)	0.64(0.58)	0.53(0.47)
SO	0.85	0.77	—
E	0.85	0.77	0.77
Ir II	0.84	0.76	—

[1] adjusted values are 0<sup>m</sup>.07 (*Sc+*), 0<sup>m</sup>.09 (*Sc-*), 0<sup>m</sup>.10 (*Sb+*, *Sb-*), and 0<sup>m</sup>.11 (*Sa*).  
[2] The corrected color indices, representing the integrated colors of the stellar con-  
[3] tents of the nebulae, are listed in the fourth column of Table 13.

[4] Four type classes (*Ir I*, *SO*, *E*, *Ir II*) have not been included in the absorption  
[5] investigation. As regards elliptical nebulae, it seems justified to assume that no  
[6] internal obscuration is present; the integrated color of the stellar content will  
[7] in that case amount to 0<sup>m</sup>.77. As regards types *SO* and *Ir II*, the material available  
[8] does not permit any definite conclusions as to the internal absorption. If the *SO*  
[9] spirals do not contain any obscuring matter, which seems likely (comp. Baade 1951),  
[10] the absorption-free color will be the same as that of elliptical nebulae, or 0<sup>m</sup>.77.  
[11] In order to get the color excess for type *Ir I* it may be permissible to assume that  
[12] the internal absorption is comparable to that found in the main bodies of *Sc* spirals,  
[13] the stellar contents being more or less the same in both cases. If a color excess  
[14] of 0<sup>m</sup>.08 is adopted, the integrated color of the stellar content of *Ir I* nebulae (0<sup>m</sup>.12)  
[15] will be the same as the color of the stellar content of the main bodies of *Sc+* spirals,  
[16] a result that seems very reasonable.

[17] The absorption-free color indices range from 0<sup>m</sup>.12 (type *Ir I*) to 0<sup>m</sup>.77 (type *E*).  
[18] These two limiting values supposedly represent the intrinsic colors of stellar popu-  
lations of type I and type II, respectively. Assuming that the stellar contents of  
nebulae of intermediate types are simply mixtures of the two kinds of populations  
(comp. Baade 1951), we are able to derive, from the intrinsic color indices, the  
ratio of type I to type II stars in the different cases. We thus find that stars of  
population I are responsible for the following relative parts of integrated photo-  
graphic luminosity: 1.00 (*Ir I*), 0.94 (*Sc+*), 0.86 (*Sc-*), 0.67 (*Sb+*), 0.52 (*Sb-*),  
and 0.44 (*Sa*). For the main bodies alone, the corresponding figures are: 1.00 (*Sc+*),  
0.97 (*Sc-*), 0.77 (*Sb+*), 0.66 (*Sb-*), and 0.54 (*Sa*). Accordingly, the greater part

of the photographic light emitted from the main bodies comes from type I stars, even in the case of *Sb-* and *Sa* spirals. It may be mentioned that this conclusion is in agreement with the results obtained by Baum and Schwarzschild (1955) in a photometric study of some outlying regions in NGC 224.

According to a previous investigation by the writer (1950a), the integrated color index (int. syst.) of the stellar content in a sphere around the sun with a radius of about 30 pc amounts to  $+0^m28$ . It is interesting to note that this color index agrees rather closely with the mean color obtained for the main bodies of *Sb+* spirals.

If the photographic luminosities are replaced by the masses, the contribution of type II stars to the stellar contents of nebulae of different types will naturally be considerably increased. The only reliable mass determinations available so far are those referring to NGC 224 and NGC 598 (Wyse and Mayall 1942); with apparent distance moduli of 24.25 and 24.15 (comp. sect. 28), the revised masses are  $2.3 \cdot 10^{11}$  and  $4.2 \cdot 10^9$  solar units, respectively. The corresponding absolute photographic magnitudes, corrected for the entire amount of internal absorption as determined in sect. 19, are  $-20.9$  and  $-18.4$ . The ratios of total mass to total unabsorbed luminosity, in solar units (abs. magn. of sun =  $+5.37$ ; comp. Stebbins and Kron 1957), will thus be 7.1 (224) and 1.3 (598). On the assumption that the increase in the mass/lum. ratio from NGC 598 to NGC 224 can be ascribed entirely to the relative increase in the type II population from *Sc+* to *Sb-*, as derived above, we find for type I and type II stars mass/lum. ratios of approximately 0.5 and 14, respectively, the quotient being 30. If the latter quotient is accepted, we arrive at the conclusion that stars of population I are responsible for the following relative parts of total nebular mass: 1.00 (*Ir I*), 0.34 (*Sc+*), 0.17 (*Sc-*), 0.06 (*Sb+*), 0.03 (*Sb-*), and 0.03 (*Sa*). For the main bodies the corresponding figures are: 1.00 (*Sc+*), 0.52 (*Sc-*), 0.10 (*Sb+*), 0.06 (*Sb-*), and 0.04 (*Sa*). It may not be necessary to add that these figures are of a provisional character; in order to get more definite results, a larger material of nebular masses is obviously needed.

#### 24. Total galactic absorption.

In the preceding sections we have assumed that the photographic absorption due to galactic obscuration can be represented by the cosecant law  $0^m25 \operatorname{cosec} B$ , as derived by Hubble (1934). It is, of course, possible to determine the galactic absorption directly from the writer's material on surface magnitudes. Unfortunately, the individual variations in surface magnitude are rather large even for nebulae of the same type; it may be recollect that for the different types of spiral nebulae a dispersion of about  $0^m3$  was obtained (comp. Table 9).

For a study of the galactic absorption we may conveniently use the same material of spiral nebulae as that selected for the investigation of internal nebular absorption (Tables 14a and 14b). If the observed photographic surface magnitude *S*, as defined in sect. 19, is corrected for the inclination effect of internal absorption (corr. given by the curves of Fig. 4), we obtain the quantity *S'*, or the surface magnitude

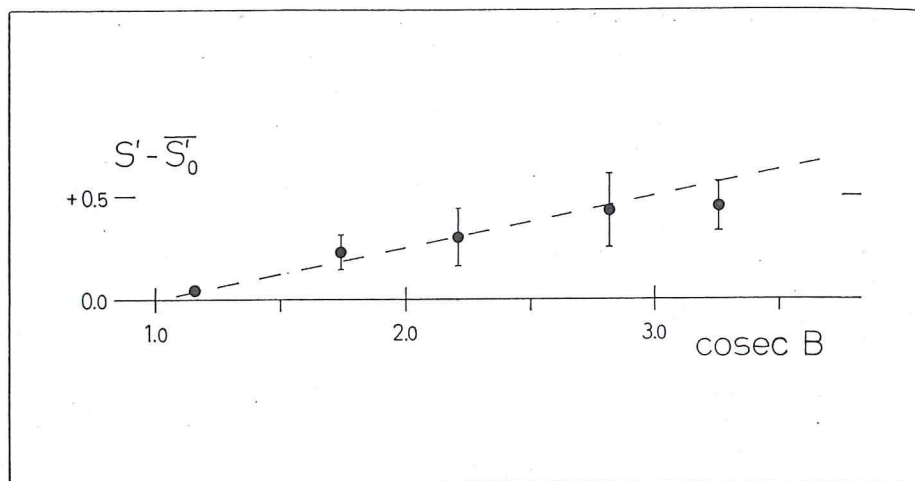


Fig. 8. Total galactic absorption, as derived from the photographic surface magnitudes (red. to incl.  $90^\circ$ ) of spiral nebulae of types  $Sc+$  to  $Sa$ . Length of each vertical line equal to twice the mean error of the average surface magnitude residual (m.e. for the high lat. group negligible). Hubble's cosecant law represented by the broken line.

red. to incl.  $90^\circ$  to the line of sight. A least squares solution based on the individual values of  $S'$  derived for all of the 119 nebulae, the latitudes of which extend from  $15^\circ$  to  $88^\circ$ , gives the result

$$A_{pg} = 0^m 22 \operatorname{cosec} B,$$

$$\pm 0.05$$

where  $A_{pg}$  is the photographic absorption, and  $B$  the galactic latitude. Owing to the considerable dispersion in the surface magnitudes, the mean error of the absorption parameter is comparatively large. A more detailed examination shows that a few objects in very low latitudes influence the result systematically. If the least squares solution is based only on nebulae with latitudes larger than  $20^\circ$  ( $N=113$ ), we arrive at a slightly different result,

$$A_{pg} = 0^m 26 \operatorname{cosec} B,$$

$$\pm 0.07$$

The absorption parameters derived from the two solutions show as good an agreement with Hubble's result as might be expected.

In order to get a more complete picture of the latitude variation in the writer's surface magnitudes, the mean residuals in  $S'$  have in Fig. 8 been computed for different intervals of  $\operatorname{cosec} B$ , the breadth of each interval being equal to 0.5. The straight-line relation represents Hubble's cosecant law. The agreement between the individual means and Hubble's relation is very satisfactory, except perhaps

S1364

Table 14a. Color indices and photographic surface magnitudes of Sc+ nebulae (first half) and Sc- nebulae (second half).

Object	Entire Nebula				Main Body			
	C <sub>o</sub>	C' <sub>o</sub>	S <sub>o</sub>	S' <sub>o</sub>	C <sub>o</sub>	C' <sub>o</sub>	S <sub>o</sub>	S' <sub>o</sub>
NGC 428	+0 <sup>m</sup> .30	+0 <sup>m</sup> .28	+15 <sup>m</sup> .40	+15 <sup>m</sup> .27	+0 <sup>m</sup> .22	+0 <sup>m</sup> .21	+16 <sup>m</sup> .20	+16 <sup>m</sup> .05
598	0.34	0.32	15.55	15.38	0.37	0.35	16.48	16.28
672	0.38	0.35	16.37	15.73	0.38	0.35	17.40	16.67
784	0.29	0.25	16.82	15.87	0.24	0.21	17.56	16.63
925	0.31	0.29	15.90	15.70	0.22	0.20	16.68	16.46
1003	0.28	0.25	15.73	15.33	0.24	0.21	16.61	16.15
1073	0.39	0.38	15.35	15.31	0.35	0.34	16.00	15.95
1337	0.41	0.38	16.46	15.82	0.33	0.30	17.22	16.49
1560	0.45	0.41	16.95	15.91	0.36	0.32	17.69	16.73
2403	0.26	0.24	15.86	15.57	0.27	0.25	16.88	16.55
2541	0.34	0.32	16.36	16.03	0.34	0.32	17.18	16.80
2805	0.33	0.32	16.07	15.97	0.28	0.27	16.64	16.52
3319	0.28	0.26	16.35	16.02	0.22	0.20	16.92	16.54
3423	0.28	0.28	15.21	15.20	0.24	0.24	15.98	15.97
3432	0.30	0.27	16.13	15.23	0.27	0.24	16.88	15.97
3556	0.44	0.41	15.75	15.26	0.39	0.36	16.41	15.85
4096	0.28	0.25	15.61	15.15	0.27	0.24	16.37	15.84
4116	0.29	0.28	15.80	15.69	0.22	0.21	16.48	16.35
4123	0.36	0.35	15.61	15.56	0.18	0.17	16.46	16.40
4242	0.37	0.37	15.78	15.77	0.35	0.35	16.45	16.43
4244	0.28	0.24	16.75	15.71	0.23	0.19	17.42	16.46
4559	0.29	0.27	15.58	15.34	0.22	0.20	16.44	16.17
4618	0.25	0.25	14.96	14.94	0.25	0.25	15.80	15.77
4631	0.42	0.38	16.10	15.07	0.33	0.29	16.79	15.84
5204	0.25	0.23	16.10	15.82	0.24	0.22	17.13	16.81
5474	0.30	0.30	15.47	15.45	0.30	0.30	16.20	16.18
5585	0.34	0.32	15.90	15.74	0.32	0.30	16.71	16.53
6015	0.42	0.39	15.58	15.20	0.34	0.31	16.45	16.01
NGC 7741	0.36	0.34	15.73	15.49	0.40	0.38	16.70	16.42
Reinm. 80	0.30	0.30	16.15	16.12	0.25	0.25	16.71	16.68
Means:	0.309		15.56		0.267		16.31	

NGC 578	+0 <sup>m</sup> .38	+0 <sup>m</sup> .33	+15 <sup>m</sup> .65	+15 <sup>m</sup> .47	+0 <sup>m</sup> .32	+0 <sup>m</sup> .27	+16 <sup>m</sup> .54	+16 <sup>m</sup> .34
628	0.38	0.38	15.04	15.04	0.26	0.26	15.82	15.82
908	0.54	0.47	15.42	15.11	0.51	0.45	16.20	15.85
1042	0.41	0.39	15.54	15.50	0.31	0.30	16.33	16.29
1058	0.42	0.42	15.13	15.13	0.41	0.41	16.32	16.32

Table 14a (cont.)

Object	Entire Nebula				Main Body				
	C <sub>o</sub>	C' <sub>o</sub>	S <sub>o</sub>	S' <sub>o</sub>	C <sub>o</sub>	C' <sub>o</sub>	S <sub>o</sub>	S' <sub>o</sub>	
NGC 1087	+0 <sup>m</sup> 41	+0 <sup>m</sup> 36	+15 <sup>m</sup> 22	+15 <sup>m</sup> 06	+0 <sup>m</sup> 45	+0 <sup>m</sup> 41	+16 <sup>m</sup> 30	+16 <sup>m</sup> 12	
1232	0.45	0.44	15.30	15.28	0.30	0.29	16.02	16.00	
1637	0.44	0.42	15.41	15.35	0.27	0.25	16.47	16.40	
1784	0.50	0.45	15.92	15.75	0.32	0.28	16.74	16.54	
2336	0.44	0.38	15.85	15.63	0.34	0.29	16.61	16.36	
2715	0.40	0.32	15.73	15.29	0.29	0.22	16.53	16.03	
2903	0.45	0.40	15.10	14.93	0.31	0.27	16.12	15.93	
3079	0.49	0.38	16.23	15.19	0.39	0.29	17.04	16.08	
3184	0.43	0.43	15.12	15.12	0.35	0.35	15.85	15.85	
3198	0.38	0.30	16.15	15.66	0.29	0.22	17.01	16.45	
3338	0.40	0.35	16.08	15.88	0.22	0.17	16.93	16.71	
3344	0.30	0.30	15.19	15.18	0.26	0.26	16.07	16.06	
3359	0.36	0.31	15.58	15.39	0.39	0.34	16.42	16.21	
[1]	3486	0.38	0.34	15.94	15.83	0.28	0.25	16.99	16.86
[2]	3631	0.45	0.45	15.16	15.16	0.45	0.45	16.09	16.09
[3]	3642	0.34	0.33	15.90	15.89	0.27	0.27	17.04	17.03
[4]	3646	0.54	0.50	15.30	15.19	0.48	0.45	16.06	15.94
[5]	3726	0.35	0.32	15.39	15.30	0.27	0.24	16.31	16.21
[6]	3756	0.50	0.44	15.71	15.47	0.42	0.37	16.50	16.22
[7]	3810	0.49	0.44	15.21	15.05	0.42	0.38	16.18	16.00
[8]	3938	0.37	0.37	14.93	14.92	0.26	0.26	15.75	15.74
[9]	4088	0.44	0.36	15.06	14.62	0.43	0.36	15.76	15.26
[10]	4517	0.60	0.50	16.59	15.66	0.57	0.48	17.14	16.22
[11]	4666	0.56	0.49	15.50	15.12	0.42	0.35	16.37	15.93
[12]	5033	0.43	0.36	16.06	15.70	0.24	0.18	16.94	16.52
[13]	5248	0.43	0.40	14.83	14.74	0.33	0.30	15.71	15.61
[14]	5364	0.52	0.51	15.61	15.59	0.47	0.46	16.37	16.34
[15]	5457	0.29	0.29	15.40	15.40	0.17	0.17	16.23	16.23
[16]	6503	0.47	0.38	15.77	15.13	0.38	0.30	17.08	16.35
[17]	NGC 6643	0.45	0.39	14.87	14.59	0.41	0.35	15.69	15.37
[18]	IC 239	0.46	0.46	15.36	15.35	0.42	0.42	16.04	16.03
	Means:		0.393		15.29		0.316		16.15

for the last group (lat. smaller than 20°). The deviation of this group, if not accidental, may be due to some slight selection effects in the writer's material, or, possibly, to a real break in the linear cosecant relation. It may be noted that from his nebular counts Hubble has found a similar deviation in low latitudes, explained by him as "a result either of selection or of a failure of the cosecant law".

S 1364

Table 14b. Color indices and photographic surface magnitudes of Sb+ nebulae (first part), Sb- nebulae (second part), and Sa nebulae (third part); a diff. redshift corr. of  $-0^m01$  applied to the colors of 8 members (Sb-, Sa) of the Virgo cluster.

Object	Entire Nebula				Main Body			
	C <sub>o</sub>	C' <sub>o</sub>	S <sub>o</sub>	S' <sub>o</sub>	C <sub>o</sub>	C' <sub>o</sub>	S <sub>o</sub>	S' <sub>o</sub>
NGC 772	+0 <sup>m</sup> 64	+0 <sup>m</sup> 60	+16 <sup>m</sup> 07	+15 <sup>m</sup> 82	+0 <sup>m</sup> 57	+0 <sup>m</sup> 55	+17 <sup>m</sup> 12	+16 <sup>m</sup> 88
891	0.67	0.58	16.11	14.80	0.57	0.52	16.80	15.64
1055	0.76	0.69	16.68	15.89	0.68	0.64	17.69	16.94
1090	0.51	0.43	16.92	16.05	0.35	0.31	17.93	17.10
1300	0.52	0.47	15.57	15.26	0.45	0.43	16.11	15.81
1325	0.63	0.55	16.26	15.39	0.56	0.52	16.97	16.14
1961	0.50	0.47	15.64	15.51	0.38	0.37	16.58	16.46
1964	0.60	0.52	15.84	14.92	0.41	0.37	16.94	16.06
2985	0.58	0.54	15.34	15.15	0.51	0.49	16.63	16.45
3351	0.71	0.67	15.27	15.06	0.60	0.58	16.20	16.00
3627	0.62	0.55	15.33	14.77	0.62	0.59	16.58	16.05
3628	0.69	0.60	16.49	15.17	0.61	0.56	17.11	15.94
3953	0.56	0.52	15.55	15.34	0.50	0.48	16.41	16.21
3992	0.69	0.65	15.50	15.28	0.55	0.53	16.20	15.99
4051	0.61	0.58	15.32	15.15	0.55	0.53	16.10	15.94
4258	0.52	0.45	15.78	14.99	0.41	0.37	16.73	15.98
4565	0.74	0.64	16.81	15.45	0.54	0.49	17.80	16.62
4725	0.61	0.59	15.48	15.39	0.49	0.48	16.20	16.11
5005	0.63	0.58	15.06	14.72	0.56	0.53	16.18	15.85
5055	0.61	0.56	15.27	14.99	0.50	0.48	16.25	15.99
5775	0.69	0.62	15.86	15.21	0.59	0.56	16.50	15.89
5850	0.56	0.56	15.36	15.36	0.48	0.48	16.17	16.17
5907	0.61	0.50	16.95	15.59	0.49	0.44	17.68	16.50
6384	0.51	0.46	15.29	14.99	0.39	0.37	16.10	15.81
NGC 7331	0.60	0.54	15.47	15.02	0.47	0.44	16.59	16.16
Means:	0.557		15.25		0.484		16.19	

NGC 224	+0 <sup>m</sup> 75	+0 <sup>m</sup> 62	+15 <sup>m</sup> 36	+14 <sup>m</sup> 80	+0 <sup>m</sup> 54	+0 <sup>m</sup> 39	+16 <sup>m</sup> 33	+15 <sup>m</sup> 80
488	0.84	0.77	15.51	15.32	0.74	0.66	16.53	16.35
1068	0.70	0.65	14.56	14.45	0.67	0.61	15.86	15.75
2683	0.78	0.61	15.80	14.54	0.70	0.51	16.98	15.78
2841	0.70	0.57	15.27	14.78	0.63	0.49	16.32	15.85
3031	0.82	0.67	15.44	14.69	0.69	0.53	16.69	15.98
3521	0.82	0.70	15.67	15.20	0.77	0.63	16.88	16.43
4216	0.93	0.77	15.95	14.97	0.87	0.69	16.81	15.88
4450	0.69	0.61	15.53	15.31	0.61	0.52	16.57	16.36
4527	0.76	0.63	15.64	15.08	0.69	0.54	16.44	15.91

Table 14b (cont.)

Object	Entire Nebula				Main Body			
	C <sub>o</sub>	C' <sub>o</sub>	S <sub>o</sub>	S' <sub>o</sub>	C <sub>o</sub>	C' <sub>o</sub>	S <sub>o</sub>	S' <sub>o</sub>
NGC 4579	+0 <sup>m</sup> .70	+0 <sup>m</sup> .62	+15 <sup>m</sup> .22	+14 <sup>m</sup> .99	+0 <sup>m</sup> .62	+0 <sup>m</sup> .53	+16 <sup>m</sup> .40	+16 <sup>m</sup> .18
4736	0.63	0.60	14.78	14.72	0.48	0.45	16.24	16.19
4826	0.76	0.68	14.72	14.49	0.70	0.61	15.81	15.59
5746	0.92	0.74	16.27	14.98	0.87	0.67	17.24	16.09
NGC 7217	0.68	0.64	14.88	14.78	0.61	0.56	16.16	16.07

Means: 0.659 14.87 0.559 16.01

NGC 936	+0 <sup>m</sup> .87	+0 <sup>m</sup> .84	+15 <sup>m</sup> .15	+15 <sup>m</sup> .08	+0 <sup>m</sup> .84	+0 <sup>m</sup> .80	+16 <sup>m</sup> .30	+16 <sup>m</sup> .23	
2655	0.71	0.66	15.14	15.03	0.63	0.58	16.36	16.26	
2681	0.65	0.65	14.86	14.86	0.62	0.62	16.24	16.24	
3166	0.77	0.64	15.59	15.05	0.77	0.62	16.80	16.29	
3169	0.68	0.64	15.08	14.99	0.58	0.54	16.02	15.94	
[1]	3190	0.85	0.70	15.76	15.01	0.81	0.65	-16.88	16.17
[2]	3368	0.75	0.68	15.18	15.00	0.70	0.62	16.37	16.20
[3]	3623	0.80	0.64	15.53	14.66	0.76	0.59	16.54	15.71
[4]	4235	0.94	0.76	16.34	15.06	0.86	0.66	17.40	16.26
[5]	4274	0.85	0.70	16.03	15.24	0.83	0.66	17.15	16.40
[6]	4586	0.90	0.77	16.18	15.69	0.87	0.73	17.07	16.60
[7]	4596	0.89	0.85	15.29	15.21	0.90	0.86	16.28	16.20
[8]	NGC 4698	0.82	0.74	15.61	15.40	0.72	0.63	16.66	16.46

Means: 0.713 15.10 0.658 16.23

Fi

[1]

[2]

[3]

[4]

[5]

[6]

[7]

[8]

[9]

[10]

[11]

[12]

[13]

[14]

[15]

[16]

[17]

[18]

## CHAPTER IV

## Investigation of the Virgo Cluster

**25. Introductory remarks.**

In order to get material for a more detailed study of the Virgo cluster, the photometric program has included as many objects in this region as has been permitted by the available observing time. By means of Palomar 48-inch plates a survey has been made of the cluster area, and all nebulae with apparent dimensions above a certain limit have been included in the observing list. Preference has been given to all outstanding objects, especially those of late types which seem to be sparsely represented in the cluster; double and multiple systems, where the components are close enough to be covered by one exposure, have also been given priority. In all, 88 nebulae have been observed, 35 with the 60-inch and 53 with the 100-inch telescope. The photographic magnitudes, as listed in the catalogue, range from 9.33 (NGC 4472) to about 14.5. The material includes only 2 objects of type *Ir I*, whereas types *Sc+* and *Sc-* are represented by 9 and 25 objects, respectively.

The above nebulae all belong to the Virgo cluster proper. With regard to the following analysis of the magnitudes and colors of cluster members it has seemed desirable to try to define the boundaries of the cluster as closely as possible. For this purpose we may conveniently use the survey catalogues by Reinmuth (1926) and by Shapley-Ames (1932). An examination of distribution curves derived from these catalogues indicates that the cluster extends in right ascension from 12<sup>h</sup> 8<sup>m</sup> to 12<sup>h</sup> 48<sup>m</sup>, and in declination from +2°.5 to +18°.5 (1950). In the following investigation it has been assumed that the cluster covers an elliptical area with diameters of the size mentioned, the minor axis being parallel to the equator. With this rather restricted definition, objects belonging to the outside field are excluded as far as possible. It may be noted that the anomalies to be discussed below have been found only for nebulae that are located within the cluster boundaries, as defined here.

**26. Colors and surface magnitudes of cluster members.**

Already in sect. 13 attention was called to the fact that certain members of the Virgo cluster seem to have abnormal colors. For that reason, nebulae in the cluster area were not (with a few exceptions) included in the previous investigations of inclination effects in color and surface magnitude. The photometric data assembled will now be used for a closer examination of the peculiar conditions in the cluster.

Table 15. Color indices and photographic surface magnitudes of Virgo cluster members.

Object	Type	$C'_o$	$\Delta C'_o$	$S'_o$	$\Delta S'_o$	
NGC 4165	Sc -	+0 <sup>m</sup> .69	+0 <sup>m</sup> .29	+16 <sup>m</sup> .04	+0 <sup>m</sup> .75	
4178	Sc +	0.30	-0.01	15.60	+0.04	
4189	Sc -	0.64	+0.24	15.11	-0.18	
4192	Sb +	0.60	+0.04	14.92	-0.33	
4193	Sb +	0.71	+0.15	15.49	+0.24	
4206	Sc -	0.44	+0.04	15.78	+0.49	
4212	Sc -	0.60	+0.20	15.03	-0.26	
4216	Sb -	0.78	+0.11	14.97	+0.10	
4224	Sa	0.89	+0.17	15.31	+0.21	
4235	Sa	0.77	+0.05	15.06	-0.04	
[1]	4241	Sa	0.86	+0.14	15.60	+0.50
[2]	4246	Sc -	0.57	+0.17	15.94	+0.65
[3]	4254	Sc -	0.45	+0.05	14.62	-0.67
[4]	4273	Sc -	0.46	+0.06	14.89	-0.40
[5]	4294	Sc -	0.31	-0.09	15.29	0.00
[6]	4298	Sc -	0.55	+0.15	15.47	+0.18
[7]	4299	Sc +	0.24	-0.07	15.15	-0.41
[8]	4301	Sc +	0.25	-0.06	15.46	-0.10
[9]	4303	Sc -	0.32	-0.08	15.01	-0.28
[10]	4321	Sc -	0.61	+0.21	15.03	-0.26
[11]	4341	Sa	0.82	+0.10	15.79	+0.69
[12]	4411A	Sc +	0.59	+0.28	16.02	+0.46
[13]	4411B	Sc +	0.50	+0.19	15.69	+0.13
[14]	4450	Sb -	0.62	-0.05	15.31	+0.44
[15]	4480	Sc -	0.54	+0.14	15.36	+0.07
[16]	4496	Sc +	0.45	+0.14	15.49	-0.07
[17]	4501	Sb +	0.54	-0.02	14.60	-0.65
[18]	4519	Sc -	0.35	-0.05	15.23	-0.06
[19]	4527	Sb -	0.64	-0.03	15.08	+0.21
[20]	4532	Ir I	0.23	-0.05	—	—
[21]	4535	Sc -	0.50	+0.10	15.31	+0.02
[22]	4536	Sc -	0.38	-0.02	15.33	+0.04
[23]	4548	Sb +	0.51	-0.05	15.11	-0.14
[24]	4567	Sc -	0.60	+0.20	15.50	+0.21
[25]	4568	Sc -	0.70	+0.30	15.50	+0.21
[26]	4569	Sb +	0.43	-0.13	14.95	-0.30
[27]	4571	Sc +	0.37	+0.06	15.27	-0.29
[28]	4576	Sc -	0.61	+0.21	15.54	+0.25
[29]	4579	Sb -	0.63	-0.04	14.99	+0.12
[30]	NGC 4586	Sa	0.78	+0.06	15.69	+0.59

Table 15 (cont.)

Object	Type	$C'_0$	$\Delta C'_0$	$S'_0$	$\Delta S'_0$
NGC 4596	Sa	+0 <sup>m</sup> .86	+0 <sup>m</sup> .14	+15 <sup>m</sup> .21	+0 <sup>m</sup> .11
4606	Sa	0.63	-0.09	15.61	+0.51
4633	Sc+	0.48	+0.17	15.98	+0.42
4639	Sb+	0.57	+0.01	15.05	-0.20
4647	Sc-	0.38	-0.02	15.30	+0.01
4651	Sc-	0.39	-0.01	15.03	-0.26
4654	Sc-	0.49	+0.09	15.12	-0.17
4689	Sc-	0.52	+0.12	15.31	+0.02
NGC 4698	Sa	0.75	+0.03	15.40	+0.30
IC 3115	Sc-	0.56	+0.16	16.02	+0.73
3259	Sc-	0.58	+0.18	16.43	+1.14
IC 3267	Sc-	0.64	+0.24	16.25	+0.96
Ho VII	Ir I	0.37	+0.09	—	—

The investigation will be based on objects of types *Ir I*, *Sc+*, *Sc-*, *Sb+*, *Sb-*, and *Sa*; only in these cases does the catalogue contain a sufficiently large number of field nebulae to make possible a detailed comparison. The material is collected in Table 15, which includes all cluster objects of the types mentioned. The third column gives the integrated color index  $C'_0$ , or the observed color reduced to gal. lat.  $90^\circ$  and to incl.  $90^\circ$  to line of sight (no incl. corr. for type *Ir I*); the corrections are  $-0^m.062$  (cosec  $B-1$ ) and  $-\beta(1-b/a)$ , respectively, as derived in sections 13 and 14. The deviation of  $C'_0$  from the corresponding mean color referring to field nebulae (Table 7) is listed in the fourth column. In column 5 we find the integrated photographic surface magnitude  $S'_0$ , as defined in sect. 19; in this case the correction to lat.  $90^\circ$  is  $-0^m.25$  (cosec  $B-1$ ), whereas the correction to incl.  $90^\circ$  is given by the curves in Fig. 4. The last column gives the deviation in surface magnitude from the mean corresponding to field nebulae (Table 9). No surface magnitudes are listed for the two nebulae of type *Ir I*.

It should be noted that no redshift corrections (comp. sect. 15) have been applied to the colors and surface magnitudes of Table 15. The *mean* differential correction to be applied to  $\Delta C'_0$  would amount to only  $-0^m.005$  (mean redshifts derived in Tables 6 and 16). Since the observed redshifts of Virgo cluster members range from about  $-500$  to about  $+2500$  km/sec, the differential corrections may in individual cases range from  $+0^m.03$  to  $-0^m.03$ ; redshifts are however available for only 21 of the 53 objects in the table. As regards the surface magnitudes, the corrections are negligible.

For the above cluster members the color deviation ranges from  $-0^m.13$  to  $+0^m.30$ ; the mean of  $\Delta C'_0$  amounts to  $+0^m.08 \pm 0^m.015$  (m. e.). A color excess effect is thus clearly indicated. The statistical distribution of the individual deviations is repro-

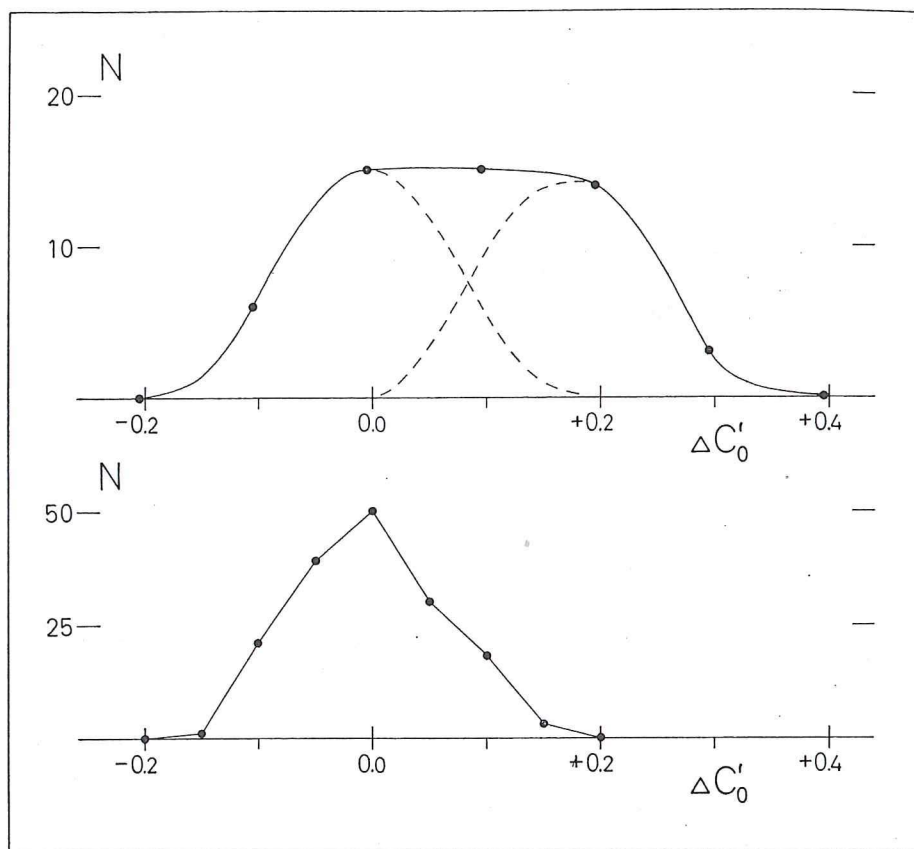


Fig. 9. Statistical distribution of color index residuals (obs. color minus mean color, both red. to lat.  $90^\circ$  and to incl.  $90^\circ$ ), as found for 53 members of the Virgo cluster (upper part). Distribution of corresponding color residuals for nebulae outside the cluster area (lower part).

[1] [2] [3] [4] [5] [6] [7] [8] [9] [10] [11] [12] [13] [14] [15] [16] [17] [18]

duced in Fig. 9, where the different class frequencies have been represented by a smooth curve. For comparison, the figure also includes the distribution curve obtained for the 162 field nebulae of the same types.

Whereas the curve referring to non-cluster objects is more or less symmetrical around  $\Delta C'_0 = 0^m 00$ , the curve corresponding to the Virgo cluster shows a considerable asymmetry. In spite of the limited size of the material it seems possible to divide the latter distribution in two parts, one representing objects of normal color, and the other objects with color excess effects. The division is in the figure indicated by dotted lines. We may conclude that approximately half the number of nebulae investigated have colors more or less the same as those observed for field nebulae, and that the remaining half suffer a color excess that, on an average, amounts to about  $0^m 16$ .

If the cluster members are divided in two groups according to type, we find that the mean color excess amounts to  $+0^m 09$  ( $Sc+$ ,  $Sc-$ ,  $Sb+$ ) and  $+0^m 05$  ( $Sb-$ ,

S1364

*Sa).* If types *SO* (13 members) and *E* (7 members) are also examined, and if the normal color in these cases is assumed to be  $0^m 85$  (comp. Table 7), we find a mean excess of  $+0^m 03$ . The color deviation thus seems to depend, to some extent, on the type of the nebula. As regards the coordinates of nebulae with pronounced color excesses, it may be noted that these objects do not favor any special part of the cluster area. However, a more detailed analysis of the apparent distribution reveals a certain "grouping effect". There are in Table 15 altogether 25 nebulae with  $\Delta C'_0 \geq +0^m 10$ ; their mean color excess amounts to  $+0^m 18$ . In circular areas around these nebulae, with a radius of  $15'$ , we find 17 other objects (probably physical comp.) which also are listed in the table; the mean color excess of these companions is  $+0^m 17$ . If the procedure is repeated for the 28 nebulae with  $\Delta C'_0 < +0^m 10$  (mean excess =  $-0^m 01$ ), we find in the corresponding survey areas 9 objects with a mean excess of  $+0^m 03$ . This result strongly suggests that, whatever is the cause of the color excess, neighboring nebulae are affected in a similar way.

An examination of the relation between color and surface magnitude is naturally an important step in trying to find an explanation of the color excess. It is indicated already by a superficial inspection of the material, that a large color excess as a rule is accompanied by a positive deviation in surface magnitude. In Fig. 10 the latter deviation, as listed in Table 15, has been plotted against the color deviation. Since the individual variations in the surface magnitudes of spiral nebulae are rather large, a dispersion of  $0^m 3$  being found for objects outside the cluster, we cannot expect any pronounced correlation between the two quantities. However, the plot clearly indicates that there is a systematic decrease in surface luminosity as the color deviation increases. In the interval  $\Delta C'_0 < +0^m 10$ , where we may expect a majority of "normal" objects, the surface luminosity is definitely brighter than in the interval  $\Delta C'_0 \geq +0^m 10$ . A numerical analysis shows that the coefficient of correlation amounts to  $+0.41$ , and that the two regression lines reproduced in the figure have inclination coefficients of  $+1.4$  and  $+8.4$ . It is interesting to note that the mean of these coefficients comes rather close to the result obtained in the preceding chapter for the ratio of total to selective absorption in spiral nebulae.

As a result of the correlation between the deviations in color and surface magnitude, a slight correlation is also obtained between color deviation and total apparent magnitude. However, if the (photographic) magnitude is corrected by  $-4\Delta C'_0$ , the correlation disappears.

The color excesses derived in Table 15, as well as the deviations in surface magnitude, ultimately depend on the types of the nebulae as determined by the writer. For the majority of the cluster objects there are, in the writer's opinion, no special difficulties of classification. It may be noted that 21 of the nebulae are included in the redshift catalogue by Humason, Mayall, and Sandage (1956), and that the types listed in this catalogue in all but two cases are in agreement with the writer's classifications. The exceptions are NGC 4501 and NGC 4536 (in redshift cat. *Sc* and *Sb*, resp.), which seem to be rather typical specimens of types *Sb+* and *Sc-*, respectively, a classification that is supported by the observed integrated colors.

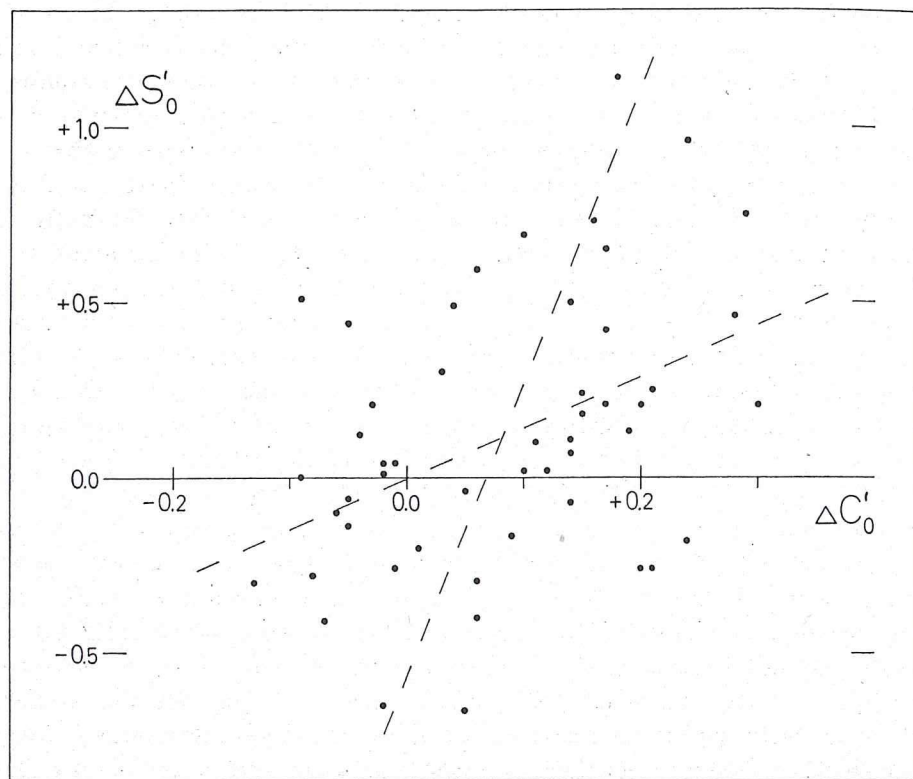


Fig. 10. Relation between color index residual and surface magnitude residual, as derived for 51 spiral nebulae in the Virgo cluster; regression lines represented by broken lines.

The material at hand is too limited to permit any definitive conclusions as to the causes of the abnormal behavior of part of the cluster members. Two possibilities may be considered: (a) the presence of obscuring clouds in the internebular space of the cluster, and (b) internal changes in individual nebulae as regards absorption and stellar content. The result obtained above as regards the ratio of color excess to surface magnitude deviation may seem to speak in favor of possibility (a). If obscuring clouds are present in the cluster, they must have a very irregular and spotty distribution, the absorption at different places ranging from zero to several tenths of a magnitude. It may be noted that the mean absorption, corresponding to the mean color excess derived above, would be very large compared to the combined absorption of the internal obscuring matter in the cluster nebulae; if the absorbing matter contained in all the nebulae were spread out as a screen in front of the cluster, the resulting absorption would probably be less than 0<sup>m</sup>01. The number of background nebulae in the Virgo area seems to be more or less normal (Shane and Wirtanen 1954); however, a certain deficiency is noted by Zwicky (1957). As regards possibility (b), we wish to refer to the investigation by Spitzer and Baade

(1951) concerning collisions between cluster members. On account of the high space density, and the large dispersion in redshifts, it seems probable that collisions between individual nebulae are a not uncommon phenomenon even in a comparatively loose cluster of the Virgo type. As a result of a collision, the interstellar matter (or part of it) is, according to Spitzer and Baade, swept out of the nebulae, whereas the stars are left more or less undisturbed. After a collision we may thus expect a decrease in internal absorption; on the other hand, we may also expect a gradual change as regards stellar content, since the presence of interstellar matter seems to be a necessary condition for the survival of the supergiants of a type I population. The decrease in absorption and the change in stellar content will work in opposite directions as regards the observed color index, and it seems difficult to decide from the material analysed here if, and to what extent, collisions between nebulae are responsible for the color excess effect.

#### 27. Relation between surface magnitude and absolute magnitude.

Although the angular dimensions of the Virgo cluster are comparatively large, all cluster nebulae may to a first approximation be assumed to be situated at the same distance in space. If the extension of the cluster along the line of sight is comparable to the largest angular diameter adopted above ( $16^{\circ}0$ ), the maximum errors in the individual absolute luminosities, as based on the mean distance, would amount to  $\pm 0.3$  magnitudes. The additional dispersion in absolute magnitude caused by variations in distance modulus would probably not be larger than 0.10—0.15 magn., a quantity that may be neglected in the following analysis. In the fainter magnitude classes, the material investigated may include objects that belong to the field behind the cluster; down to  $m_{pg}=13$  the relative number of background objects is however very small, as will be shown in sect. 29.

In this section we shall examine the dependence of surface magnitude on total magnitude. The integrated photographic surface magnitude,  $S'_0$ , has in Table 15 been derived for cluster nebulae of types *Sc+* to *Sa*; the listed magnitude is corrected for differential galactic absorption and for inclination effect. The same corrections will be applied to the total apparent photographic magnitude, as given in the catalogue, the corrected magnitude being denoted by  $m'_0$ . Since the quantity  $S'_0$  is equal to  $m'_0 + 5 \log A$ , according to our previous definition (comp. sect. 19;  $a = \text{app. maj. diam. in min.}$ ), the relation between surface magnitude and total absolute magnitude is given by the expression

$$S'_0 = M' + 5 \log A + 12.93,$$

where  $M'$  is the absolute photographic magnitude reduced to incl.  $90^{\circ}$  to the line of sight, and  $A$  the major diameter in parsec. The degree of correlation to be expected between  $S'_0$  and  $M'$  apparently depends on the variations in the absolute diameters of the nebulae investigated.

In Fig. 11 a plot has been made of  $S'_0$  against  $m'_0$  for cluster spirals of the types

mentioned. In order to avoid the systematic effects discussed in the preceding section, the figure only includes the 36 nebulae for which the color deviation  $\Delta C'_0$  does not exceed  $+0^m 15$ . The selected objects have a mean surface magnitude of 15.25, whereas the mean of  $m'_0$  is 11.37. In spite of the fact that the different types of spirals have been taken together in one group, the relation between the two variables is rather pronounced, the coefficient of correlation amounting to  $+0.64 \pm \pm 0.10$  (m.e.). The regression line reproduced in the figure gives the mean surface magnitude corresponding to a given total magnitude,

$$S'_0 = +0.181 m'_0 + 13.19. \quad (11a)$$

When  $m'_0$  changes from 9.6 to 13.2, the surface magnitude thus decreases by about  $0^m 7$ .

On account of the systematic variation with total magnitude, the observed surface magnitude may apparently be used as an indicator of absolute luminosity. The regression line giving the mean absolute magnitude (red. to incl.  $90^\circ$ ) as a function of surface magnitude is represented by the relation

$$M' = +2.27 S'_0 - 23.3 - D, \quad (11b)$$

where  $D$  is the apparent distance modulus of the Virgo cluster. There are several indications that this modulus is not far from 30; as is shown in the following section, an analysis of the present material leads to  $D=30.2$ .

The dispersion in total magnitude about the above regression line amounts to  $0^m 8$ , and in an individual case the mean error of the derived absolute luminosity is thus comparatively large. However, if the method is applied to *groups* of nebulae, the mean results seem to be comparable in accuracy to those obtained when the observed redshifts are used as distance indicators (comp. next sect.). A somewhat higher accuracy may be attained when a larger material becomes available, and the relation between surface magnitude and total luminosity can be determined for each nebular type separately.

It should be noted that the regression lines derived above only represent spiral nebulae with absolute magnitudes brighter than about  $-17.0$ . The magnitude cut-off may have no serious effects as regards relation (11a); on the other hand, it is obvious that relation (11b) would be somewhat changed if objects of fainter magnitude classes were added to the material. The use of the latter relation for estimates of absolute luminosities should thus be restricted to samples of nebulae in which the absolute magnitude distribution is more or less the same as in the material investigated here — that is, to samples for which the apparent magnitude has been the main selection parameter.

### 28. Determination of the redshift parameter $H$ .

The recent redshift catalogue by Humason, Mayall, and Sandage (1956), with detailed redshift data for 806 extragalactic nebulae, includes a photometric analysis

S 1964

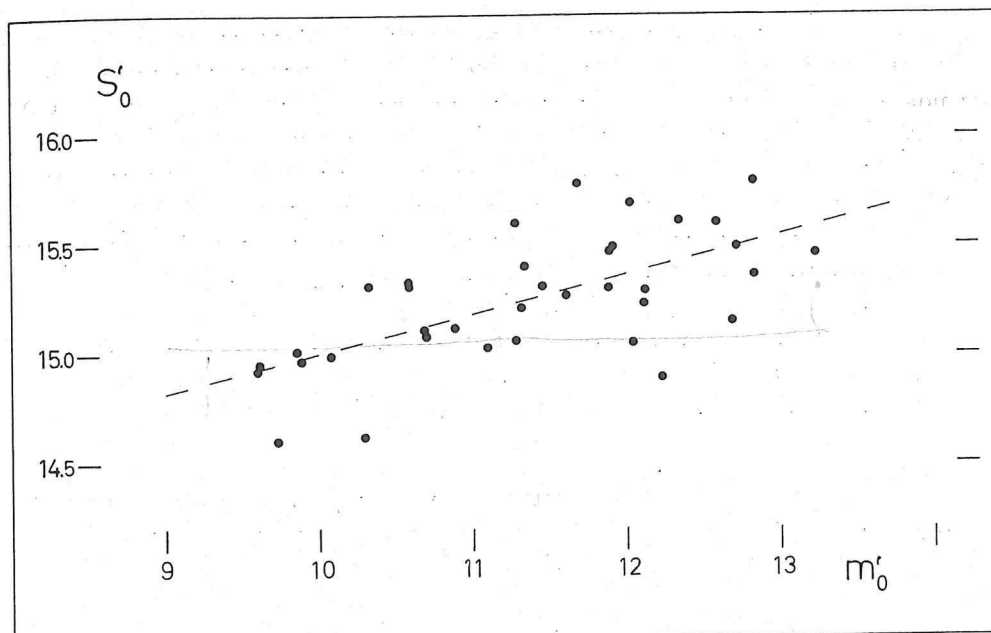


Fig. 11. Relation between photographic surface magnitude and total photographic magnitude (both red. to lat.  $90^\circ$  and to incl.  $90^\circ$ ), as derived for 36 spiral nebulae in the Virgo cluster; the broken line gives the mean surface magnitude as a function of total magnitude.

by Sandage that, among other things, aims at a determination of the Hubble redshift parameter  $H$ . The results, which according to Sandage are of a provisional character, range from 176 to 211 km/sec per  $10^6$  ps, the adopted mean being 180 (comp. also Hoyle and Sandage 1956; Baum 1957). On account of the importance of this fundamental parameter, it may be of interest to examine whether any additional information can be derived from the present material. The investigation will be limited to (a) the Virgo cluster and (b) spiral nebulae in the general field, the distance moduli of the latter objects being estimated by means of relation (11b).

Obviously, the results to be derived from the two groups of nebulae as regards the redshift parameter will be entirely dependent on the distance modulus adopted for the Virgo cluster. In the above-mentioned analysis, Sandage has accepted an apparent modulus of 29.3, as determined from the apparent magnitudes of the brightest resolved stars in the cluster member NGC 4321, and from the assumption that the mean absolute magnitude of these stars is  $-8.5$ . However, this assumption is necessarily somewhat uncertain; it may furthermore be noted that NGC 4321 is one of the "abnormal" spirals in the cluster, the color excess (Table 15) amounting to  $+0^m.21$  (color index confirmed by Stebbins-Whitford; comp. Table 3).

From an analysis of the present photometric material we are supplied with several arguments indicating an apparent cluster modulus of about 30.2. Four reasons for the acceptance of this rather high modulus are given below.

1. The apparent photographic magnitudes of the three brightest *spiral* nebulae in the cluster, NGC 4192, 4501, and 4569, are nearly the same (9.61, 9.74, and 9.62, resp., as red. to incl. 90°). If the mean absolute luminosity of these nebulae is assumed to agree with that of NGC 224 ( $-20.48$ , as red. to incl. 90°; app. mod. =  $=24.25$  acc. to Baade and Swope 1955), which presumably is one of the most luminous spiral nebulae in the sky, the apparent modulus of the cluster will be 30.1. It may be noted that the three spirals are all of type *Sb*, that their colors are normal (Table 15), and that their mean surface magnitude ( $\bar{S}'_0=14.82$ ) is practically the same as that of NGC 224 ( $S'_0=14.80$ ; Table 14b); an agreement in luminosity will thus also lead to an agreement in the absolute diameters. Incidentally, the absolute magnitude of the brightest cluster member, the elliptical nebula NGC 4472, will be about the same as the absolute magnitude of NGC 224 corrected for internal absorption ( $-20.48 - 0.43 = -20.9$ ; comp. sect. 19).
2. If the relation between absolute magnitude and surface magnitude, as given in eq. (11b), is calibrated by means of NGC 224 (app. mod. =  $24.25$ ), NGC 598 (app. mod. =  $24.15$  acc. to Sandage), and NGC 3031 (app. mod. =  $27.1$ ; Sandage 1954), the apparent cluster modulus will be equal to 30.2; the individual results are 30.8, 29.7, and 30.0, respectively.
3. In the three groups (local group, groups around NGC 3031 and NGC 5457) previously investigated by the writer (1950a) there are 9 nebulae brighter than absolute magnitude  $-17.0$ ; the magnitudes are based on revised distance moduli (app. mod. of NGC 5457 assumed to be =  $27$ ). If we adopt for the Virgo cluster a distance modulus of only 29.3, the corresponding number of cluster members will amount to 70 (comp. the lum. curve of Fig. 13). The ratio of these numbers (8:1) certainly appears too small; although no exact figures are available regarding the size of the two populations, it seems likely that the true ratio must be approximately twice as large. In order to get a ratio of 16:1 the distance modulus of the cluster has to be changed to about 30.3.
4. Finally, some information about the cluster modulus is obtained, indirectly, by a comparison, as regards luminosity, between the brightest field nebulae and NGC 224. The absolute magnitudes of spiral nebulae may be estimated (a) from their surface magnitudes by means of relation (11b), which includes the cluster modulus as a constant term, and (b) from the observed redshifts, in which case the parameter  $H$  must be known. The cluster modulus and the redshift parameter are apparently related; with a modulus of 30.2, the material analysed below yields a parameter, corresponding to the mean redshift of the cluster, of  $130 \text{ km/sec}$  per  $10^6 \text{ ps}$ . If these results are adopted, we find that the three most luminous spiral nebulae (present material) outside the cluster, NGC 1068 (*Sb*—), NGC 6643 (*Sc*—), and NGC 5746 (*Sb*—), have absolute magnitudes (means of  $a$  and  $b$ ; magn. red. to incl. 90°) equal to  $-20.6$ ,  $-20.2$ , and  $-20.1$ , respectively. If we want an agreement in luminosity between NGC 1068 and NGC 224, the cluster modulus must, accordingly, be reduced to 30.1. On the other hand, we must increase the modulus

Table 16. Mean redshift of the Virgo cluster. 26

Decl. interval	Decl.	N	$\bar{V}$ (km/sec)
+ 2°5 — +18°5	+11°1	65	+1206
+ 2.5 — +10.5	+ 7.2	23	+1456
+10.5 — +18.5	+13.3	42	+1068

to 30.4 in order to make the *mean* luminosity of the three field nebulae equal to the luminosity of NGC 224; it may be added that the agreement in luminosity is accompanied by an agreement in absolute diameters.

Although each of the above arguments may not be quite conclusive, the good agreement between the individual results seems to leave no doubt about an apparent cluster modulus slightly larger than 30. In the following analysis we shall accept the mean result, or 30.2. It is interesting to note that this modulus happens to agree with the tentative modulus derived by Baum (1955) from a photometric comparison between globular clusters in NGC 224 and the elliptical cluster member NGC 4486.

As regards the redshifts of cluster members, we find that, within the cluster boundaries as defined in sect. 25, measures are available for 65 nebulae in the above redshift catalogue. The arithmetical mean of these redshifts, corrected for solar motion with respect to the local group, is +1206 km/sec. However, the somewhat flattened shape of the cluster may be an indication of rotation, and it has seemed advisable to examine the distribution of the measured nebulae. If the cluster is divided in two halves, north and south of decl.  $+10^{\circ}5$  (1950), we arrive at the results summarized in Table 16. The southern half appears to have a mean redshift that is about 400 km/sec larger than that of the northern half; on the other hand, almost two thirds of the measured nebulae are located in the latter area. This asymmetry in the apparent distribution must be partly an effect of a certain excess of bright nebulae in northern declinations, and partly an effect of observational selection. Since no large differences are found between the two halves of the cluster as regards the numbers of fainter nebulae, it seems justified to accept the unweighted mean of the redshifts of the northern and the southern area, or +1262 km/sec. The mean error, as derived from the dispersion in the individual redshifts, amounts to about 85 km/sec.

With an apparent distance modulus of 30.2, and a mean galactic absorption in the cluster area of 0.26 magn., the distance of the cluster is  $9.7 \cdot 10^6$  ps. Accordingly, the redshift parameter  $H$  will amount to  $130 \pm 9$  km/sec per  $10^6$  ps. It may be noted that the result is based on the assumption that the mean peculiar motion of the cluster along the line of sight is negligible.

The analysis of the writer's photometric material will be based on the spiral nebulae listed in Tables 14a and 14b, or on the same material that was used for

the absorption investigation of the preceding chapter. As appears from the second column of Table 17, redshift measures are available for 92 of these nebulae. Members of the local group have been omitted, and also NGC 3031, which is the only other case where the redshift is smaller than 100 km/sec. The third column gives for each nebular type the mean of  $S'_0$ , or the average photographic surface magnitude as defined above (comp. Table 14). It is interesting to note that in all the type classes these magnitudes are slightly brighter than those previously derived in Table 9, an indication of the observational selection in the redshift program.

The observed surface magnitude will now be transformed into total absolute magnitude by means of eq. (11b). This relation, as derived from the Virgo cluster members, is undoubtedly applicable to the material investigated here, an examination of the resulting magnitudes showing that their statistical distribution is more or less the same as the distribution found for the cluster nebulae. The fourth column of Table 17 gives the mean photographic luminosity (red. to incl. 90°) of each type of spiral nebulae. We find that the absolute magnitude ranges from  $-18.34$  (type  $Sc+$ ) to  $-19.88$  (type  $Sb-$ ), the mean for all the types taken together being  $-18.93$ .

From the mean absolute luminosities and the mean logarithmic redshifts, as listed in column 5, we are able to determine the redshift parameter  $H$ . Thus

$$5 \log H = M'_s - m'_0 + 5 \log V + 25.25.$$

The resulting means of  $\log H$  (with mean errors) are found in the sixth column of the table. From the entire material we get the final result,  $H=138 \pm 9$  km/sec per  $10^6$  ps.

The result obtained by means of the surface magnitudes of the field nebulae agrees rather closely with that found above from the Virgo cluster. We may conclude that the mean,  $H=134 \pm 6$  km/sec per  $10^6$  ps, represents the best possible solution from the photometric material analysed in this section.

In the seventh column of Table 17 we find the mean absolute photographic magnitudes (red. to incl. 90°) as derived from the observed redshifts by means of the above parameter ( $H=134$ ). Considering the mean errors, the agreement between  $M'_s$  and  $M'_v$  is reasonably good. If the two means are combined with equal weights, we arrive at the magnitudes contained in the last column of the table. These magnitudes represent the final results, as far as the present material is concerned, of the mean absolute luminosities of spiral nebulae of different types; obviously, the means correspond to a given apparent magnitude, and not to a given volume of space. It may be added that the final luminosities, combined with the mean surface magnitudes, lead to the following mean logarithmic diameters:  $\log A=4.15$  ( $Sc+$ ), 4.25 ( $Sc-$ ), 4.33 ( $Sb+$ ), 4.30 ( $Sb-$ ), and 4.25 ( $Sa$ ). The diameters thus range from 14000 to 21000 parsec.

The Virgo cluster undoubtedly is of the greatest importance for the extrapolation of the distance scale from nearby nebulae to the outer space. It may be recollect- ed that the results derived above are based on an apparent modulus of the cluster of 30.2. The long-term extragalactic program in progress at the Mount Wilson and

S 1964

Table 17. Determination of the redshift parameter  $H$  by means of distance moduli derived from surface magnitudes. Mean absolute magnitudes of spiral nebulae of different types.  
(app. dist. mod. of Virgo cluster = 30.2)

Type	N	$\bar{S}'_o$	$\bar{M}'_S$	$\log V$	$\log H$	$\bar{M}'_V$	$\frac{1}{2}(\bar{M}'_S + \bar{M}'_V)$
Sc+	20	+15.49	-18.34 ±.23	2.834	2.08 ±.05	-18.12 ±.23	-18.2
Sc-	33	15.28	18.81 ±.19	2.987	2.16 ±.05	18.95 ±.23	18.9
Sb+	21	15.18	19.04 ±.19	3.022	2.27 ±.06	19.76 ±.22	19.4
Sb-	9	14.81	19.88 ±.34	2.882	2.02 ±.10	19.35 ±.36	19.6
Sa	9	14.99	19.47 ±.22	2.997	2.03 ±.05	18.97 ±.20	19.2
All	92	+15.23	-18.93 ±.16	2.952	2.14 ±.029	-19.00 ±.13	-19.0

Palomar Observatories will eventually yield additional data regarding the cluster modulus. As pointed out by Sandage (in redshift cat.), there are some other smaller groups of nebulae that may also be used as stepping-stones for an extension of the distance scale. The most important of the groups listed by Sandage is the "Leo group", where redshifts are available for 18 members; the mean redshift amounts to  $788 \pm 62$  km/sec. Seven of these nebulae (NGC 3338—51—68, 3623—27—28, 3810) are included in the present catalogue; their mean surface magnitude is 15.08 ( $S'_o$  listed in Table 14), and the mean app. magnitude 9.95 (red. to incl.  $90^\circ$ ). In the writer's distance system (Virgo clust. mod.=30.2,  $H=134$ ) the apparent modulus of the Leo group will thus be 29.13 (from redshifts; gal. abs.= $0^m28$ ), or 29.22 (from surf. magn.), the mean errors being 0.2 and 0.3, respectively.

In conclusion, it will be recalled that Sandage (redshift cat.) has derived a redshift parameter from the Virgo cluster data of 176 km/sec per  $10^6$  ps. The deviation from the writer's result is mainly due to the different assumption concerning the distance modulus of the cluster. The rather high values derived from field nebulae ( $H=211$ ), and from clusters ( $H=180$ ), may be explained in a similar way. If, for instance, the upper limit of nebular luminosity is assumed to be  $-20.9$  ( $=-20.8$  in Sandage's photom. syst.), which is the abs. magnitude of the brightest Virgo cluster member (NGC 4472) as determined by the writer, the parameter obtained from field nebulae is reduced to 134 km/sec per  $10^6$  ps. The result found by Sandage was based on the assumption that the absolute magnitude of NGC 224, or  $-19.9$  as corresponding to the apparent magnitude (no incl. corr.) measured by the writer, represents the upper luminosity limit. However, it has been shown above that the luminosity is increased to  $-20.5$ , if the magnitude is reduced to incl.  $90^\circ$  to the line of sight.

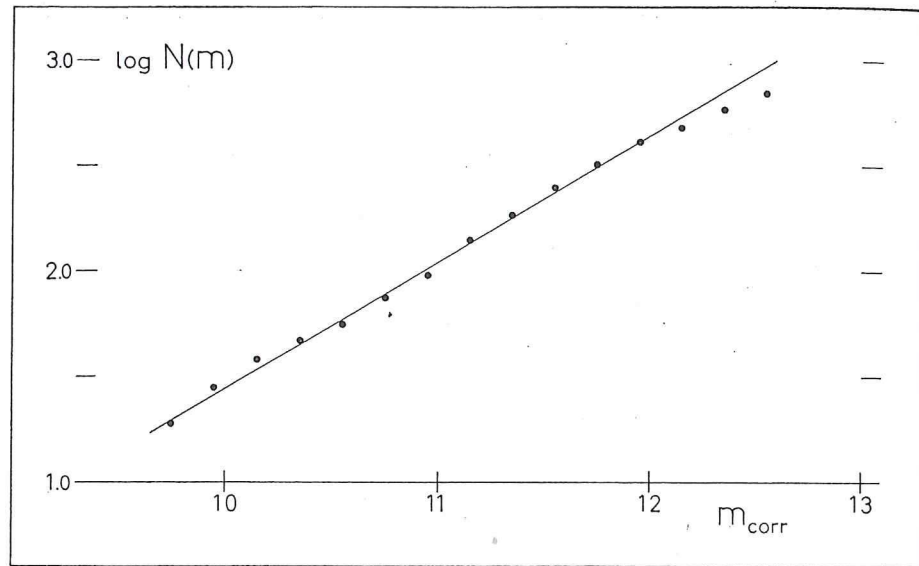


Fig. 12. Logarithmic distribution of apparent magnitudes, reduced to the writer's photometric system and to gal. lat.  $90^\circ$ , as found for nebulae in the Shapley-Ames survey catalogue.

#### 29. Magnitude distribution in Virgo cluster.

An examination of the statistical distribution of the apparent magnitudes of cluster members may be expected to yield some information about the general luminosity function of extragalactic nebulae. Unfortunately, the cluster population is not quite comparable to a random sample of non-cluster objects, the cluster exhibiting a certain excess of early-type nebulae; furthermore, the systematic changes in surface magnitude and color, as found in sect. 26, will have a disturbing effect. Since, however, the dispersion in absolute magnitude is very large, it does not seem likely that these deviations will cause any radical changes in the luminosity curve.

In order to correct for the background, we first have to determine the distribution of apparent magnitudes for nebulae in the general field. Since it covers the entire sky, the survey catalogue by Shapley-Ames (1932) gives the most complete data for this purpose. The systematic errors in the estimated magnitudes have been examined in sect. 10; comparisons with the writer's magnitudes and with the photoelectric measures by Stebbins-Whitford gave the result that the errors mainly depend on the surface magnitudes of the objects. If the corrections given by eq. (1b) are applied, and if the magnitudes are reduced to the galactic pole, we find for all nebulae with gal. lat.  $|B| > 30^\circ$  (Virgo area not included) the distribution curve reproduced in Fig. 12. The quantity  $\log N(m)$ , or the logarithmic number of objects brighter than the corrected magnitude  $m$ , appears to be a linear function

S 1964

of  $m$ . The inclination coefficient amounts to +0.60 — that is, the inclination corresponds to a *constant space density* of nebulae. A negative deviation is found only for objects fainter than magnitude 11.9. This effect is to be expected since the corrections applied to the estimated magnitudes (limit=13.0) are usually negative and in some cases reach, and even exceed, one magnitude. If  $\log N(m)$  is reduced to an area of one square degree, we arrive at the final relation,

$$\log N(m) = 0.6 m - 8.87. \quad (12)$$

The determination of the magnitude distribution in the Virgo cluster area will be based (a) on the photometric measures by the writer and by Stebbins-Whitford (1952), and (b) on the magnitudes estimated by Adelaide Ames (1930) in her survey catalogue referring to the cluster area. The photoelectric magnitudes are given a diaphragm correction of  $-0^m 1$ , as derived in sect. 8. Systematic corrections to the estimated magnitudes have been determined from comparisons with the photometric measures; from 100 objects we find the following correction to  $m_A$ :

$$\Delta m = -0.24 x - 0.36 y - 0.25, \quad (13)$$

where  $x$  means  $(m_A - 12.0)$ , and  $y$  stands for  $(2.5 \log ab - 1.0)$ ,  $a$  and  $b$  being the apparent diameters in minutes as computed from the data listed in the Ames catalogue. The correction formula, by which the estimated magnitudes are reduced to the writer's photometric system, may be compared with that derived for the Shapley-Ames magnitudes (eq. 1b). Since the dispersion of  $m_A$  about the above regression line amounts to  $0^m 29$ , the mean error of a corrected magnitude will be approximately equal to  $0^m 28$ .

About 70 % of the elliptical cluster area, as defined in sect. 25 (=124 square degrees), is covered by the plates of the Harvard survey. Within this smaller area, we find a distribution of apparent photographic magnitudes as given in the second column of Table 18. The first figure corresponds to photometric magnitudes, mainly measures by the writer, and the second figure to estimated magnitudes as corrected by the above formula. Down to magnitude 13.4 photometric measures are available for about half the number of nebulae. The third column of the table gives, for each magnitude interval, the number of background objects, as derived from eq. (12). By subtraction, we arrive at the probable number of cluster members listed in column 4. The disturbance caused by the background is rather small down to  $m=13.0 - 13.5$ , but increases fast as the magnitude becomes fainter.

The luminosity distribution derived for the cluster is reproduced in Fig. 13, where the absolute photographic magnitude (app. modulus=30.2) has been chosen as abscissa. The highest luminosity is obtained for NGC 4472 ( $M=-20.9$ ). For fainter magnitudes the class frequencies increase steadily down to  $M=-16.8$ ; below this limit we find a decrease, the observed numbers being considerably smaller than the expected ones (dotted curve). Since this effect cannot be eliminated by any reasonably large changes in the assumed background distribution, it seems

Table 18. Distribution of photographic magnitudes in the Virgo cluster.

Magnitude interval	Number of nebulae		
	Observed	Background	Cluster
9 <sup>m</sup> 0—9 <sup>m</sup> 4	1+0	0.0	1
9.5—9.9	2+0	0.1	2
10.0—10.4	9+0	0.1	9
10.5—10.9	4+1	0.2	5
11.0—11.4	5+4	0.4	9
11.5—11.9	12+4	0.9	15
12.0—12.4	13+13	1.7	24
12.5—12.9	12+17	3.4	26
13.0—13.4	11+27	6.9	31
13.5—13.9	7+27	14	(20)
14.0—14.4	5+29	27	(7)
14.5—14.9	4+63	55	(12)

[1] likely that it is caused by deficiencies in the Harvard catalogue. It is also possible [2] that the magnitude corrections derived above are not applicable to the fainter [3] magnitude classes, where the number of comparison objects is rather small. Thus, [4] the material discussed here does not permit any conclusions as regards the luminosity curve for the region below  $M = -16.8$ .

[5] Even with a complete observational material, it would not be possible to establish [6] the luminosity curve below  $M = -15$ , on account of the rapidly increasing [7] number of background objects. There is, however, no reason to assume that, for [8] medium and low luminosities, the curve deviates considerably from the curve [9] representing the local group of nebulae. It may be mentioned that Reaves (1956), [10] in a detailed study of the cluster area, has examined the possibilities of identifying [11] faint cluster members.

[12] If the median absolute magnitude of all cluster members is fainter than  $M = -15$ , [13] which seems likely, an integration of the curve in Fig. 13 leads to a total number [14] of cluster objects of at least 600. Since the curve only refers to the area covered [15] by the Harvard survey plates, the observed numbers have been multiplied by [16] the factor 1.25 in order to reduce them to the entire cluster area, as defined in [17] sect. 25. Without any special assumptions, the material available allows the determination [18] of two quantities which mainly depend on the most luminous magnitude classes, the total magnitude of the cluster, and the mean magnitude  $\bar{M}_m$ . The small contributions of nebulae with magnitudes fainter than  $M = -16.8$  may in both cases be estimated with a sufficient accuracy. We find that  $M_{tot} = -24.2$  ( $m_{tot} = +6.0$ ), as reduced to the entire cluster area, whereas  $\bar{M}_m = -19.6$ . The latter quantity, which in the general field (constant space density) represents the mean luminosity corresponding to a given class of apparent magnitude, is the weighted mean of the magnitudes of the individual cluster members, the weight

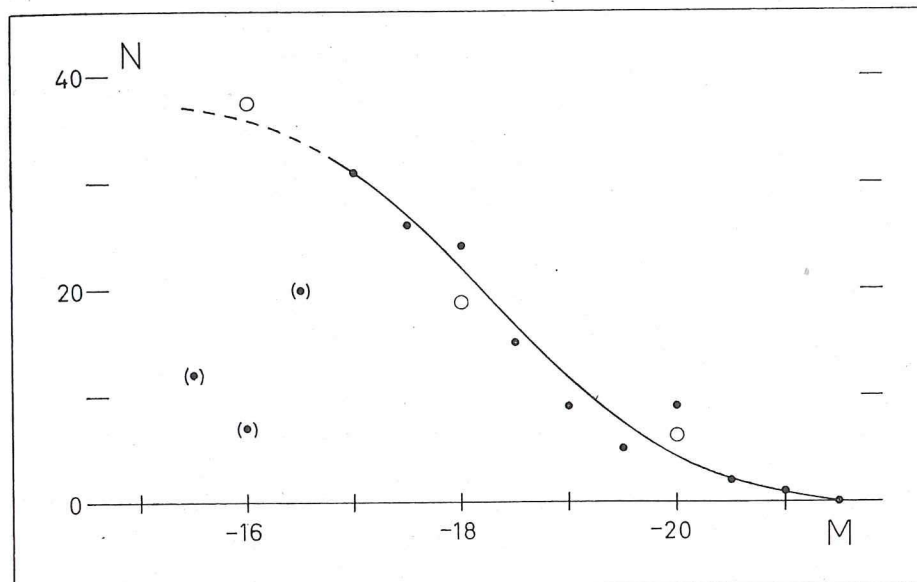


Fig. 13. Statistical distribution (corr. for background; dist. mod. = 30.2) of absolute photographic magnitudes of Virgo cluster nebulae (full circles). For comparison, the open circles give the distribution referring to the 20 brightest nebulae ( $M < -15$ ; abs. magn. based on rev. dist. mod.) of the local group and the groups around NGC 3031 and NGC 5457 (Holmberg 1950a; conversion factor = 12.5).

being proportional to  $10^{-0.6M}$ . The mean luminosity may seem to be rather high, as compared with the luminosities derived previously in Table 17 (last column) for spiral nebulae outside the cluster; it will be recollected that the magnitudes listed in this table are reduced to incl.  $90^\circ$  (mean corr. = -0.3 magn.), whereas the magnitudes of the cluster members are uncorrected. The difference is explained by the fact that among the most luminous cluster objects the elliptical nebulae are dominant: NGC 4472 ( $9^m3$ ), NGC 4486 ( $9^m6$ ), NGC 4649 ( $9^m9$ ), and NGC 4406 ( $10^m1$ ). If these four exceptional objects are omitted,  $\bar{M}_m$  is reduced to  $-19.1$ , a result that is in good agreement with the mean magnitudes derived in Table 17 for *Sb* and *Sa* spirals.

According to Table 18 (second column), photometric magnitudes are available for 69 of the nebulae with  $m \leq 13.4$ ; 67 of these objects have also been measured for color. If all the measured nebulae belong to the cluster, and if they are assumed to form a random sample as regards color, their integrated color index,  $+0^m74$ , would represent the difference between the total photographic and photovisual apparent magnitudes of the cluster. With a galactic selective absorption of  $0^m06$  (comp. sect. 14), and a mean redshift effect of  $0^m02$  (comp. sect. 15), the difference between the corresponding absolute magnitudes would amount to  $0^m66$ . The integrated color index of the Virgo cluster thus seems to be about the same as the mean color found for spiral nebulae of type *Sa* (comp. Table 13).

## CHAPTER V

## Investigation of Double Nebulae

## 30. Double nebulae as physical systems.

Among the various smaller agglomerations of extragalactic objects, the close double systems are of special interest from several points of view. The frequency of nebulae that are members of close pairs is comparatively high, and all types in the classification scheme are represented. The present catalogue includes a rather large number of double nebulae, the most well-known pairs being NGC 221—24, 4485—90, 4567—68, and 5194—95.

In some previous papers the writer (1937, 1940, 1941) has investigated the properties of double (and multiple) nebulae, either by examining the objects as they are revealed on photographic plates, or by using a statistical method of analysis. Data on close double systems may be assembled from survey plates by selecting all pairs for which the angular separation is less than a suitably defined maximum distance. If the separation is small enough, there is in most cases no doubt about a physical relationship between the components; the relationship is usually confirmed by subsequent redshift observations. On the other hand, it is possible (in a statistical sense) to separate physical and optical systems by an analysis of the distribution over the sky of all nebulae down to a certain limiting magnitude. This procedure, which is not based on any assumptions, leads to a complete statistical description of the physical systems as they actually exist in the sky.

In an attempt to find an explanation of the clustering tendencies among the nebulae, the writer has previously suggested that the agglomerations may be the results of captures between individual objects, brought about by tidal forces at close encounters. The theory seemed to be supported by the comparatively large number of double systems exhibiting strong tidal disturbances. Even with optimistic assumptions regarding the capture process, the time interval needed to transform a supposedly random space distribution of nebulae to the present spatial arrangement would however be considerably longer than the generally adopted time scale. It seems quite clear that during an interval of  $5 \cdot 10^9$  years relatively few close encounters, and consequently few captures, could have taken place. Only in exceptional cases (possibly NGC 5194—95; comp. sect. 32) could a capture by tidal forces be responsible for the formation of a double system. For the main part of the double nebulae, the time scale available seems *a priori* to permit only one formation process, namely, the disintegration of a larger system.

In the following sections a detailed investigation will be made of close double nebulae, particularly with regard to the possibility of finding any clues as to their origin from the observational data available.

### 31. Selection of material.

A study of magnitudes and colors of members of close physical systems may be based on the double nebulae listed in the catalogue. The writer has tried to include all well-known and interesting double systems in the original photometric program. Besides, a number of faint companions to bright program-nebulae have afterwards been found on the plates; when feasible, the magnitudes and colors of these additional objects have also been measured. The final catalogue includes a comparatively large number of close double (triple) nebulae; it has not seemed necessary to try to enlarge the material further by adding systems that may possibly be found in other photometric lists.

The selection of a material of supposedly physical systems, suitable for a statistical discussion, will in the first place be based on the angular separation of the components. In a previous analysis of the distribution of extragalactic objects over the sky, the writer (1940) has shown that the mean separation of physically related nebulae ranges from  $60'$  to  $15'$  as the mean apparent magnitude (Shapley-Ames magn. scale) of the components ranges from 10.0 to 13.0; a mean magnitude of about 12.5, as found for the nebulae selected below, corresponds to an average separation of approximately  $20'$ . In order to reduce the number of optical systems as far as possible, the latter distance will in the present case be adopted as the *maximum separation* permissible. As may be expected, practically all optical doubles are eliminated by this rigorous definition.

In the second place, the selection of physical systems may be based on the observed redshifts. If the difference in redshift between the components is small, for instance smaller than  $250 \text{ km/sec}$ , the system is in all probability a physical one. Unfortunately, redshifts are available only for a part of the material to be discussed below.

Outside the Virgo cluster area, as defined in sect. 25, 31 double nebulae with separations not exceeding  $20'$  are listed in the catalogue. They are collected in Table 19a. Among the double objects we find several well-known systems, as NGC 3623—27, NGC 4485—90, and NGC 5194—95. In two cases, as appears from the table, a third nebula is located within a distance of  $20'$  from the brightest component. The first column gives the NGC number (or other denotation), the nebulae in each group being listed in order of decreasing magnitude. Columns 2 and 3 give the color index  $C'_0$  and the photographic surface magnitude  $S'_0$  (only spirals  $Sa$  to  $Sc+$ ), respectively. The color index is reduced to gal. lat.  $90^\circ$  (comp. sect. 14) and to incl.  $90^\circ$  to the line of sight (only spirals; comp. sect. 13); the surface magnitude is also reduced to gal. lat.  $90^\circ$  and to incl.  $90^\circ$  (comp. sect. 19). In the last column of the table we find the redshifts (corr. for solar motion) of the individual nebulae, as observed at Mount Wilson-Palomar and at Lick (Humason, Mayall, and Sandage 1956); if two observations are available, the arithmetical mean has been accepted.

Tabel 19a. Double and triple nebulae in the writer's material (Virgo cluster excl.); maximum separation = 20'.

	NGC	C <sub>o</sub> '	S <sub>o</sub> '	V		NGC	C <sub>o</sub> '	S <sub>o</sub> '	V
	672	0 <sup>m</sup> 35	15 <sup>m</sup> 73	+ 496		4258	0 <sup>m</sup> 45	14 <sup>m</sup> 99	+ 494
	IC 1727	0. 26		518		4248	0. 46		—
	936	0. 84	15. 08	1367		4278	0. 77		615
	941	0. 36	15. 86	—		4283	0. 81		1062
	1042	0. 39	15. 50	334		4382	0. 78		721
	1052	0. 79		1466		4394	0. 82	15. 08	720
	1087	0. 36	15. 06	1835		4490	0. 26	14. 55	675
	1090	0. 43	16. 05	—		4485	0. 22	14. 80	—
	1325	0. 55	15. 39	—		4517	0. 50	15. 66	1098
	Ho VI	0. 43	15. 76	—		R 80	0. 30	16. 12	—
[1]	2276	0. 30	14. 64	2595		4618	0. 25	14. 94	541
[2]	2300	0. 96		2221		4625	0. 36	15. 41	—
[3]	2805	0. 32	15. 97	2021		4631	0. 38	15. 07	611
[4]	2820	0. 29	15. 51	—		4627	0. 48		—
[5]	2964	0. 43	14. 73	1286		4666	0. 49	15. 12	1531
[6]	2968	0. 99		—		4653	0. 36	15. 84	—
[7]	3169	0. 64	14. 99	1117		4668	0. 30		—
[8]	3166	0. 64	15. 05	1201		4725	0. 59	15. 39	1108
[9]	3193	0. 80		1272		4712	0. 35	15. 86	—
[10]	3190	0. 70	15. 01	1252		5194	0. 49	14. 47	546
[11]	3185	0. 61	15. 58	1142		5195	0. 98		650
[12]	3627	0. 55	14. 77	633		5364	0. 51	15. 59	1357
[13]	3623	0. 64	14. 66	588		5363	0. 85		1102
[14]	3718	0. 60		1128		5427	0. 50	14. 86	—
[15]	3729	0. 42	15. 00	—		5426	0. 42	15. 40	—
[16]	3738	0. 25		—		5746	0. 74	14. 98	1830
[17]	3756	0. 44	15. 47	—		5740	0. 57	15. 48	—
[18]	4036	0. 76		1506		5775	0. 62	15. 21	—
	4041	0. 38	14. 54	—		5774	0. 44	15. 76	—
	4088	0. 36	14. 62	820		5846	0. 84		1784
	4085	0. 36	15. 11	—		5850	0. 56	15. 36	2412
	4123	0. 35	15. 56	—					
	4116	0. 28	15. 69	1175					

S 1864

For five of the systems listed in the above table the redshift difference exceeds 250 km/sec, and four of these probably are optical pairs, as will be shown below. In a number of cases the redshifts of the components are very nearly the same. It may be noted that differential redshifts for two systems, NGC 4490—85 and NGC 5427—26, have been measured by Page (1952), the results being 155 and 96 km/sec, respectively.

A somewhat more extensive list of physically related nebulae is obtained by combining the above two selection principles. On the condition that redshifts are available for both components, and that the redshift difference is smaller than 250 km/sec, the angular separation permitted may be increased from 20' to 40'; owing to the limited redshift interval the great majority of optical pairs will probably still be eliminated. The result appears in Table 19 b, where the different columns contain the same information as in the previous table. As regards the nearby nebulae NGC 2403, NGC 3031, and NGC 5457, a maximum separation considerably larger than 40' has in fact been permitted, since there does not seem to be any doubt that the groups listed are physical ones; in the case of NGC 224 a distance of 40' is large enough to include the two elliptical companions. It is, of course, well known that each of the nearby groups actually contains more than three members; in order to restrict the investigation, only the two companions (satisfying the redshift condition) that are closest to the main nebula have however been included.

Outside the Virgo cluster area, the writer's material includes practically no nebulae that are fainter than  $13^m0 - 13^m5$ . If, down to this magnitude limit, the majority of extragalactic objects are assumed to have a more or less random distribution over the sky, it is possible to compute the relative number of optical companions that may have been included in the material selected above. By using the magnitude distribution curve derived in sect. 29 from the Shapley-Ames survey catalogue, we find that within a circular area of the sky having a radius of 20' we have to expect, accidentally, an average number of nebulae amounting to 0.03 (limit. magn. = 13.0), or 0.06 (limit. magn. = 13.5). This result implies that, if the redshift condition cannot be applied, 3 to 6 % of the companions listed in Table 19 a may be optical companions.

In the ideal case, a study of the properties of physical systems of nebulae should be based on a random sample from a given volume of space. Since this condition cannot be fulfilled, it is important that no serious selection effects be present in the material, especially effects that are related to the properties that are being investigated. The following analysis will mainly deal with the color indices and surface magnitudes of the selected nebulae. Since the writer's choice of double (triple) systems to be included in the photometric program has in no way been influenced by the colors, or the surface magnitudes, of the components (except for the necessary restriction due to the limiting magnitude), it may be assumed that the principal results to be derived below are representative of a more or less random sample.

### 32. Colors and surface magnitudes of double nebulae.

The integrated color indices listed in Tables 19 a and 19 b are in good systematic agreement with the mean colors (Table 7) derived previously for the different types

Table 19b. Double and triple nebulae in the writer's material (Virgo cluster excl.); maximum redshift diff. = 250 km/sec, maximum sep. = 40' (except for comp. of NGC 2403, 3031, 5457).

NGC	$C'_0$	$S'_0$	V	NGC	$C'_0$	$S'_0$	V
224	0m.62	14m.80	+ 5	3627	0m.55	14m.77	+ 633
205	0. 61		- 3	3628	0. 60	15. 17	728
221	0. 79		+ 28				
2403	0. 24	15. 57	187	4278	0. 77		615
2366	0. 28		229	4274	0. 70	15. 24	758
				4631	0. 38	15. 07	611
3031	0. 67	14. 69	+ 74	4656	0. 24		742
3077	0. 65		- 26	5457	0. 29	15. 40	394
2976	0. 61		+ 171	5474	0. 30	15. 45	394
				5585	0. 32	15. 74	466
3368	0. 68	15. 00	792				
3351	0. 67	15. 06	553				

[1] of nebulae. There is, however, a pronounced correlation between the colors of the members of each group. In the following analysis the brightest component (photogr. magn.) of a double (triple) system will be denoted by  $a$ , and the second (third) brightest with  $b$  ( $c$ ). The relation between the color indices  $C'_0$  of components  $a$  and  $b$  ( $c$ ) appears from the plot in Fig. 14. The open circles refer to those five pairs in Table 19a that have differential redshifts exceeding 250 km/sec, whereas the full circles represent the remaining part of the material.

[2] The figure indicates quite clearly that there is a marked agreement between the colors, all but 4 of the 39 full circles being distributed along the  $45^\circ$ -line in a comparatively narrow lane. It seems possible, or even likely, that three of the discordant pairs (NGC 936—41, 2964—68, 4036—41) are optical systems. None of them is a close pair, and the components do not exhibit any signs of gravitational disturbance; redshifts are available for only one component in each system. In the fourth case (NGC 5194—95), the physical relationship is apparently well established; on account of the strong tidal disturbances it is however tempting to assume that this pair has been formed by a capture process, in which case there would be no reason to expect any correlation between the colors of the components. It is interesting to note that the pairs with large redshift differences (open circles) have a distribution in the color diagram that is quite different from the distribution corresponding to the main part of the material.

[3] If we omit the systems with diff. redshifts larger than 250 km/sec, and the four discordant pairs mentioned above, the following coefficient of correlation is obtained:

$$r = +0.80 \pm 0.06 \text{ (m.e.)}$$

[4] The agreement indicated by the figure is thus confirmed numerically. It may be remarked that the correlation is to some degree disturbed by the accidental errors

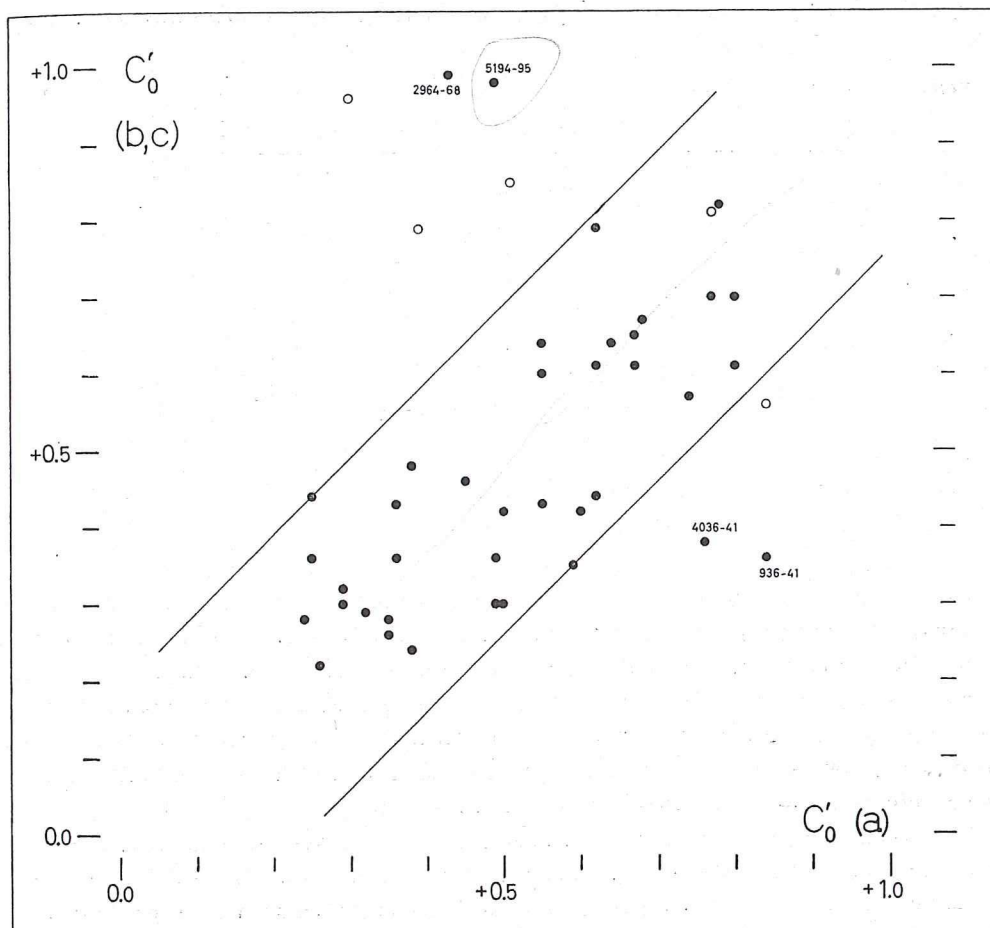


Fig. 14. Relation between comp.  $a$  and comp.  $b$  ( $c$ ) in double (triple) systems as regards integrated color index (red. to lat.  $90^\circ$  and to incl.  $90^\circ$ ).

in the color measures. The derived coefficient is inversely proportional to the product of the dispersions in the color indices of comp.  $a$  and comp.  $b$  ( $c$ ); if these dispersions are corrected for the effect caused by the mean error ( $\epsilon = 0^m 052$ ; comp. Table 2), the coefficient will be increased to  $+0.88$ .

Since the integrated color of a nebula is closely related to the type (comp. Table 7), it would be of interest to extend the statistical investigation to the types of the above objects. The types are listed in the catalogue; in a few cases the type description is not complete, in other cases the type has been denoted as peculiar (*Ep*, *SOp*). If the latter objects are omitted, and if the material is otherwise the same as that used for the computation of the coefficient  $r$ , we get the result reproduced in Table 20. The correlation is high, but not quite so pronounced as that

6\*

Table 20. Relation between the type of component *a* and the type of component *b* (*c*).

	E	Component <i>a</i>							
		Ir II	SO	Sa	Sb-	Sb+	Sc-	Sc+	Ir I
Component <i>b</i> ( <i>c</i> )	E, Ir II	—	—	—	2	—	—	—	—
	SO	—	—	—	—	—	—	—	—
	Sa	3	—	1	—	1	—	—	—
	Sb-	—	1	—	—	—	—	—	—
	Sb+	—	—	1	1	1	—	—	—
	Sc-	—	—	—	—	3	3	—	1
	Sc+	—	—	—	—	—	3	4	—
	Ir I	—	—	—	—	—	1	3	—

found for the colors. It seems likely that the agreement between the types is only a secondary effect.

The photographic surface magnitudes,  $S'_0$ , of the individual spiral nebulae in Tables 19a and 19b are in good systematic agreement with the mean magnitudes previously derived in Table 9 for the different spiral classes. Also in this case there is, surprisingly enough, a pronounced relation between comp. *a* and comp. *b* (*c*), as appears from the plot in Fig. 15 (936—41 omitted). In order to reduce the disturbing effects of the internal nebular absorption, the comparison is based on the photovisual surface magnitudes  $S'_0 - C'_0$ ; in fact, the photovisual magnitudes have been corrected by  $-0^m 21$  ( $Sc+$ ,  $Sc-$ ), and by  $-0^m 32$  ( $Sb+$ ,  $Sb-$ ,  $Sa$ ), to eliminate the internal absorption entirely (comp. sect. 19). To get a larger material, the figure includes not only the 20 pairs of spirals, but also five pairs (672—1727, 3738—56, 4666—68, 2403—2366, 4631—56) in which a spiral is combined with an *Ir I* system. In the computation of surface magnitude and absorption correction, the *Ir I* nebulae have been treated as if they were  $Sc+$  nebulae, the internal absorption in both cases apparently being more or less the same (comp. sect. 23); the five pairs (denoted by crosses) agree well with the other part of the material.

Of the 25 pairs investigated, 24 are distributed in a comparatively narrow lane in the figure. As regards the deviating pair, NGC 2805—20, it may be recollected that the colors agree well with the previous color diagram; since, however, only one redshift determination is available, the possibility of an optical system cannot be excluded. If NGC 2805—20 is omitted, we find a correlation between comp. *a* and comp. *b* (*c*) that is measured by the coefficient

$$r = +0.82 \pm 0.07 \text{ (m.e.)}.$$

The correlation in surface magnitude is thus comparable to that found in the colors. If the result is corrected for the disturbances caused by the accidental errors in the magnitude and diameter measures, the coefficient is increased to about +0.9.

It seems quite certain that the observed correlation between the surface magni-

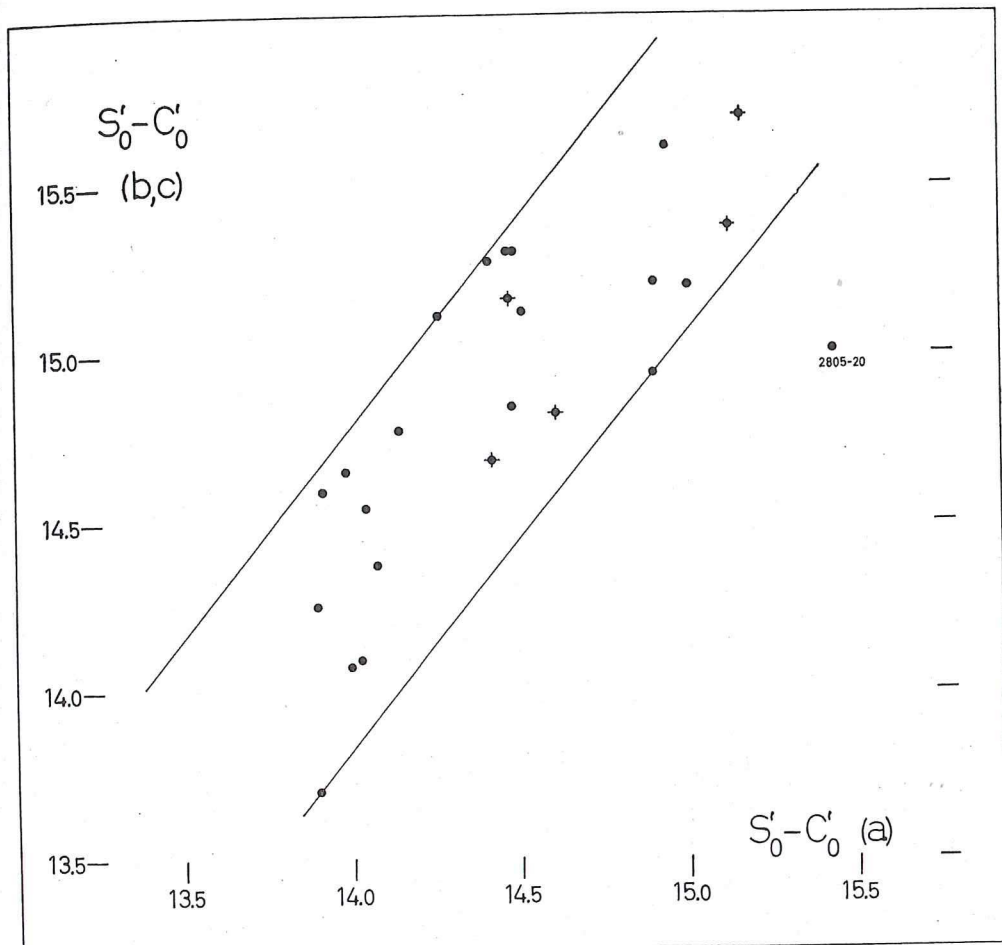


Fig. 15. Relation between comp. *a* and comp. *b* (*c*) in double (triple) systems as regards photo-visual surface magnitude (red. to lat.  $90^\circ$  and corr. for internal absorption).

tudes is to be explained as an indirect result of an agreement between the mean luminosity densities (aver. amount of light per cubic ps) of the physically related nebulae. The difference between surface magnitude (multipl. by  $-0.4$ ) and logarithmic luminosity density is, apart from a constant, equal to the logarithm of the smallest diameter (in ps), or the thickness, of the nebular disc; since this diameter is not known, the luminosity density cannot be directly computed. It should however be noted that the relation derived in Fig. 15 deviates from the  $45^\circ$ -line, the surface magnitude of comp. *b* (*c*) being fainter than that of comp. *a*; if the luminosity densities are more or less the same, the deviation is explained by the fact that comp. *b* (*c*) in practically all cases has a smaller apparent (major) diameter, and supposedly a smaller thickness, than comp. *a*. In fact, if we assume that the densities

of the two components are *exactly* the same, we are able to compute (from the surf. magn.) the relative thickness of  $b$  ( $c$ ), expressed in units of the relative thickness of  $a$ ; the resulting ratios have a geometric mean close to 1.0, and the dispersion is reasonably small. We may thus conclude that if the surface magnitudes could be replaced by the corresponding logarithmic luminosity densities, the observed relation would be turned into a  $45^\circ$ -relation. The agreement in mean luminosity density between the physically related nebulae must be equivalent to an agreement in mean mass density, the mass/lum. ratio being approximately the same for nebulae of the same intrinsic colors.

The results of the above analyses indicate that the components of a close physical system have (a) stellar contents of a similar type, and (b) mean luminosity densities (mean mass densities) that are approximately the same. The simplest, and most direct explanation of this agreement would be obtained if we assume that the majority of double systems were formed (by disintegrations of single nebulae) quite recently, in which case the two components may be considered as separate, but quite comparable parts of the same nebula. If the double systems were formed at an early stage, we have to face the difficulty of explaining why the evolutionary process has been the same for both components, as is indicated by the stellar contents observed at present. Since the mass densities are correlated (but apparently not the total masses; comp. next sect.), a possible explanation is offered by the hypothesis that the mass density is a fundamental evolutionary parameter.

An inspection of the writer's plate material shows that there are a number of nebulae in which a disintegration seems to be in progress at the present time; the most interesting cases are NGC 2366, 4088, 4485—90, and 4656.

As regards a possible influence of the mass density on the evolution of a stellar system, the writer would like to refer to a previous investigation (Holmberg 1952) of the masses of nebulae of different types. According to the preliminary results derived in this paper, the mean mass density increases by a factor of about 10 as we pass along the type sequence from *Ir I* systems to "early" spirals and elliptical nebulae. The results obtained in the investigation of the surface magnitudes of spiral nebulae (sect. 19) point in the same direction. The mean surface luminosity increases considerably from *Sc+* (or *Ir I*) to *Sb-* (or *Sa*); since the relative number of type II stars, having a higher mass/lum. ratio than type I stars, also gets larger (comp. sect. 23), the result will be a substantial increase in the projected mass density.

### 33. Examination of total magnitudes.

A study of the material listed in the previous tables will give some information about the total magnitudes of the members of close physical systems. As before, we shall omit the four pairs not agreeing with the color diagram, and the systems with diff. redshifts larger than 250 km/sec. It appears that the difference in integrated photographic magnitude, comp.  $a$  minus comp.  $b$  ( $c$ ), ranges from —0.05 (3738—56) to —4.73 (224—21), the mean being —1.68. On an average, the principal nebula is thus almost five times as bright as its companion.

S1364

The dispersion in the magnitude differences amounts to 2.1. A dispersion of this size seems to exclude the possibility of any appreciable correlation between the absolute luminosities of the components. If the correlation is zero, the dispersion in the absolute magnitudes of the individual nebulae would amount to  $2.1/\sqrt{2}$ , or 1.5. Considering the fact that this figure is a minimum value, the photometric program not including objects below a certain limiting magnitude, we may conclude that the magnitude dispersion for nebulae that are members of physical groups is very likely of the same order of size as the dispersion corresponding to a random sample of nebulae in a given volume of space (probably at least 2 magn.). It should be added that, if the correlation between the luminosities of physically related nebulae is small, or zero, no appreciable correlation can be expected between the masses of the same objects.

The mean absolute magnitude of the spiral nebulae in the above tables can be derived by means of the observed redshifts. Adopting a redshift parameter  $H$  of 134 km/sec per  $10^6$  ps (comp. sect. 28), we find a mean magnitude, reduced to incl.  $90^\circ$ , of  $-18.5$ . This mean may be compared with the results listed in columns 7 and 8 of Table 17; for the same mixture of spiral types we get from both columns a mean magnitude of  $-18.8$ . The physically related nebulae included in the writer's material have thus practically the same mean luminosity as that found for the entire material. The same conclusion may be drawn from an examination of the surface magnitudes, the latter quantities being used previously (comp. sect. 27) as indicators of absolute luminosity. The mean surface magnitude,  $S'_0$ , of the spiral nebulae in the physical groups is almost exactly the same as the mean obtained from Table 9 for a similar distribution of types. Indirectly, the agreements in total magnitude and surface magnitude indicate that there must be a similar agreement as regards absolute dimensions.

Finally, the data listed in the tables may be used to check the relation between surface magnitude and absolute magnitude, as established in sect. 27 by means of the members of the Virgo cluster. A comparison, referring to the pairs of spiral nebulae in the tables, between differential surface magnitude  $\Delta S'_0$  and differential apparent magnitude  $\Delta m'_0$  (photogr. magn. red. to lat.  $90^\circ$  and to incl.  $90^\circ$ ) gives the mean result,  $\Delta S'_0 = +0.18 \Delta m'_0$ . The coefficient is the same as that derived in sect. 27.

The above comparisons have not revealed any significant divergencies. In the magnitude interval covered by the writer's photometric program, there does not seem to be any systematic differences between the individual members of close physical systems and a random sample of nebulae. We may conclude that if the systems have been formed by disintegrations, the original parent nebulae must, on an average, have had brighter absolute magnitudes, and probably larger masses, than those corresponding to single nebulae observed at present.

### References

- Ames, Adelaide 1930, *Ann. Harv. Coll. Obs.* 88, 1. A catalogue of 2778 nebulae, including the Coma-Virgo group.
- Arp, H. C. 1956, *A.J.* 61, 15. Novae in the Andromeda nebula.
- Baade, W. 1951, *Mich. Obs. Pub.* 10, 7. Galaxies — present day problems.
- Baade, W., and Mayall, N. U. 1951, *Problems of cosmical aerodynamics*, 165, Central air documents office, Dayton, Ohio. Distribution and motions of gaseous masses in spirals.
- Baade, W., and Swope, Henrietta H. 1955, *A.J.* 60, 151. The Palomar survey of variables in M 31 (First results).
- Baum, W. A. 1955, *Pub. A.S.P.* 67, 328. The distribution of luminosity in elliptical galaxies.
- . 1957, *A.J.* 62, 6. Photoelectric determinations of redshifts beyond 0.2 c.
- Baum, W. A., and Schwarzschild, M. 1955, *A.J.* 60, 247. A comparison of stellar populations in the Andromeda galaxy and its elliptical companion.
- Bigay, J. H. 1951, *Ann. Astroph.* 14, 319. Photométrie photographique des nébuleuses extragalactiques.
- Bigay, J. H., and Dumont, R. 1954, *ibid.* 17, 78. Déterminations photoélectriques de magnitudes globales de nébuleuses extragalactiques.
- Bigay, J. H., Dumont, R., Lenouvel, F., and Lunel, M. 1953, *ibid.* 16, 133. Photométrie photoélectrique de nébuleuses extragalactiques.
- Elvius, Aina 1956, *Ann. Obs. Stockholm* 18, No. 9. Diffraction of light by interstellar particles in spiral galaxies.
- Harrington, R. G., and Wilson, A. G. 1950, *Pub. A.S.P.* 62, 118. Two new stellar systems in Leo.
- Holmberg, E. 1937, *Ann. Obs. Lund*, No. 6. A study of double and multiple galaxies.
- . 1940, *Ap.J.* 92, 200. On the clustering tendencies among the nebulae.
- . 1941, *ibid.* 94, 385. On the clustering tendencies among the nebulae. II.
- . 1946, *Medd. Lunds Astr. Obs.*, Ser. II, No. 117. On the apparent diameters and the orientation in space of extragalactic nebulae.
- . 1950a, *ibid.*, No. 128. A photometric study of nearby galaxies.
- . 1950b, *Medd. Lunds Astr. Obs.*, Ser. I, No. 170. A study of the absorption in NGC 5195.
- . 1952, *ibid.*, No. 180. On the masses and luminosities of extragalactic nebulae.
- van Houten, C. J., Oort, J. H., and Hiltner, W. A. 1954, *Ap.J.* 120, 439. Photoelectric measurements of extragalactic nebulae.
- Hoyle, F., and Sandage, A. 1956, *Pub. A.S.P.* 68, 301. The second-order term in the redshift-magnitude relation.
- Hubble, E. 1926, *Ap.J.* 64, 321. Extra-galactic nebulae.
- . 1934, *ibid.* 79, 8. The distribution of extra-galactic nebulae.
- Humason, M. L., Mayall, N. U., and Sandage, A. R. 1956, *A.J.* 61, 97. Redshifts and magnitudes of extragalactic nebulae.
- van de Kamp, P. 1932, *A.J.* 42, 97. On the absorption of light in the galactic system.
- Lindblad, B. 1941, *Ann. Obs. Stockholm* 13, No. 8. On the distribution of light-intensity and colour in the spiral nebula NGC 7331.
- . 1942, *ibid.* 14, No. 3. On the absorption of light in the central region of the spiral nebula NGC 7331 and related subjects.

## Catalogue

The catalogue gives the results obtained in the photographic photometry of 300 extragalactic nebulae. The different columns are explained as follows:

Column 1: Designation of the object. The nebulae are listed in the following order:

(a) NGC objects, (b) IC objects, and (c) Anon. objects. Additional information concerning some of the nebulae (also coordinates of anon. objects) are found in the notes at the end of the catalogue.

Column 2: Galactic coordinates from the Lund Observatory tables (Ohlsson 1932), interpolated from the position reduced to 1900. The position corrections given by Reinmuth (1926) and by Shapley-Ames (1932) have been taken into account.

Column 3: Telescope used in the observations. Most of the plates have been taken with the 60-inch (60) and 100-inch (100) reflectors at Mount Wilson; for a few nebulae plates have been taken with the 10-inch refractor (10) at Mount Wilson, with the 24-inch and 40-inch reflectors (40) at the Hamburg Observatory, and with the 48-inch Schmidt telescope (48) at the Palomar Observatory.

Column 4: Type of the nebula, as determined by the writer. The classification system, which is described in sect. 12, includes the sub-types *E*, *Ir II*, *SO*, *Sa*, *Sb-*, *Sb+*, *Sc-*, *Sc+*, and *Ir I*.

Column 5: Apparent major and minor diameters, as derived from microphtometer tracings of 103a-0 plates (photogr. reg.). The diameters refer to the part of the nebula contained within a standard isophote (comp. sect. 2).

Column 6: Integrated photographic and photovisual magnitudes in int. system, and numbers of individual measures (in parentheses). The magnitudes represent the amounts of light contained within a standard isophote (comp. sect. 2); the mean errors are listed in Table 2.

Column 7: Integrated color index, as derived from the magnitude measures; the mean errors are listed in Table 2.

## CATALOGUE

Object	L	B	Instr.	Type	Diam.	$m_{pg}$	$m_{pv}$	C
NGC 147	87°.9	-14°.0	60, 40	Ep	18' 12'	10 <sup>m</sup> 57(5)	9 <sup>m</sup> 73(4)	+0 <sup>m</sup> 84
157	82.3	-70.8	60	Sc-	5.8 3.8	11. 17(2)	10. 46(2)	0. 71
185	88.9	-14.2	60, 40	Ep	14. 12.	10. 29(5)	9. 43(4)	0. 86
205	89.0	-20.9	60, 40	Ep	26. 16.	8. 89(5)	8. 17(4)	0. 72
221	89.4	-21.7	60	E	12. 8.	9. 06(3)	8. 16(3)	0. 90
224	89.5	-21.3	10	Sb-	197. 92.	4. 33(3)	3. 47(3)	0. 86
247	94.1	-83.3	10	Sc	28. 10.	9. 47(2)	—	—
404	95.4	-26.6	60	SO	5.5 5.5	11. 16(1)	10. 24(2)	0. 92
428	104.4	-60.8	60	Sc+	5.5 3.8	11. 74(2)	11. 43(2)	0. 31
488	106.5	-56.1	60	Sb-	7.8 5.5	11. 10(1)	10. 25(2)	0. 85
520	108.4	-57.3	60	Ir II	6.8 2.9	12. 35(2)	11. 54(2)	0. 81
578	157.4	-78.6	60	Sc-	7.2 4.5	11. 37(3)	10. 99(2)	0. 38
598	102.1	-30.7	10	Sc+	83. 53.	6. 19(3)	5. 79(3)	0. 40
628	107.6	-45.0	60	Sc-	12.0 12.0	9. 74(2)	9. 33(2)	0. 41
660	110.6	-46.5	60	Sp	9.8 4.4	11. 85(2)	11. 12(2)	0. 73
672	106.6	-33.1	60	Sc+	11.3 4.1	11. 31(2)	10. 88(2)	0. 43
753	106.0	-24.4	60	Sc-	4.0 3.5	12. 91(2)	12. 41(2)	0. 50
772	113.2	-40.2	60	Sb+	10.5 6.8	11. 10(3)	10. 43(2)	0. 67
784	109.4	-30.8	60	Sc+	9.7 2.6	12. 13(2)	11. 78(2)	0. 35
803	116.0	-42.5	60	Sc-	4.6 2.3	12. 90(1)	12. 38(1)	0. 52
891	108.5	-16.7	60	Sb+	15.0 3.8	10. 85(2)	10. 03(2)	0. 82
908	169.7	-66.8	60	Sc-	8.7 4.4	10. 74(3)	10. 19(2)	0. 55
925	113.1	-24.3	60	Sc+	14.0 8.6	10. 53(2)	10. 13(2)	0. 40
936	137.4	-54.0	60	Sa	6.3 5.5	11. 21(2)	10. 33(2)	0. 88
941	137.6	-53.8	60	Sc+	4.5 2.8	12. 84(2)	12. 45(2)	0. 39
1003	112.1	-16.7	60	Sc+	7.7 3.5	11. 92(2)	11. 49(2)	0. 43
1023	113.1	-18.2	60	SO	11.6 4.3	10. 48(2)	9. 51(2)	0. 97
1042	150.5	-56.7	60	Sc-	6.8 6.0	11. 43(2)	11. 01(2)	0. 42
1052	150.4	-56.6	60	E	4.5 2.9	11. 69(1)	10. 89(2)	0. 80
1055	139.9	-50.4	60	Sb+	11.9 4.8	11. 38(2)	10. 60(2)	0. 78
1058	114.5	-19.5	60	Sc-	6.0 6.0	11. 74(2)	11. 20(2)	0. 54
1068	140.7	-50.6	60	Sb-	10.0 8.0	9. 63(2)	8. 91(2)	0. 72
1073	139.5	-49.4	60	Sc+	6.3 5.5	11. 43(2)	11. 02(2)	0. 41
1087	142.3	-50.3	60	Sc-	5.9 3.9	11. 45(2)	11. 02(2)	0. 43
1090	142.0	-50.1	60	Sb+	7.9 3.0	12. 51(2)	11. 98(2)	0. 53
1156	124.5	-28.1	60	Ir I	5.9 5.9	11. 85(2)	11. 47(2)	0. 38
1232	176.1	-56.3	60	Sc-	9.5 8.9	10. 46(2)	10. 00(2)	0. 46
1300	175.6	-53.8	60	Sb+	8.0 4.8	11. 11(2)	10. 58(2)	0. 53
1325	179.6	-53.4	60	Sb+	6.6 2.5	12. 22(2)	11. 57(2)	0. 65
NGC 1337	161.4	-47.0	60	Sc+	7.2 2.6	12. 26(3)	11. 83(2)	0. 43

Object	L	B	Instr.	Type	Diam.		m <sub>pg</sub>	m <sub>pV</sub>	C
NGC 1560	105°.6	+16°.7	60	Sc+	11'.9	2'.2	12m19(2)	11m59(2)	+0m60
1569	111.1	+12.1	60	Ir I	6.9	3.2	11.75(2)	11.17(2)	0.58
1637	167.2	-28.5	60	Sc-	7.7	6.3	11.26(2)	10.75(2)	0.51
1784	179.4	-27.4	60	Sc-	5.8	3.7	12.39(2)	11.82(2)	0.57
1961	111.0	+20.3	60	Sb+	7.7	6.0	11.68(2)	11.06(2)	0.62
1964	192.7	-25.2	60	Sb+	8.2	3.0	11.61(2)	10.93(1)	0.68
2146	102.7	+25.5	60	Sp	8.4	4.8	11.26(2)	10.68(2)	0.58
2268	96.2	+28.0	60	Sc-	4.6	2.8	12.18(2)	11.57(2)	0.61
2276	94.6	+28.2	60	Sc+	4.0	4.0	11.91(2)	11.54(2)	0.37
2300	94.6	+28.2	60	E	3.5	3.3	12.25(2)	11.22(2)	1.03
2336	100.9	+28.7	60	Sc-	10.4	6.1	11.03(2)	10.52(2)	0.51
2366	113.7	+29.4	60	Ir I	10.0	5.3	11.41(3)	11.07(3)	0.34
2403	117.6	+30.2	60, 40	Sc+	29.	15.	8.80(5)	8.48(2)	0.32
2500	135.2	+32.8	60	Sc+	3.9	3.7	12.13(2)	11.67(2)	0.46
2525	199.7	+12.0	60	Sc-	4.2	3.2	12.30(2)	11.67(2)	0.63
2541	137.3	+34.8	60	Sc+	8.6	4.2	11.88(2)	11.49(2)	0.39
2655	101.7	+33.3	60	Sa	7.7	6.2	10.92(2)	10.16(2)	0.76
2681	134.3	+40.9	60	Sa	5.4	5.4	11.33(2)	10.65(2)	0.68
2683	157.9	+40.2	60	Sb-	12.1	3.9	10.53(2)	9.72(2)	0.81
2685	124.6	+40.0	60	SO <sub>P</sub>	5.5	3.6	12.04(1)	11.38(1)	0.66
2715	101.5	+34.0	60	Sc-	6.5	2.8	11.87(3)	11.42(2)	0.45
2763	212.1	+21.9	60	Sc-	3.4	3.4	12.57(2)	12.09(2)	0.48
2805	116.7	+41.2	60	Sc+	8.0	6.0	11.68(2)	11.32(1)	0.36
2820	116.5	+41.2	60	Sc+	4.7	1.4	13.16(3)	12.81(2)	0.35
2841	133.8	+45.4	60	Sb-	11.3	5.7	10.10(2)	9.38(2)	0.72
2903	176.7	+46.1	60	Sc-	13.9	9.0	9.48(2)	9.01(2)	0.47
2964	162.1	+50.5	60, 100	Sc-	4.3	2.4	11.89(2)	11.38(2)	0.51
2968	162.0	+50.6	60, 100	Ir II	3.9	2.9	12.79(2)	11.78(2)	1.01
2976	110.5	+41.7	60	Sp	9.7	5.7	10.73(4)	10.09(3)	0.64
2977	103.4	+37.4	60	S	2.9	1.3	13.25(1)	—	—
2985	105.6	+39.4	60	Sb+	7.5	5.3	11.11(2)	10.49(2)	0.62
3003	159.8	+51.8	60	Sc	7.5	3.3	12.04(2)	11.74(2)	0.30
3027	105.4	+39.8	60	Sc+	6.4	3.6	12.31(1)	—	—
3031	108.7	+41.7	60, 40, 10	Sb-	35.	14.4	7.85(5)	7.00(6)	0.85
3034	108.0	+41.3	60	Ir II	13.4	8.5	9.20(3)	8.39(3)	0.81
3061	101.8	+37.4	60	Sc-	2.6	2.6	13.44(1)	—	—
3077	108.4	+42.4	60	Ir II	8.8	8.0	10.57(3)	9.89(3)	0.68
3079	124.3	+49.4	60	Sc-	11.0	2.3	11.10(2)	10.59(2)	0.51
3166	206.8	+46.7	60	Sa	6.9	3.3	11.49(2)	10.70(2)	0.79
NGC 3169	206.9	+46.8	60	Sa	6.1	5.1	11.24(2)	10.54(2)	0.70

31964

Object	L	B	Instr.	Type	Diam.	$m_{pg}$	$m_{pv}$	C
NGC 3183	101°9	+39°8	60	Sb+	3'.6	2'.5	12 <sup>m</sup> 59(1)	—
3184	145.2	+57.0	60	Sc-	9.5	9.5	10. 28(2)	9. 84(2)
3185	181.4	+56.1	100	Sa	3.9	2.6	12. 90(2)	12. 20(2)
3187	181.1	+56.2	100	S	4.3	1.6	13. 62(2)	13. 27(2)
3190	181.2	+56.3	100	Sa	5.9	2.4	11. 96(2)	11. 10(2)
3193	181.2	+56.4	100	E	4.8	4.6	11. 83(2)	11. 02(2)
3198	137.8	+56.1	60	Sc-	11.9	4.9	10. 82(2)	10. 43(2)
3319	142.6	+60.7	60	Sc+	8.8	4.3	11. 67(2)	11. 38(2)
3338	199.2	+58.3	60	Sc-	9.4	5.7	11. 25(2)	10. 84(2)
3344	178.2	+62.7	60	Sc-	9.3	9.0	10. 38(2)	10. 07(2)
3351	202.9	+57.6	60	Sb+	9.3	6.4	10. 48(2)	9. 76(2)
3359	109.9	+49.4	60	Sc-	9.0	5.6	10. 89(2)	10. 51(2)
3364	101.3	+42.3	60	Sc-	2.2	2.2	13. 40(1)	—
3368	203.5	+58.2	60	Sa	10.8	7.8	10. 05(2)	9. 29(2)
3423	213.4	+55.4	60	Sc+	5.7	5.5	11. 48(2)	11. 19(2)
3432	151.7	+64.6	60	Sc+	8.2	2.4	11. 59(1)	11. 28(2)
3486	169.9	+67.0	60	Sc-	9.8	7.2	11. 00(2)	10. 61(2)
3521	224.9	+53.6	60, 100	Sb-	13.6	7.0	10. 06(3)	9. 23(3)
3556	114.2	+57.2	60	Sc+	11.1	4.5	10. 57(2)	10. 12(2)
3623	211.1	+65.3	60	Sa	11.9	4.5	10. 18(2)	9. 37(2)
3627	211.8	+65.5	60	Sb+	13.8	6.5	9. 65(2)	9. 02(2)
3628	210.7	+65.9	60	Sb+	18.	4.3	10. 23(2)	9. 53(2)
3631	115.2	+60.0	60	Sc-	7.2	7.2	10. 91(2)	10. 45(2)
3642	108.4	+55.3	60	Sc-	7.7	7.4	11. 52(2)	11. 17(2)
3646	196.4	+69.7	60	Sc-	5.0	3.7	11. 82(2)	11. 28(2)
3718	112.6	+61.1	60	SO <sub>p</sub>	8.1	4.7	11. 24(2)	10. 63(2)
3726	120.7	+65.9	60	Sc-	8.2	6.3	10. 84(2)	10. 48(2)
3729	112.2	+61.2	60	Sc-	4.6	3.1	11. 88(2)	11. 41(2)
3738	110.1	+60.1	60	Ir I	4.4	3.2	12. 00(2)	11. 74(2)
3756	110.1	+60.4	60	Sc-	5.5	3.1	12. 05(2)	11. 54(2)
3810	223.6	+68.1	60	Sc-	6.1	4.0	11. 30(3)	10. 81(2)
3938	118.6	+70.3	60	Sc-	6.8	6.6	10. 79(2)	10. 42(2)
3953	107.4	+63.4	60	Sb+	9.4	6.5	10. 71(2)	10. 14(2)
3992	105.3	+62.6	60	Sb+	9.6	6.5	10. 62(2)	9. 92(2)
4036	98.8	+54.8	60	SO	5.0	3.0	11. 48(2)	10. 70(2)
4041	98.5	+54.6	60	Sc-	4.2	4.1	11. 48(2)	11. 09(2)
4051	113.2	+71.0	60	Sb+	8.0	5.8	10. 81(2)	10. 20(1)
4085	105.4	+65.9	60	Sc-	3.7	1.5	12. 79(2)	12. 34(2)
4088	105.2	+65.7	60	Sc-	6.5	2.8	11. 03(2)	10. 58(2)
NGC 4096	108.1	+68.6	60	Sc+	8.9	3.7	10. 88(2)	10. 60(2)

Object	L	B	Instr.	Type	Diam.	$m_{pg}$	$m_{pv}$	C	
NGC 4111	113°6	+72°6	60	SO	6'3	1'8	11 <sup>m</sup> 63(2)	10 <sup>m</sup> 91(2)	+0 <sup>m</sup> 72
4116	248.5	+63.7	60	Sc+	5.1	3.7	12. 29(3)	11. 99(2)	0. 30
4123	248.7	+63.9	60	Sc+	5.9	5.0	11. 79(3)	11. 42(2)	0. 37
4165	240.0	+73.9	100	Sc-	2.2	1.6	14. 45(1)	13. 72(1)	0. 73
4168	240.1	+73.8	100	E	4.2	3.6	12. 32(1)	11. 39(1)	0. 93
4178	243.8	+71.8	60	Sc+	7.3	3.1	11. 75(2)	11. 42(2)	0. 33
4189	241.0	+74.2	100	Sc-	3.4	2.9	12. 51(2)	11. 85(2)	0. 66
4192	238.3	+75.5	60	Sb+	11.6	3.2	10. 89(2)	10. 20(2)	0. 69
4193	241.4	+74.0	100	Sb+	3.6	1.9	13. 15(2)	12. 38(2)	0. 77
4206	242.8	+74.0	60	Sc-	6.6	1.6	12. 69(2)	12. 14(2)	0. 55
4212	241.7	+74.8	100	Sc-	4.8	3.8	11. 71(2)	11. 08(2)	0. 63
4214	123.0	+79.2	60	Ir I	10.6	10.6	10. 12(1)	9. 85(2)	0. 27
4216	243.2	+74.2	60	Sb-	10.4	3.7	10. 88(2)	9. 94(2)	0. 94
4224	250.0	+68.9	100	Sa	4.2	1.8	12. 89(2)	11. 86(2)	1. 03
4233	250.3	+69.1	100	SO	3.7	1.9	13. 03(2)	12. 02(2)	1. 01
4235	250.6	+68.7	100	Sa	5.7	1.6	12. 58(2)	11. 63(2)	0. 95
4236	93.6	+47.8	60	Sc+	26.	8.7	10. 05(2)	9. 82(2)	0. 23
4241	251.3	+68.2	100	Sa	4.0	2.2	13. 00(2)	12. 03(2)	0. 97
4242	104.8	+71.0	60	Sc+	7.6	7.2	11. 39(1)	11. 02(1)	0. 37
4244	117.2	+78.1	60	Sc+	18.	2.9	10. 48(2)	10. 20(2)	0. 28
4246	251.1	+68.8	100	Sc-	3.6	2.4	13. 33(2)	12. 72(2)	0. 61
4248	103.0	+69.3	60	S	5.0	2.1	13. 07(2)	12. 61(2)	0. 46
4254	243.7	+75.6	60	Sc-	7.3	6.0	10. 37(2)	9. 90(2)	0. 47
4258	102.5	+69.5	60	Sb+	24.	9.6	8. 90(2)	8. 38(2)	0. 52
4259	253.4	+67.1	100	SO	2.0	1.1	14. 58(2)	13. 67(2)	0. 91
4268	253.7	+67.0	100	SO	2.7	1.4	13. 79(2)	12. 77(2)	1. 02
4270	253.6	+67.2	100	SO	2.7	1.8	13. 13(2)	12. 24(2)	0. 89
4273	253.8	+67.1	100	Sc-	3.4	2.6	12. 35(2)	11. 85(2)	0. 50
4274	156.8	+84.1	100	Sa	8.7	3.5	11. 33(1)	10. 48(1)	0. 85
4277	253.9	+67.1	100	S	2.0	1.8	14. 48(2)	13. 54(2)	0. 94
4278	159.8	+84.2	100	E	6.3	6.1	11. 20(1)	10. 43(1)	0. 77
4281	254.0	+67.2	100	SO	4.8	3.0	12. 32(2)	11. 37(2)	0. 95
4283	159.4	+84.3	100	E	2.3	2.3	13. 27(1)	12. 46(1)	0. 81
4294	249.6	+73.1	100	Sc-	4.3	2.1	12. 46(2)	12. 08(2)	0. 38
4298	245.8	+76.1	60, 100	Sc-	5.2	4.4	11. 95(2)	11. 38(2)	0. 57
4299	249.9	+73.2	100	Sc+	3.1	3.0	12. 71(2)	12. 47(2)	0. 24
4301	255.7	+66.4	60	Sc+	2.8	2.4	13. 29(2)	13. 02(2)	0. 27
4302	246.0	+76.1	60, 100	S	7.7	2.5	12. 44(2)	11. 64(2)	0. 80
4303	255.4	+66.4	60	Sc-	10.7	7.4	10. 01(2)	9. 64(2)	0. 37
NGC 4312	245.2	+77.0	60	S	6.3	2.0	12. 50(2)	11. 80(2)	0. 70

Object	L	B	Instr.	Type	Diam.	$m_{pg}$	$m_{pv}$	C
NGC 4321	245°1	+77°3	60	Sc-	10'.0	9'.1	10 <sup>m</sup> 07(2)	9 <sup>m</sup> 45(2)
4341	255.1	+68.9	100	Sa	3.9	2.2	13. 22(2)	12. 29(2)
4342	255.0	+69.0	100	E	2.0	1.3	13. 48(2)	12. 60(2)
4343	255.2	+69.1	100	SO	2.9	1.4	14. 16(2)	13. 29(2)
4371	252.4	+73.6	100	SO	6.3	3.9	11. 83(2)	10. 91(2)
4374	251.2	+74.7	60	SO	10.7	10.5	10. 21(3)	9. 36(3)
4382	243.0	+79.7	100	SO	10.9	8.3	10. 05(2)	9. 27(2)
4388	252.2	+74.5	60	S	8.6	2.7	11. 73(3)	11. 06(3)
4394	243.6	+79.8	100	Sb-	4.5	4.5	11. 81(2)	10. 99(2)
4395	122.6	+82.6	60	Sc+	15.	11.	10. 66(2)	10. 29(1)
4402	251.9	+75.0	60	S	5.6	2.1	12. 47(3)	11. 78(3)
4406	252.2	+74.9	60	E	12.0	10.3	10. 10(3)	9. 25(3)
4410A	255.7	+71.1	100	S	2.4	2.0	13. 73(2)	12. 79(2)
4410B	255.7	+71.1	100	S	2.0	2.0		
4411A	255.8	+70.9	100	Sc+	3.3	3.3	13. 45(2)	12. 86(2)
4411B	256.1	+70.9	100	Sc+	3.6	3.6	12. 93(2)	12. 43(2)
4417	255.6	+71.6	100	SO	4.9	3.0	12. 11(1)	11. 33(1)
4424	256.0	+71.5	100	S	5.6	2.8	12. 32(1)	11. 75(1)
4425	253.3	+74.7	60	S	3.7	1.9	12. 84(3)	11. 96(3)
4429	255.0	+73.2	100	SO	7.7	4.7	11. 09(2)	10. 15(2)
4435	253.5	+75.1	60	SO	4.1	3.1	11. 86(3)	11. 03(3)
4438	253.5	+75.0	60	Sap	10.5	5.5	10. 92(3)	10. 20(3)
4442	256.4	+71.9	100	SO	6.8	3.0	11. 61(1)	10. 74(1)
4445	256.8	+71.6	100	S	3.9	1.1	13. 61(1)	12. 88(1)
4449	100.2	+73.0	60	Ir I	10.1	8.7	9. 90(2)	9. 68(2)
4450	249.0	+79.0	60	Sb-	8.8	6.0	10. 81(2)	10. 11(2)
4472	258.8	+70.2	60	E	11.7	11.0	9. 33(2)	8. 49(2)
4480	260.8	+66.5	100	Sc-	3.2	2.0	13. 03(1)	12. 43(1)
4485	100.6	+75.4	60	Sc+	3.3	3.1	12. 24(2)	12. 02(2)
4486	256.9	+74.6	60	E	10.7	10.7	9. 56(2)	8. 74(2)
4490	100.6	+75.5	60	Sc+	8.9	4.7	10. 09(2)	9. 81(2)
4496A	261.7	+66.3	100	Sc+	5.2	5.2	11. 93(2)	11. 47(2)
4496B	261.7	+66.3	100	Sc+	2.1	2.1		
4501	256.3	+76.6	60	Sb+	9.4	5.5	10. 07(2)	9. 48(2)
4517	263.3	+62.5	60	Sc-	12.7	3.5	11. 10(2)	10. 49(2)
4519	261.2	+71.0	60	Sc-	4.2	3.2	12. 22(3)	11. 84(2)
4527	263.5	+65.1	60	Sb-	7.5	3.5	11. 29(2)	10. 51(2)
4532	262.6	+68.9	100	Ir I	4.0	2.6	12. 17(2)	11. 94(2)
4535	262.0	+70.6	60	Sc-	9.9	8.9	10. 38(3)	9. 87(2)
NGC 4536	263.8	+64.6	60	Sc-	8.9	4.4	10. 94(2)	10. 48(2)

	Object	L	B	Instr.	Type	Diam.	$m_{pg}$	$m_{pv}$	C
	NGC 4539	255°0	+80°5	100	Sa	4'.5	2'.3	12 <sup>m</sup> 81(1)	12 <sup>m</sup> 06(1)
	4548	259.8	+76.9	60	Sb+	7.7	5.6	10. 86(2)	10. 32(2)
	4559	165.	+87.9	60	Sc+	11.6	6.6	10. 26(2)	9. 97(2)
	4564	262.4	+73.9	60	E	5.2	2.9	12. 17(1)	11. 33(1)
	4565	217.	+87.6	60	Sb+	20.	3.6	10. 30(2)	9. 56(2)
	4567	262.5	+73.7	60	Sc-	5.4	3.7	11. 98(2)	11. 34(2)
	4568	262.6	+73.7	60	Sc-	6.8	3.5	11. 66(2)	10. 89(2)
	4569	262.0	+75.6	60	Sb+	11.7	5.8	10. 11(2)	9. 62(2)
	4571	261.5	+76.6	60	Sc+	5.4	5.2	11. 63(2)	11. 26(2)
	4576	265.2	+66.8	100	Sc-	2.0	1.4	14. 18(2)	13. 52(2)
Fi	4579	263.4	+74.3	60	Sb-	9.6	6.4	10. 32(2)	9. 61(2)
	4586	265.8	+66.8	100	Sa	5.4	2.7	12. 54(2)	11. 62(2)
	4594	268.0	+50.9	60, 100	Sa	12.0	10.6	9. 18(2)	8. 29(2)
	4596	265.8	+72.7	100	Sa	6.0	5.1	11. 41(1)	10. 51(1)
	4606	266.3	+74.4	100	Sa	4.5	2.7	12. 66(2)	11. 93(2)
[1]	4607	266.4	+74.4	100	S	4.2	1.4	13. 72(2)	12. 89(2)
[2]	4608	266.9	+72.7	100	SO	4.6	4.4	12. 02(1)	11. 16(1)
[3]	4618	92.5	+76.3	60	Sc+	6.0	5.6	11. 08(2)	10. 83(2)
[4]	4625	92.3	+76.3	60	Sc+	3.5	2.5	12. 82(2)	12. 45(2)
[5]	4627	96.8	+84.8	60	S	3.7	3.4	13. 01(2)	12. 53(1)
[6]	4631	96.3	+84.9	60	Sc+	19.	4.4	9. 71(2)	9. 29(2)
[7]	4633	267.2	+76.9	100	Sc+	3.4	1.6	13. 69(2)	13. 18(2)
[8]	4634	267.6	+76.8	100	S	4.3	1.5	13. 10(2)	12. 44(2)
[9]	4639	267.8	+75.8	60	Sb+	4.0	3.5	12. 11(2)	11. 53(2)
[10]	4647	268.7	+74.1	100	Sc-	4.8	3.2	12. 05(2)	11. 63(2)
[11]	4649	268.8	+74.1	100	E	9.9	9.1	9. 88(2)	8. 97(2)
[12]	4651	268.5	+78.9	60	Sc-	6.1	4.5	11. 21(2)	10. 78(2)
[13]	4653	269.4	+62.0	100	Sc-	4.4	3.9	12. 69(2)	12. 31(2)
[14]	4654	269.0	+75.7	60	Sc-	7.0	4.9	11. 03(2)	10. 50(2)
[15]	4656	92.	+85.3	60	Ir I	14.5	4.1	10. 74(2)	10. 50(1)
[16]	4666	270.0	+62.1	100	Sc-	6.7	3.1	11. 40(2)	10. 83(2)
[17]	4668	270.2	+62.0	100	Ir I	2.4	1.7	13. 44(2)	13. 13(2)
[18]	4689	272.8	+76.3	60	Sc-	5.9	5.6	11. 48(2)	10. 95(2)
	4698	272.6	+71.0	100	Sa	6.5	4.5	11. 56(2)	10. 73(2)
	4712	297.	+87.7	60, 100	Sc-	3.7	1.6	13. 46(2)	13. 03(2)
	4725	302.	+87.7	100	Sb+	12.1	10.0	10. 07(1)	9. 46(1)
	4736	85.1	+76.3	60	Sb-	15.	13.3	8. 91(2)	8. 28(2)
	4747	313.	+87.7	100	Sc-	4.5	2.6	12. 90(1)	12. 40(1)
	4826	295.5	+83.6	60	Sb-	12.3	8.3	9. 27(2)	8. 51(2)
	NGC 5005	61.8	+78.9	60	Sb+	8.1	4.7	10. 52(2)	9. 89(2)

S1364

Object	L	B	Instr.	Type	Diam.	$m_{pg}$	$m_{pv}$	C
NGC 5033	58°2	+79°0	60	Sc-	12'3 5'8	10 <sup>m</sup> 61(2)	10 <sup>m</sup> 18(2)	+0 <sup>m</sup> 43
	68.5	+74.1	60	Sb+	16. 10.1	9. 26(2)	8. 65(2)	0. 61
	277.7	+18.9	48	Ep	31. 25.	7. 87(2)	6. 98(2)	0. 89
	68.8	+68.4	60	Sc-	14.2 9.5	8. 88(3)	8. 35(3)	0. 53
	68.8	+68.3	60	Ir II	8.9 7.4	10. 47(3)	9. 49(3)	0. 98
	5204	+58.0	60	Sc+	8.0 4.2	11. 62(2)	11. 36(2)	0. 26
	306.2	+67.6	60	Sc-	7.9 6.1	10. 36(2)	9. 93(2)	0. 43
	310.4	+62.1	60	Ir II	6.4 4.5	11. 13(2)	10. 27(2)	0. 86
	310.2	+61.9	60	Sc-	8.3 7.7	11. 04(2)	10. 51(2)	0. 53
	302.3	+51.5	60, 100	Sc-	4.0 2.2	12. 71(3)	12. 21(3)	0. 50
NGC 5427	302.4	+51.5	60, 100	Sc-	3.9 3.8	11. 98(3)	11. 46(3)	0. 52
	67.2	+59.5	10, 40	Sc-	28. 28.	8. 20(3)	7. 90(3)	0. 30
	66.0	+59.9	60	Sc+	7.2 6.8	11. 22(3)	10. 91(2)	0. 31
	66.5	+56.2	60	Sc+	8.7 5.7	11. 25(2)	10. 90(2)	0. 35
	323.0	+51.5	60, 100	Sb+	4.8 2.6	12. 55(2)	11. 90(2)	0. 65
NGC 5746	323.5	+51.6	60, 100	Sb-	9.0 2.4	11. 57(2)	10. 63(2)	0. 94
	327.8	+51.1	100	Sc-	4.3 3.7	12. 71(2)	12. 23(2)	0. 48
	327.8	+51.0	100	Sb+	5.7 2.5	12. 15(2)	11. 44(2)	0. 71
	328.7	+47.4	60	E	5.3 5.3	11. 16(2)	10. 30(2)	0. 86
	328.8	+47.2	60	Sb+	6.0 6.0	11. 56(2)	10. 98(2)	0. 58
NGC 5907	57.5	+50.6	60	Sb+	15.7 2.0	11. 04(2)	10. 41(2)	0. 63
	62.0	+43.7	60	Sc+	6.3 2.9	11. 69(2)	11. 24(2)	0. 45
	357.9	+19.3	60	Sb+	8.2 5.0	11. 23(2)	10. 59(2)	0. 64
	74.0	+31.2	60	Sc-	3.8 3.4	12. 19(2)	11. 80(2)	0. 39
	67.4	+30.4	60	Sc-	11.2 4.0	10. 77(2)	10. 24(2)	0. 53
NGC 6643	72.4	+28.1	60	Sc-	5.1 2.7	11. 61(2)	11. 09(2)	0. 52
	353.1	-19.9	10	Ir I	20. 20.	9. 21(3)	—	—
	63.1	+11.3	60	Sc-	14.4 12.6	9. 67(3)	8. 96(3)	0. 71
	68.2	+14.6	60	Sb+	6.4 5.2	11. 84(2)	11. 09(2)	0. 75
	54.7	-20.3	60	Sb-	7.4 6.1	11. 00(2)	10. 20(2)	0. 80
NGC 7331	62.0	-21.1	60	Sb+	13.5 7.0	10. 27(2)	9. 56(2)	0. 71
	73.5	-19.0	60	Sc+	13.5 3.6	11. 31(2)	11. 00(2)	0. 31
	73.2	-34.5	60	Sc+	7.2 4.0	11. 63(2)	11. 22(2)	0. 41
	112.4	-18.7	60	Sc-	6.5 6.3	11. 83(1)	11. 24(1)	0. 59
	105.8	+36.6	60	Sc-	5.5 2.4	12. 54(1)	—	—
IC 1613	99.2	-60.3	10, 40	Ir I	23. 23.	10. 00(6)	9. 61(5)	0. 39
	106.5	-33.2	60	Ir I	10.2 3.4	12. 10(2)	11. 79(2)	0. 31
	111.2	-26.1	60	Sb+	3.1 1.6	13. 98(1)	13. 17(1)	0. 81
	141.4	+34.4	60	S	6.7 1.3	12. 99(2)	12. 64(2)	0. 35
	106.6	+44.3	60	Ir I	16. 8.0	10. 91(3)	10. 62(3)	0. 29

	Object	L	B	Instr.	Type	Diam.	$m_{pg}$	$m_{pv}$	C
IC	3061	241°0	+74°9	100	S	3'.5 0'9	14 <sup>m</sup> 27(2)	13 <sup>m</sup> 61(2)	+0 <sup>m</sup> 66
	3115	251.6	+68.2	100	Sc-	3.0 2.9	13. 66(2)	13. 10(2)	0. 56
	3259	255.0	+69.1	100	Sc-	3.0 1.9	14. 24(2)	13. 61(2)	0. 63
IC	3267	255.3	+69.0	100	Sc-	2.7 2.6	14. 12(2)	13. 47(2)	0. 65
Ho	I	107.4	+39.4	60	Ir I	5.3 5.1	13. 27(4)	12. 98(2)	0. 29
Ho	II	111.2	+33.6	60	Ir I	11.0 8.9	11. 14(4)	10. 80(2)	0. 34
	III	105.4	+36.2	60	Sc+	4.0 4.0	12. 94(1)	—	—
	IV	68.8	+60.6	60	S	6.5 2.7	12. 95(1)	—	—
	V	72.9	+61.2	60	Sc-	3.5 2.6	13. 23(1)	—	—
	VI	179.3	-53.2	60	Sc-	3.2 2.8	13. 33(2)	12. 86(2)	0. 47
Ho	VII	262.9	+68.7	100	Ir I	2.5 2.5	14. 59(2)	14. 22(2)	0. 37
	VIII	57.1	+79.4	60	Ir I	3.2 3.1	13. 46(2)	13. 28(2)	0. 18
	Reinm. 80	263.1	+62.7	60	Sc+	5.4 4.9	12. 52(2)	12. 21(2)	0. 31
	Wolf-Lundm.	48.4	-74.5	60	Ir I	12.6 6.5	11. 14(4)	10. 87(2)	0. 27
	Leo A	164.5	+53.9	60	Ir I	7.0 4.5	12. 96(2)	12. 69(2)	0. 27
[1]	Leo B	189.1	+68.6	60	Ep	11.0 10.0	12. 85(2)	12. 04(2)	0. 81
[2]	Pegasus	63.9	-43.9	60	Ir I	7.7 4.6	12. 50(2)	12. 06(2)	0. 44
[3]	Regulus	194.5	+50.4	60	Ep	12.0 9.5	11. 27(3)	10. 40(3)	0. 87
[4]	Sextans A	214.8	+40.9	60	Ir I	9.3 8.6	11. 55(2)	11. 32(1)	0. 23
[5]	Sextans B	201.7	+45.0	60	Ir I	7.7 5.9	11. 82(2)	11. 49(2)	0. 33

## Notes

- [6] NGC 147, 185. The photographic magnitudes are slightly fainter than those given previously (Holmberg 1950a); in each case, three of the former plates (long exp., heavy sky fog) have been replaced by new exposures.
- [7] NGC 221. Diameter measures are uncertain on account of the heterogeneous background (NGC 224); the listed diameters are very likely too small.
- [8] NGC 224. In a recent investigation (soon to be published), based on the same photometric method as that used in the present paper, G. Lyngå has derived an integrated photographic magnitude of 4.23 (int. syst.) for NGC 224. The result is obtained from four Palomar 18-inch Schmidt plates (long-exp.), supplemented by 60-inch plates (short-exp.), taken by the writer in 1951 (all plates calibrated by means of NP-stars). Since the magnitude refers to a limiting isophote of about 28<sup>m</sup>0 per square second, the result is in good agreement with the integrated magnitude listed in the present catalogue.
- [9] NGC 404. Measurement somewhat disturbed by nearby bright star ( $\beta$  Androm. only 7' from nebula).
- [10] NGC 1961. Note the coordinate corrections given by Reinmuth (1926).
- [11] NGC 2276. Measurement slightly disturbed by nearby bright star.
- [12] NGC 2805. Previously listed by the writer (1950a) as a possible member of the group around NGC 3031; recent redshift determination (Humason, Mayall, and Sandage 1956) rules out membership.
- [13] NGC 2820. Companion of NGC 2805.

S1364

- NGC 2977. According to identification by Reinmuth (1926); nebula belongs to the survey area around NGC 3031.
- NGC 3027. Previously listed as a possible member of the NGC 3031 group; recent redshift determination rules out membership.
- NGC 3061. According to identification by Reinmuth (1926); nebula belongs to survey area around NGC 3031.
- NGC 3187. This nebula belongs to the group around NGC 3190; except for the peculiar shape of the spiral arms (gravitational disturbance from NGC 3190?), the object would have been classified as a  $Sc+$  spiral.
- NGC 3338. Measurement slightly disturbed by nearby bright star; major diameter assumed to be twice the radius of the undisturbed half of the nebula.
- NGC 3364. Belongs to the survey area around NGC 3031.
- NGC 4165. Faint companion of NGC 4168.
- NGC 4241. Measurement slightly disturbed by nearby bright star.
- NGC 4259. Faint companion of NGC 4273.
- NGC 4277. Faint companion of NGC 4273.
- NGC 4301. Companion of NGC 4303; note coordinate corrections given by Reinmuth (1926).
- NGC 4342. According to identification by Reinmuth (1926).
- NGC 4343. According to identification by Reinmuth (1926); both 4342 and 4343 are companions of NGC 4341.
- NGC 4410 A,B. Close pair of two small spirals on same plate as NGC 4411 A, B; the components have approximately the same magnitude and color (separation =  $0'3$ ).
- NGC 4411 A,B. Double system of two spiral nebulae (separation =  $4'4$ ). Component A has the position listed in the NGC for 4411; however, IC 3339 has practically the same position (description also correct). The position of component B agrees with the revised position suggested by Dreyer for NGC 4411 in his «Notes and Corrections to the New General Catalogue», given as a supplement to the Second Index Catalogue.
- NGC 4429. Measurement slightly disturbed by nearby bright star.
- NGC 4496 A,B. Close double system (separation =  $0'9$ ) of two spirals of similar color; magnitude difference = 1.5—2.0.
- NGC 4517. Note right ascension correction given by Reinmuth (1926).
- NGC 4567—68. The total magnitudes represent the integrated light on either side of the division line between the two nebulae that corresponds to minimum plate density; the diameters of the components have been put equal to twice the corresponding radii, as derived for the undisturbed halves of the nebulae.
- NGC 4571. Measurement disturbed by nearby bright star.
- NGC 4576. Faint companion of NGC 4586.
- NGC 4594. On account of the unusually large and prominent central bulge, this nebula is not quite comparable to other early-type spirals in the catalogue; although the orientation is almost edgewise, the ratio of the measured diameters amounts to 0.9.
- NGC 4647—49. Very interesting close pair (separation =  $2'6$ ); the faint spiral system is almost entirely within the boundaries of the bright elliptical nebula. In this case the tracings have been made parallel to a line connecting the two nuclei, and the total magnitudes of the components have been derived on the assumption that the surface luminosity distribution in the elliptical nebula is symmetrical.
- NGC 5128. This well-known radio source has been measured (by request of Dr. R. Minkowski) on two  $103\alpha-O$  plates and two  $103\alpha-D$  plates (yellow plexiglas filter) taken with the Palomar 48-inch Schmidt telescope by Mr. G. O. Abell on March 28—29, 1955; the plates are calibrated by means of polar exposures.

Although the nebula has been observed close to the meridian, the altitude is only about  $14^\circ$ , and the extinction corrections are naturally somewhat uncertain. Since the derived color index (red. to gal. lat.  $90^\circ$ ) is rather close to the mean color found for elliptical nebulae (Table 7), the adopted extinction values are probably of the right order of magnitude. The distribution of surface luminosity, and the absorption produced by obscuring material in the superposed spiral system, will be studied in a subsequent paper.

- NGC 5194—95. Compare note given for NGC 4567—68.  
 NGC 5363. Measurement disturbed by projected star close to the nucleus.  
 NGC 5426—27. Close double system; compare note given for NGC 4567—68.  
 NGC 5907. According to Reinmuth (1926)=NGC 5906—07.  
 IC 239. Measurement disturbed by nearby stars.  
 IC 529. One of the nebulae in the survey area around NGC 3031 (Holmberg 1950a).  
 IC 1727. This nebula and NGC 672 form an interesting double system (separation= $8'$ ).  
 IC 1784. When possible, IC-nebulae that are described as "large" have been included in the photometric program; the description does not seem to be justified in this case.  
 IC 2233. One of the "large" objects in the IC.  
 IC 3061. Faint companion of NGC 4212.  
 IC 3115. Companion of NGC 4241.  
 IC 3259. Companion of NGC 4343; identification according to Reinmuth (1926).  
 IC 3267. Companion of NGC 4343; identification according to Reinmuth (1926).  
 Ho I. One of the nebulae discovered in the survey area around NGC 3031;  $\alpha = 9^h 36^m 2$ ,  $\delta = +71^\circ 26'$  (1950).  
 Ho II. Discovery in survey area around NGC 3031;  $\alpha = 8^h 14^m 1$ ,  $\delta = +70^\circ 52'$  (1950).  
 According to recent redshift determination (Humason, Mayall, and Sandage 1956) the nebula is a member of the 3031-group.  
 Ho III. Discovery in survey area around NGC 3031;  $\alpha = 9^h 9^m 5$ ,  $\delta = +74^\circ 28'$  (1950).  
 Ho IV. Discovery in survey area around NGC 5457;  $\alpha = 13^h 53^m 0$ ,  $\delta = +54^\circ 8'$  (1950). According to recent redshift determination the nebula is a member of the 5457-group.  
 Ho V. Discovery in survey area around NGC 5457;  $\alpha = 13^h 38^m 8$ ,  $\delta = +54^\circ 35'$  (1950).  
 Ho VI. Companion of NGC 1325;  $\alpha = 3^h 22^m 7$ ,  $\delta = -21^\circ 31'$  (1950).  
 Ho VII. Faint companion of NGC 4532;  $\alpha = 12^h 32^m 2$ ,  $\delta = +6^\circ 34'$  (1950).  
 Ho VIII. Companion of NGC 5033;  $\alpha = 13^h 11^m 0$ ,  $\delta = +36^\circ 28'$  (1950).  
 Reinm. 80. Companion of NGC 4517 (comp. Shapley-Ames 1932);  $\alpha = 12^h 30^m 0$ ,  $\delta = +0^\circ 38'$  (1950).  
 Wolf-Lundm. This remarkable system was first noted by M. Wolf at Heidelberg, and was later rediscovered by K. Lundmark and P. J. Melotte (comp. MN 86, 636, 1926);  $\alpha = 0^h 0^m$ ,  $\delta = -15^\circ 45'$  (1950).  
 Leo A. Palomar discovery (Zwicky 1942);  $\alpha = 9^h 56^m 5$ ,  $\delta = +30^\circ 59'$  (1950).  
 Leo B. Palomar discovery (Harrington and Wilson 1950);  $\alpha = 11^h 10^m 8$ ,  $\delta = +22^\circ 26'$  (1950).  
 Pegasus. Palomar discovery (Wilson);  $\alpha = 23^h 26^m 1$ ,  $\delta = +14^\circ 29'$  (1950).  
 Regulus. Palomar discovery (Harrington and Wilson 1950);  $\alpha = 10^h 5^m 8$ ,  $\delta = +12^\circ 33'$  (1950). Measurement is somewhat disturbed by nearby  $\alpha$  Leonis.  
 Sextans A. Palomar discovery (Zwicky 1942);  $\alpha = 10^h 8^m 6$ ,  $\delta = -4^\circ 27'$  (1950).  
 Sextans B. Palomar discovery (Wilson);  $\alpha = 9^h 57^m 3$ ,  $\delta = +5^\circ 34'$  (1950).

- Lindblad, B., and Delhayé, J. 1949, *ibid.* **15**, No. 9. On the distribution of light-intensity and colour in the spiral nebula Messier 63.
- Lindblad, B., and Elvius, Aina 1952, *Nature* **169**, 1042. A diffraction corona near the centre of the spiral nebula NGC 4216.
- McVittie, G. C. 1956, *Chapman and Hill, London*. General relativity and cosmology.
- Morgan, W. W., and Mayall, N. U. 1957, *Pub. A.S.P.* **69**, 291. A spectral classification of galaxies.
- Ohlsson, J. 1932, *Ann. Obs. Lund*, No. 3. Lund Observatory tables for the conversion of equatorial coordinates into galactic coordinates.
- Page, T. 1952, *Ap.J.* **116**, 63. Radial velocities and masses of double galaxies.
- Pettit, E. 1954, *Ap.J.* **120**, 413. Magnitudes and color indices of extragalactic nebulae determined photoelectrically.
- Reaves, G. 1956, *A.J.* **61**, 69. Dwarf galaxies in the Virgo cluster.
- Redman, R. O. 1936, *M.N.* **96**, 588. Photographic photometry of the elliptical nebulae.
- Redman, R. O., and Shirley, E. G. 1938, *M.N.* **98**, 613. Photographic photometry of the elliptical nebulae. (Second paper.)
- Reinmuth, K. 1926, *Abh. Heidelberg Akad. Wissenschaft.* **13**. Die Herschel-Nebel.
- Sandage, A. R. 1954, *A.J.* **59**, 180. The first four years of extragalactic research with the Hale 200-inch telescope.
- [1] Seares, F. H. 1922, *Trans. I.A.U.* **1**, 69. Report of commission 25.
- [2] Seares, F. H., and Joyner, Mary C. 1945, *Ap.J.* **101**, 15. Revised standards of color index for polar stars.
- [3] Seares, F. H., Ross, F. E., and Joyner, Mary C. 1941, *Pub. Carnegie Instrn.* **532**. Magnitudes and colors of stars north of  $+80^\circ$ .
- [4] Shane, C. D., and Wirtanen, C. A. 1954, *A.J.* **59**, 285. The distribution of extragalactic nebulae.
- [5] Shapley, H. 1938, *Nature* **142**, 715. Two stellar systems of a new kind.
- [6] Shapley, H., and Ames, Adelaide 1932, *Ann. Harv. Coll. Obs.* **88**, 43. A survey of the external galaxies brighter than the thirteenth magnitude.
- [7] Shapley, H. 1951, *Proc. Nat. Acad. Sci.* **37**, 133. Magellanic Clouds. I. Transparency.
- [8] Shapley, H., and Nail, Virginia M. 1952, *ibid.* **38**, 281. Magellanic Clouds. III. Differential absorption within the large cloud.
- [9] Spitzer, L., and Baade, W. 1951, *Ap.J.* **113**, 413. Stellar populations and collisions of galaxies.
- [10] Stebbins, J. 1950, *M.N.* **110**, 416. The electrical photometry of stars and nebulae.
- [11] Stebbins, J., and Kron, G. E. 1957, *Ap.J.* **126**, 266. Six-color photometry of stars. X. The stellar magnitude and color index of the sun.
- [12] Stebbins, J., and Whitford, A. E. 1937, *Ap.J.* **86**, 247. Photoelectric magnitudes and colors of extragalactic nebulae.
- [13] —. 1948, *ibid.* **108**, 413. Six-color photometry of stars VI. The colors of extragalactic nebulae.
- [14] —. 1952, *ibid.* **115**, 284. Magnitudes and colors of 176 extragalactic nebulae.
- [15] Stebbins, J., Whitford, A. E., and Johnson, H. L. 1950, *Ap.J.* **112**, 469. Photoelectric magnitudes and colors of stars in selected areas 57, 61, and 68.
- [16] Whitford, A. E. 1953, *A.J.* **58**, 49. Colors of distant spiral and elliptical nebulae.
- [17] —. 1954, *Ap.J.* **120**, 599. Observational status of the color-excess effect in distant galaxies.
- [18] —. 1956, *A.J.* **61**, 352. Report of Washburn Observatory.
- Wilson, A. G. 1955, *Pub. A.S.P.* **67**, 27. Sculptor-type systems in the local group of galaxies.
- Wyse, A. B., and Mayall, N. U. 1942, *Ap.J.* **95**, 24. Distribution of mass in the spiral nebulae Messier 31 and Messier 33.
- Zwicky, F. 1942, *Phys. Rev. II* **61**, 489. On the large scale distribution of matter in the universe.
- . 1957, *Springer-Verlag, Berlin, Göttingen, Heidelberg*. Morphological astronomy.

## Table of Contents

Summary . . . . .	3
Chapter I. Observational Method and Photometric Results.	
1. Scope of photometric program . . . . .	5
2. Photometric method . . . . .	6
3. Instruments and plate material . . . . .	8
4. Measuring procedure . . . . .	10
5. Color equation and extinction . . . . .	12
6. Discussion of possible systematic errors . . . . .	13
7. The final magnitudes and their mean errors . . . . .	15
8. Comparison with Stebbins-Whitford . . . . .	17
9. Comparison with Pettit . . . . .	21
10. Comparison with Shapley-Ames . . . . .	22
11. Comparison with other magnitude lists . . . . .	23
Chapter II. Integrated Colors of Extragalactic Nebulae.	
12. Classification system . . . . .	25
13. Inclination effect in color index . . . . .	26
14. Selective galactic absorption . . . . .	29
15. Redshift effect in color index . . . . .	32
16. Mean colors of different types of nebulae . . . . .	35
Chapter III. Internal Absorption in Spiral Nebulae.	
17. Previous results . . . . .	37
18. Selective absorption in spiral nebulae . . . . .	38
19. Total absorption in spiral nebulae . . . . .	40
20. Ratio of total to selective absorption . . . . .	45
21. Absorption in the main bodies of spiral nebulae . . . . .	46
22. Theoretical analysis of the absorption problem . . . . .	50
23. Intrinsic colors of stellar contents . . . . .	54
24. Total galactic absorption . . . . .	57
Chapter IV. Investigation of the Virgo Cluster.	
25. Introductory remarks . . . . .	63
26. Colors and surface magnitudes of cluster members . . . . .	63
27. Relation between surface magnitude and absolute magnitude . . . . .	69
28. Determination of the redshift parameter $H$ . . . . .	70
29. Magnitude distribution in Virgo cluster . . . . .	76
Chapter V. Investigation of Double Nebulae.	
30. Double nebulae as physical systems . . . . .	80
31. Selection of material . . . . .	81
32. Colors and surface magnitudes of double nebulae . . . . .	83
33. Examination of total magnitudes . . . . .	88
Catalogue . . . . .	90
References . . . . .	101